Investigation of the *Plasmodiophora brassicae* life cycle and its interactions with host plants

A Thesis Submitted to the College of Graduate and Postdoctoral Studies

In Partial Fulfillment of the Requirements

For the Degree of Doctor of Philosophy

In the Department of Biology

University of Saskatchewan

Saskatoon, Saskachewan

By

Jiangying Tu

Permission to Use

In presenting this thesis/dissertation in partial fulfillment of the requirements for a Postgraduate degree from the University of Saskatchewan, I agree that the Libraries of this University may make it freely available for inspection. I further agree that permission for copying of this thesis/dissertation in any manner, in whole or in part, for scholarly purposes may be granted by the professor or professors who supervised my thesis/dissertation work or, in their absence, by the Head of the Department or the Dean of the College in which my thesis work was done. It is understood that any copying or publication or use of this thesis/dissertation or parts thereof for financial gain shall not be allowed without my written permission. It is also understood that due recognition shall be given to me and to the University of Saskatchewan in any scholarly use which may be made of any material in my thesis/dissertation.

Disclaimer

Reference in this thesis/dissertation to any specific commercial products, process, or service by trade name, trademark, manufacturer, or otherwise, does not constitute or imply its endorsement, recommendation, or favoring by the University of Saskatchewan. The views and opinions of the author expressed herein do not state or reflect those of the University of Saskatchewan, and shall not be used for advertising or product endorsement purposes.

Requests for permission to copy or to make other uses of materials in this thesis/dissertation in whole or part should be addressed to:

Head of the Department of Biology
University of Saskatchewan
112 Science Place
Saskatoon, Saskatchewan S7N 5E2
Canada

OR

Dean
College of Graduate and Postdoctoral Studies
University of Saskatchewan
116 Thorvaldson Building, 110 Science
Saskatoon, Saskatchewan S7N 5C9
Canada

Abstract

Plasmodiophora brassicae is a soilborne parasitic protist and the causal agent of clubroot disease in the family Brassicaceae. The formation of characteristic galls on the roots of susceptible hosts disrupts the uptake of water and nutrients by the plant roots, causing stunting, wilting and yellowing of above-ground parts and even premature plant death, resulting in large yield losses and lower oil quality. As an intracellular pathogen, the life cycle of *P. brassicae* that displays various developmental stages during pathogenesis, is complex. This dissertation describes my efforts during my graduate studies to coordinate the *P. brassicae* cellular study, investigating the *P. brassicae* infection process, with the recent published genome sequence and develop tools with which to help in answering the burning question of what happens in resistant cultivars and non-host cultivars, in relation to their susceptible relatives, to prevent cortical infection and terminate disease initiation.

I have established a new protocol based on a two-step axenic culture of *P. brassicae* with its host tissues, for easy and *in-planta* observation of cellular interactions between *P. brassicae* and host plants. The double staining of *P. brassicae* with fluorescent dyes, as established in this study, provides a promising technique for observing the infection process *in-planta.* Using the live-cell imaging protocols established in the axenic culture, together with transmission electron microscopy, the life cycle of *P. brassicae* was investigate in its natural pathosystem in soil. *P. brassicae* infecting a root har or epidermal cell underwent zoosporogenesis between five and 10 days post inoculation (dpi) and completed its life cycle with the production of resting spores, after meiosis and cytoplasmic cleavage of sporulating plasmodia in cortical cells, around 28 dpi. From all the genes involved in meiosis and flagella production, from a diverse array of sequenced eukaryotes, I have identified novel stage specific molecular markers for meiosis and flagella development during the *P. brassicae* infection cycle.

Auxin accumulation in infected root tissues, resulting in cell enlargement to form root galls, could be due to auxin directly secreted by *P. brassicae* or could be a result of redirected auxin transport towards the site of infection. I carried out a study of the role of the auxin transport system governed by the AUX1 influx protein and the PIN FORMED (PIN)-family efflux proteins during clubroot development in *A. thaliana*. Transcript analysis of infected tissue showed that host auxin transport was upregulated in early infection stages and down-regulated at the later stages of gall

formation. Mutants in auxin eflux proteins PIN1 and PIN3 bear smaller galls, suggesting that auxin import into the infected cell is needed for gall formation.

Understanding the *P. brassicae* life cycle and the role of auxin flow in gall development will benefit plant pathologists and plant breeders in developing clubroot disease resistance in canola and other cruciferae vegetables worldwide.

Preface

This thesis is based on the findings presented in the following papers and manuscripts:

I. Irani, S., Trost, B., Waldner, M., Nayidu, N., **Tu, J.,** Kusalik, A. J., Todd, C. D., Wei, Y. and Bonham-Smith, P. C. (2018). Transcriptome analysis of response to *Plasmodiophora brassicae* infection in the Arabidopsis shoot and root. BMC genomics 19:23. (not included in the thesis but parts of results from my Ph.D. project)

II. **Tu, J.,** Bush, J., Wei, Y. and Bonham-Smith, P. C. Live cell imaging of *Plasmodiophora brassicae* - host plants interactions based on a two-step axenic culture system. Microbiology Open. Accepted on October 18, 2018. Manuscript ID: MBO3-2018-08-0279R2 (Chapter 3)

III. Pérez-López, E., **Tu, J.,** Waldner, M., Kusalik, A. J., Wei, Y., Todd, C. D., and Bonham-Smith, P. C. Genome-wide transcriptomic analysis identified putative small-secreted *Plasmodiophora brassicae* proteins. In preparation. To be submitted to Frontiers in Microbiology. (not included in the thesis but parts of results from my Ph.D. project)

IV. **Tu, J.,** Wei, Y. and Bonham-Smith, P. C. Cellular tracking and gene profiling of *Plasmodiophora brassicae* during clubroot disease development elucidate life stage specific markers. In preparation. To be submitted to Molecular Plant Pathology. (Chapter 4)

Acknowledgements

This dissertation is a milestone in my academic career path at University of Saskatchewan. I have been fortunate to learn theories, concepts and theniques which would have been impossible if I had not extensively carried out the needed research and teaching in Department of Biology. I am grateful to a number of people who have guided and supported me throughout my Ph.D. study and provided assistance for my venture.

The persons I have interacted with the most during my study and who I am deeply indebted to and owe my heartfelt gratitude to are easily my supervisors, Dr. Peta Bonham-Smith and Dr. Yangdou Wei. For all the time, encouragement and patience you invested in me, be it personal or professional, influenced my thoughts and guided my roads on science, a big thank you.

I would like to express my deep appreciation to my advisory committee, Dr. Carlos Egydio Carvalho, Dr. Aaron Beattie and Dr. Pierre Forbert for their support, guidance and helpful suggestions. I would like to thank Dr. Stephen Strelkov for serving as my external examiner.

Members of Dr. Bonham-Smith and Dr. Wei lab also deserve my sincerest thanks, their friendship and assistance has meant more to me than I could ever express. I also would like to thank Dr. Guosheng Liu for his technique support in Department of Biology. A very special thanks to Mrs. LaRhonda Sobchishin (Western College of Veterinary Medicine, University of Saskatchewan) for her help and support with transimission electron microsopy techniques. I would like to acknowledge the financial support provided by Saskatchewan Agriculture Development Fund, Canola Coucil of Canada, University of Saskatchewan and China Scholarship Council for funding my projects.

I consider myself very lucky to be one of the few individuals who have had the freedom to pursue what they want in life. I understand now, that this privilege is largely due to my fanily and my freedom is the end result of their struggles and persistence. I would like to express my great appreciations to my parents, who gave me life and brought me up. My husband, Luyu Liu, has always supported my decisions and shared my enthusiasm for my research work. And my daughter, Raven Liu, who made me understand the true meaning of life. I also want to thank my parents-in-law for their unconditional support and love.

Table of Contents

List of Figures

List of Tables

List of Abbreviations

ABA	abscisic acid
ABRC	Arabidopsis Biological Resources Center
ACC	aminocyclopropane carboxylic acid
ACO	ACC oxidase
AFB	auxin signaling F-box protein
ABP	auxin binding protein
ADK	adenosine kinase
ARF	auxin response factor
BCAs	biocontrol agents
BLAST	basic local alignment search tool
bp	base pair
cDNA	complementary DNA
CFW	calcofluor white
CKX	cytokinin oxidase/dehydrogenase
CPR	constitutive expresser of PR genes
CR	clubroot resistant
DAG	days after germination
DAPI	4′,6-Diamidine-2′-phenylindole dihydrochloride
DEG	differentially expressed gene
DI	disease index
DMC1	disrupted meiotic c-DNA1
DND	defence-no death
dpi	days post inoculation
ER	endoplasmic reticulum
EIN	ethylene insensitive
EIR	ehhylene insensitive root
ET	ehhylene
ETO	ethylene overaccumulating
ETR	ethylene receptor
GCS1	generatice cell specific1
GH3	Gretchen Hagen 3
HAP2	Hapless2
HLS	hookless
HOP	homologous paring protein
IAA	indole-3-acetic acid
IAN	indole-3-acetonitrile
IGLs	indole glucosinolates
IAOx	indole-3-acetaldoxime
IPA	isopentenyl adenine
ISR	induced systemic resistance

JA	jasmonic acid
JAR	jasmonate resistant
Kb	kilo basepair
LB	Luria-Bertani
LSCM	laser scannig confocal microscopy
LTP	lipid transfer protein
Mb	million basepair
MeSA	methyl salicylate
MES	MeSA esterase
MND1	meiotic nuclear division protein1
MS	Murashige and Skoog
MZ	mature zoosporangium
NCBI	National Center for Biotechnology Information
NIT	nitrilase
OD	optical density
PAD3	phytoalexin deficient 3
Pb	*Plasmodiophora brassicae*
PFGE	pulse-field gel electrophoresis
PCR	polymerase chain reaction
PL	secondary plasmodium
PDA	potato dextrose agar
PP	primary plasmodium
PR	pathogenesis related
PIN	pin-formed
QTL	quantitative trait locus
RAB	responsive to ABA
RD	responsive to dehydration
RNA	ribonucleic acid
RNA-seq	RNA sequencing
RS	resting spore
RT-PCR	reverse-transcription polymerase chain reaction
SA	salicylic acid
SAR	systemic acquired resistance
SCF	skp1p, Cdc53p/cullin, and F-box protein
SPO	sporulation-specific protein
SP	sporulating plasmodium
TAG	tricylglycerol
TEM	transmission electron microscopy
TIR	F-box transport inhibitor response
YZ	young zoosporangium

Chapter 1 Literature Review

1.1 Importance of clubroot disease

Clubroot (caused by *Plasmodiophora brassicae*) is a major disease of the brassicas, including the economically important crops and vegetables including cabbage, cauliflower, canola and radish. The pathogen has been reported in more than 60 countries where brassica crops are grown (Dixon 2009, 2014). After infection with *P. brassicae*, an infected host root swells, resulting into tumorous galls with impaired vascular tissue, often restricting the uptake of water and nutrients and transport to the aboveground plant tissues. In heavily infested fields, early infection at the seedling stage can result in wilting, stunting and yellowing of aboveground plant tissues, possibly resulting in premature death of the plants.

The global impact on annual yield has been estimated at to 10-15%, but loss of yield can be up to 100% in heavily infested fields (Dixon 2009, 2014). Canola, the third most widely grown oil crop in the world after oil palm and soybean, produces a healthy oil rich in unsaturated fatty acids containing less than 2% erucic acid and lower than 30 μmol g^{-1} glucosinolates (Matheshawari and Kovalchuk 2016). In Canada, canola is the second largest grown crop next to wheat, however, canola is the most economically important crop for Canadian agriculture, food, and animal industries (https://www.canolacouncil.org/markets-stats/industry-overview/). Annually, more than nine million hectares of canola are grown in Canada, with 21 million tons (MT) of canola product (Annual report of Canola Council of Canada, 2017). In the past decade nearly 10 MT of canola seeds have been exported annually along with a further three MT of canola oil (https://www.canolacouncil.org/markets-stats/industry-overview/). In 2017, canola contributed more than $26.7 billion to the Canadian economy (https://www.canolacouncil.org/markets-stats/industry-overview/). In addition to the thousands of producers who derive an income from growing canola, canola is also important in the value-added industries such as canola oil and canola meal for animal feed and canola honey production. Pollination of canola is a major activity for the Canadian honeybee industry (https://www.canolacouncil.org/markets-stats/industry-overview/bees-and-canola-a-sweet-relationship/).

In Canada, clubroot disease is a major problem of brassica vegetables in the Atlantic provinces and brassica crops in the Prairie provinces. Infected canola plants ripen prematurely and seeds do not fully develop, thus yield, oil quality and oil content are dramatically reduced. To build on Canada's position as a supplier of premium quality canola seed and canola oil requires the development of robust clubroot disease resistance.

1.2 *P. brassicae* taxonomy

Clubroot research goes back to the discovery of its causal agent *P. brassicae* by the Russian scientist Woronin (reviewed in Ludwig-Müller 2016). Traditionally, *P. brassicae* was considered a fungus, however, subsequent analysis of small subunit ribosomal RNA genes, actin and polyubiquitin genes has led to a reclassification as a monophyletic group, not closely related to true fungi or to other zoosporic plant parasites, such as the Stramenopiles (including the oomycetes) and the chytridiomycetes (Cavalier-Smith and Chao 2003; Archibald and Keeling 2004). Today, *P. brassicae* is clearly established as an obligate biotrophic protist, belonging to the eukaryotic super group Rhizaria (Bulman and Braselton 2014). The Rhizaria together with the Stramenopiles and Alveolata form the S-A-R group, one of the largest clades of the eukaryotes tree (Fig. 1.1, Burki et al. 2010; Burki and Keeling 2014). Parasitic rhizarians are poorly studied organisms that are divided into two major assemblages based on their hosts, either animals: the Ascetosporea or plants: the Phytomyxea (Sierra et al. 2015). Molecular studies have recognized two orders within the Phytomyxea: Plasmodiophorids (Plasmodiophorida) and Phagomyxids (Phagomyxida) (Neuhauser et al. 2014). Plasmodiophorids (Rhizaria) are distantly but more closely related to oomycetes (Stramenopiles) or the human malaria parasite Plasmodium (Alveolata) than to fungal pathogens in the Ophisthokonts. Ten genera have been assigned to the order Plasmodiophorids: *Ligniera*; *Membranosorus* Ostenfeld & Whiffen; *Octomyxa* Couch, Leitner and Whiffen; *Plasmodiophora*; *Polymyxa*; *Sorodiscu* Lagerheim & Winge; *Sorosphaera*; *Spongospora* Brunchorst; *Tetramyxa* Goebel, and *Woronina* (Bulman and Braselton 2014).

P. brassicae is the most studied species in the Plasmodiophorids. Other well-studied species include *Spongospora subterranea*, causing powdery scab on potato, and *Spongospora nasturtii*, causing crook root in watercress and also acting as the vector for the *Potato mop-top virus (PMTV)* (Schwelm et al. 2018). The otherwise symptomless *Polymyxa graminis* transmits economically important viruses to a number of grain crops, while *Polymyxa betae* is the vector for the beet

necrotic yellow vein virus, that causes “rhizomania” in sugar beet (McGrann et al. 2009). Phylogenetic analysis of rDNA suggests that *P. brassicae* is more distantly related to *Spongospora* than *Polymyxa* (Bulmen et al. 2001; Cavalier-Smith and Chao 2003; Neuhauser et al. 2014; Schwelm et al. 2018).

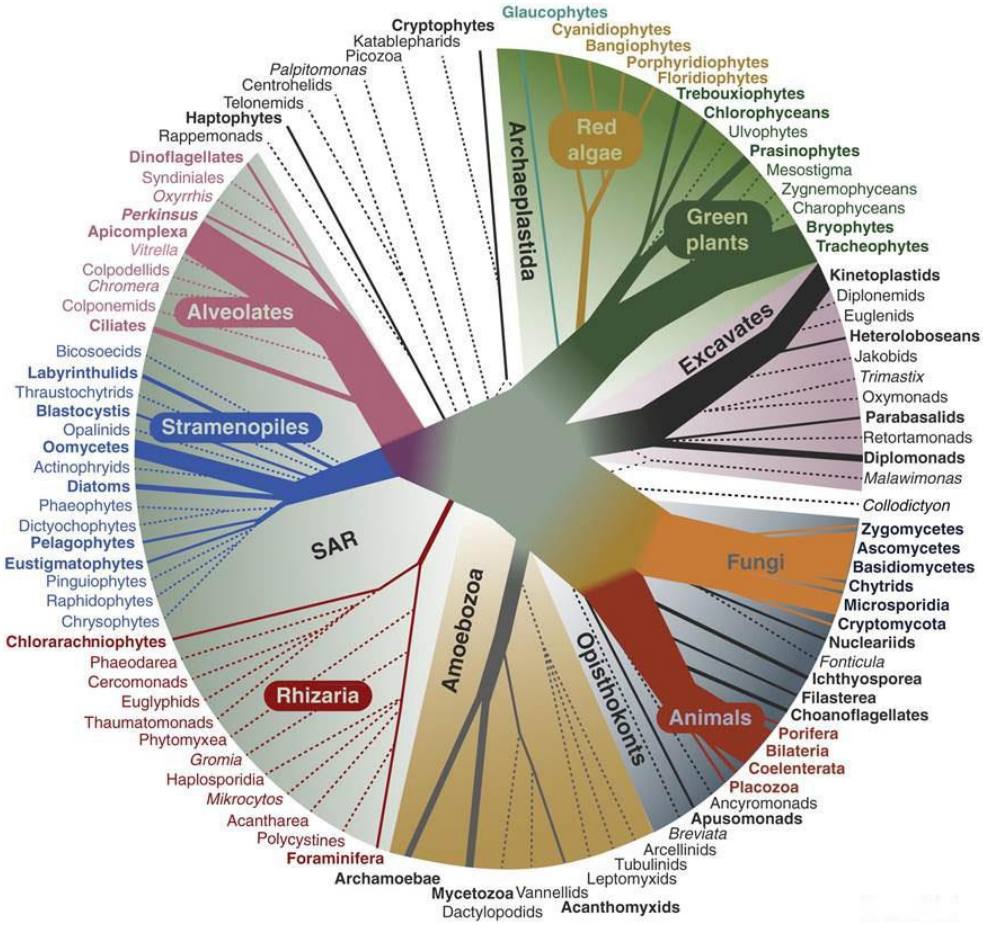

Figure 1.1 Evolutionary relationship among eukaryotes.

Rhizaria (i.e. *Plasmodiophora brassicae, Spongospora subterranea, Polymyxa betae*) are more closely related to oomycetes in the Stramenopiles (i.e. *Phytophthora spp*.) or the human malaria parasite Plasmodium in the Alveolata (i.e. *Plasmodium spp*.) than to the fungal pathogens in the Ophisthokonts (i.e. *Ustilago spp.*, *Verticillium spp*.). S-A-R = eukaryotic supergroup consisting of Stramenopiles, Alveolata and Rhizaria. Figure taken from Burki and Keeling 2014 with copyright permission.

1.3 *P. brassicae* genomics

The chromosome size and number of *P. brassicae* were investigated by electron microscopy and pulse-field gel electrophoresis (PFGE). Electron microscopy studies estimated 20 synaptonemal complexes in *P. brassicae* (Braselton 1982). Trying to determine karyotypes (chromosome size and number) for *P. brassicae* isolates by PFGE has been inconclusive, identifying between six and 16 chromosomal bands ranging between 680 kb and 2.2 Mb in size (Bryan et al. 1996; Graf et al. 2001; Fähling et al. 2004; Graf et al. 2004). PFGE analyses of three *P. brassicae* single-spore isolates did identify chromosome polymorphisms that might explain the differences in chromosome numbers (Graf et al. 2004). Based on chromosome numbers and size estimates from the PFGE studies the genome size of *P. brassicae* has been suggested to be between 18-20.3 Mb (Graf et al. 2004).

To avoid complications in using genetically diverse field isolates, the first reference genome for *P. brassicae* was created from a callus culture harboring *P. brassicae* propagates from a single spore isolate (Bulmen et al. 2011). More recently, using next generation sequencing, the 24Mb draft genome of *P. brassicae* has been completed for isolate e3 (Schwelm et al. 2015). In total, 9731 protein encoding genes were annotated with an average coding sequence length of 1405 bp. Comparision of the e3 transcriptome from germinating resting spores, secondary plasmodia and mature resting spores to the annonated genome of other Rhizaria resulted in the annotation of 66 % of the e3 genome. In 2016, the genomes of the single spore isolates representing pathotype 3 (Pb3, predominant pathotype in canola growing region) and Pb6 (predominant pathotype in cabbage growing region) were released (Rolfe et al. 2016). The size of the assembled genomes for both pathotypes was similar and approximately 24.2 Mb (Rolfe et al. 2016), close to pre-existing estimates (Siemen et al. 2009b) and to the genome of the e3 isolate (Schwelm et al. 2015). The assembled genome of Pb3 was less fragmented than that of e3 (107 versus 165 scaffolds), while the assembled genome of Pb6 was more fragmented (356 versus 165 scaffolds). A higher number of genes were predicted in both Pb3 (10851) and Pb6 (10070) than in e3 (9730). Annotated genes were compared to other Rhizaria core genes by their transcriptome expression in plasmodia (16 dpi) and maturing spores (26 dpi) for pathotypes Pb3 and Pb6. All three *P. brassicae* genomes are smaller than the previously sequenced genomes of the two free-living Rhizaria, *B. natans* (~100 Mb) and the repeat rich *R. filosa* genome (~320 Mb) (Schwelm et al. 2015). In order, through comparative genomic studies, to identify genes that determine pathogenesis in *P. brassicae*. The *P.*

brassicae genome project by Rolfe et al. (2016) is involved in sequencing multiple isolates from diverse regions.

The small size of the three sequenced *P. brassicae* genomes is characterized by a high gene density and a low percentage of repetitive sequences and transposable elements, whereas the genome of *S. subterranea* is enriched in transposon and virus-related genes (Bulman et al. 2011; Schwelm et al. 2015). How characteristic this is for *P. brassicae* remains to be determined. Like other biotrophic pathogens, the genome of *P. brassicae* lacks genes involved in numerous metabolic pathways, but contains a wide range of transport protein genes including some unique to *P. brassicae* (Rolfe et al. 2016). Genes encoding phytohormone biosynthesis, that may contribute to the clubroot gall phenotype of infected roots, were identified in both genome sequencing projects. A gene endocing the protein (PbGH3) that can modify auxin and jasmonic acid was identified in e3 (Schwelm et al. 2015). Genes involved in auxin (PbPT3Sc00039_A_3.298_1) and cytokinin (PbPT3Sc00024_Sm_2.181_1 and PbPT3Sc00040_Am_6.202_1) biosynthesis were identified in Pb3 and Pb6 genome (Rolfe et al. 2016). The information available through these genome sequence resources will provide the tools to answer questions about the biology, evolution, and pathogenesis of *P. brassicae*.

1.4 *P. brassicae* interactions with the plant host

Clubroot disease arises from a compatible interaction between a host plant and *P. brassicae*. As an intracellular biotrophic protist, once inside the host plant cell, it is likely that *P. brassicae* secretes proteins in order to suppress or evade plant immunity as well as to induce cooperation of the host cell for the establishment of a compatible interaction.

During the primary infection stage (of root hairs and epidermal cells), *P. brassicae* infection results in few obvious changes to the strucuture of the host plant cells, however, gene expression studies have identified genes involved in signal transduction and transcription, as well as cell wall enzymes and phytohormone biosynthesis and metabolism, with altered transcript levels (Agarwal et al. 2011). A more recent study of *P. brassicae* infected Arabidopsis root tissue described over 1000 host plant genes up- or down-regulated and confirmed the involvement of signal transduction and transcription pathways as well as cell wall enzymes and phytohormone genes during the early stages of infection (Zhao et al. 2017). In *P. brassicae*-infected *Brassica rapa* roots of near-isogenic lines carrying the resistant or susceptible allele at the *CRb* locus, transcripts were elevated for PR

genes involved in the salicylic acid signaling pathway and genes encoding effector receptors (resistance proteins) for the resistance allele. In contrast, transcripts of genes involved in uncontrolled cell division and cell expansion were suppressed (Chen et al. 2016).

During secondary infection (of root cortical cells), host cells expand and proliferate, leading to root swelling and characteristic gall formation that inhibits nutrient and water transport, resulting in reduced growth of the aerial parts of an infected plant. The most damaging aspect for the host plant occurs during the secondary infection. Genes involved in cell division and cell expansion were up-regulated in *Arabidopsis thaliana* during secondary infection by *P. brassicae* (Siemens et al. 2006), whereas genes for cell enlargement and proliferation were actively inhibited in a partial quantitative resistance response compared to a susceptible response in *A. thaliana* (Jubault at el. 2013).

As a biotrophic parasite, *P. brassicae* takes in nutrients, such as carbohydrates, amino acids and lipids for its rapid proliferation during secondary infection stages, from its host (Ludwig-Müller 2009a). Host cells harboring secondary plasmodia are also metabolically highly active (Schuller et al. 2014, 2015). Clubroot gall cells containing secondary plasmodia are transformed into metabolic sinks accumulating starch, as a carbohydate rescource for secondary plasmodia development (Brodmann et al. 2002). Genes involved in sugar or starch metabolism, including sucrose synthase, invertase, starch synthase, and ß-amylase, were up-regulated either at 10 dpi with very few secondary plasmodia in cortical cells, or at 23 dpi with large secondary plasmodia in more then 60% of root cells (Siemens et al. 2006). Extracellular invertases may also play an important role in supplying sugars to the pathogen during gall formation (Siemens et al. 2011).

While the *P. brassicae* genome does not contain any fatty acid synthase genes, it does contain lipase genes (Schwelm et al. 2015). Fatty acids need to be acquired from the host and secreted *P. brassicae* lipases, expressed highest in the secondary plasmodia stage, might be involved in this process by providing the pathogen with fatty acid starter molecules. In the *P. brassicae* genome, genes involved in fatty acid modification and elongation were mainly expressed during the secondary plasmodia stage (Schwelm et al. 2015). In infected Arabidopsis roots, *LIPID TRANSFER PROTEIN (LTP)* genes were also highly up-regulated during secondary infection stages, suggesting transport and delivery of lipids to tissues in which the pathogen resides (Siemens et al. 2006). A *LTP* gene was also up-regulated in *Beta vulgaris* after *P. betae* infection (Desoignies et al. 2014).

More recently, microarray data on laser capture microdissected populations of stage-specific *P. brassicae* infected cells show that cells containing secondary plasmodia were metabolically highly active with major altered pathways including sugar metabolism, lipid synthesis and metabolism and fermentative processes (Schuller et al. 2014). The transcription of plant growth-promoting hormone genes was also up-regulated, however, the transcription of most plant-defence hormone genes was either not changed, or suppressed in cells with large and older secondary plasmodia (Schuller et al. 2014).

The complex interaction of *P. brassicae* with its host makes the interpretation of transcriptome data difficult. *P. brassicae* secretes effector proteins into the host cell, while the host tries to combat the pathogen. It is often uncertain if up- or down-regulated plant genes are actually controlled by the plant in an effort to provide resistance against the pathogen or if host genes have been commandeered by the pathogen to enhance susceptibility.

1.5 Hormone homeostasis caused by *P. brassicae* infection

The development of clubroot galls during the secondary infection cycle is dependent on uncontrolled cell expansion and cell division regulated by plant hormones such as auxins, cytokinins and brassinosteroids. Plant cell division is regulated by shifting levels of cytokinin and auxin, while the hypertrophied gall cells are most likely the result of increased auxin levels (reviewed by Ludwig-Müller et al. 2009). As well as plant growth promoting hormones, plant defence-related hormones such as salicyclic acid and jasmonic acid/ethylene are also involved in the *P. brassicae*-host interaction. *P. brassicae*-induced changes in host cell hormone levels and the corresponding effects on clubroot gall phenotype in *A. thaliana,* is summarized in Table 1.1.

Table 1.1 Selected changes in hormone metabolism and corresponding effects on clubroot phenotype in *Arabidopsis.*

Hormone	Gene or pathway altered	Type of alteration	Clubroot phenotype	Reference
Auxin	biosynthesis pathways	mutant *nit1*	reduced gall size	Grsic-Rausch et al. (2000)
		antisense *NIT2*	delayed gall formation	Neuhaus et al. (2000)
		overexpression *NIT2*	none	Neuhaus et al. (2000)
Auxin/glucosinolate	biosynthesis pathway	double mutant *cyp79b2/b3*	none	Siement et al. (2008)
	conjugate hydrolysis gene	mutant *ilr1*	none	Siemens et al. (2002)
	conjugate synthesis gene	single mutant for *gh* gene	none	Jahn et al. (2013)
		double mutant *gh3.5/gh3.17*	slightly more susceptible	Jahn et al. (2013)
Glucosinolate (GL)	*TU8* (heterochromatin protein, lower IGL levels)	mutant *tu8*	reduced gall size	Ludwig-Müller et al. (1995)
Camalexin	biosynthesis pathway	mutant *pad3*	none	Siement et al. (2002), (2008)
Cytokinin	degradation pathway	overexpression lines of *CKX*	reduced gall size	Siement et al. (2006)
Jasmonic acid	conjugation/activation pathway	mutant j*ar1*	higher susceptibility	Siement et al. (2002)
	N/A	exogenous MeJA treatment	reduced gall size	Lemarié et al. (2015)
Ethylene	signalling pathway	receptor mutant *etr1*	higher susceptibility	Knaust and Ludwig-Müller (2013)
Salicyclic acid	biosynthesis pathway	mutant *sid2*	none	Lovelock et al. (2016)
		mutant *crp1*	reduced in gall scores	Lovelock et al. (2016)
		mutant *dnd1*	reduced in gall scores	Lovelock et al. (2016)
	signalling pathway	mutant *npr1*	reduced in gall scores	Lovelock et al. (2016)
		mutant n*ahG*	none	Lovelock et al. (2016)
	N/A	exogenous SA treatment	reduced in gall scores	Lemarié et al. (2015)

1.5.1 Auxin

Auxin distribution within plant tissues is regulated by biosynthesis, inactivation and transport pathways. Auxin can be biosynthesized in Arabidopsis via several different pathways occurring in parallel (Zhao 2014, Fig. 1.2). The main pathway in the Brassicaceae family is via indole-3-acetaldoxime (IAOx), indole glucosinolates (IGLs) and indole-3-acetonitrile (IAN). The availability of *A. thaliana* mutants in the IAOx /IGLs pathway has been exploited to investigate the role of auxin in the *P. brassicae*-Arabidopsis interaction.

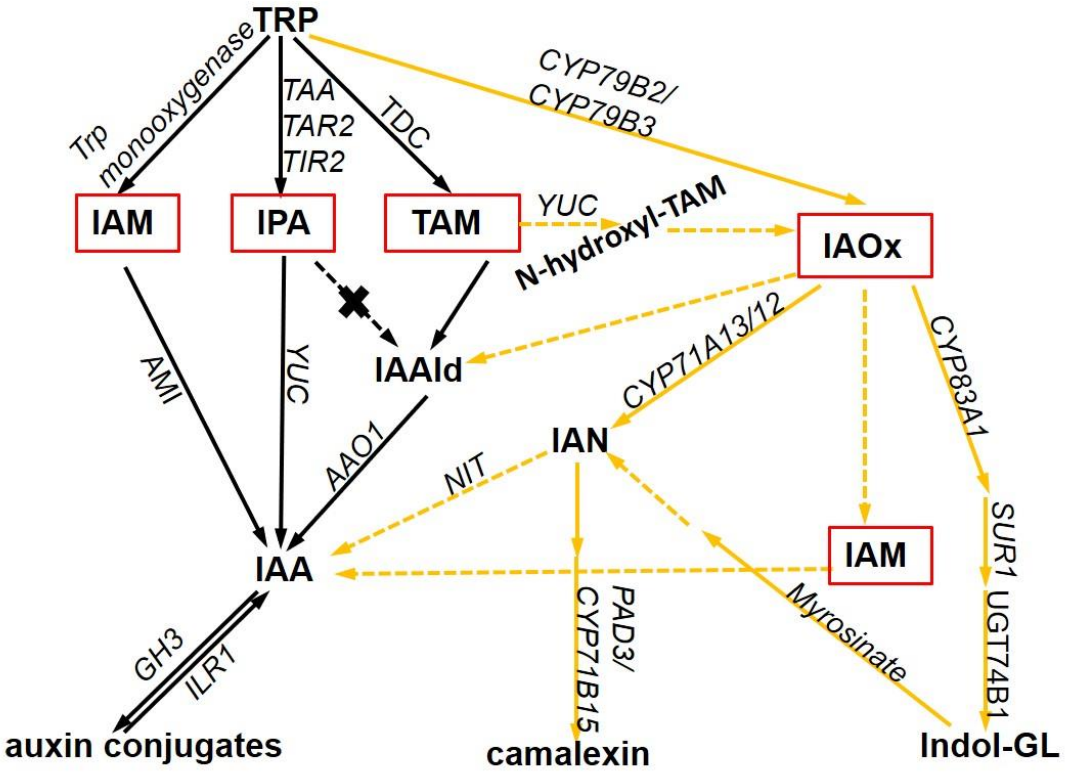

Figure 1.2 Overview of the possible route of auxin biosynthesis in *Arabidopsis*.

Mustard-coloured arrows indicate the Brassicaceae species-specific pathway. Dashed arrows indicate steps for which the gene and enzymatic function(s) remain unknown or poorly understood. Letters in italics show genes involved in the conversion process. Red boxes indicate the main auxin biosynthesis pathways. TRP: tryptophan; IAM: indole-3-acetamide; IPA, indole-3-pyruvic acid; TAM, tryptamine; IAOx, indole-3-acetaldehyde;
IAAld, indole-3-acetaldehyde; IAN, indole-3-acetonitrile; IAA: indole-3-acetic acid; GL, glucosinolate.

Previously, the size of clubroot galls in brassica species has been shown to correlate with level of glucosinolates in gall cells, which have been discussed as precursor of auxin (reviewed in Ludwig-Müller and Schuller 2008; Ludwig-Müller et al. 2009). After infection by *P. brassicae*, host plants displayed a strong induction of genes involved in the biosynthesis of indol glucosinolates (IGLs), however the Arabidopsis *cyp79b2/b3* double mutant that compromised in the first committed step, TRP to IAOx in the biosynthesis of camelexin and IGLs and almost completely devoid of IGLs, demonstrated normal clubroot symptoms and free IAA levels comparable to those of wild type galls (Siemens et al. 2008; Ludwig-Müller 2009b). In the Arabidopsis heterochromatin-like protein 1 (*tu8*) mutant, lower levels of IAN and IGL correlated with smaller clubroot galls (Bennett et al. 2005). Together, these results suggest that an increased level of IAA in clubroot tissues is produced via different pathway(s) and is not a product of the conversion of IGLs. IGLs are probably not a constraint on *P. brassicae* infection and disease development.

Interestingly, mutations in later steps of IAA synthesis, via the IAOx pathway, influence clubroot gall size. The *nitrilase1* (*nit1*) mutant in Arabidopsis, with lower free IAA levels, was more tolerant to *P. brassicae* infection and showed reduced gall size (Grsic-Rausch et al. 2000). In addition, in antisense *NITRILASE2* (NIT2) plants, gall development was slower compared to wild type plants (Neuhaus et al. 2000). By contrast, a *cyp79b2/b3* double mutant, blocked in the first step in the pathway devoted to the synthesis of IAA, camalexin and indole glucosinolates via IAOx, showed no reduction in gall size or change in endogenous IAA levels compared to wild type plants (Siemens et al. 2008), suggesting that blocking early steps in the IAOx pathway can induce alternative pathways to produce IAA, while blocking later steps resultes in a reduction in IAA and an inhibtory effect on gall formation.

In the nucleus, auxin can trigger broad but specific transcriptional responses through the action of three protein families: the F-box TRANSPORT INHIBITOR RESPONSE 1/AUXIN SIGNALING F-BOX PROTEIN (TIR1/AFB) auxin co-receptors, the Auxin/INDOLE-3-ACETIC ACID (Aux/IAA) transcriptional repressors, and the AUXIN RESPONSE FACTOR (ARF) transcription factors (Lavy and Estelle 2016). During clubroot disease progression, transcription and transcript levels for *ABP1* and *TIR1* auxin receptors were upregulated, while TIR-class receptor double mutants showed less susceptibility to *P. brassicae* (Jahn et al. 2013). As targets for auxin perception via the TIR pathway, the *GH3* genes could be required, as these are also involved in

regulating auxin homeostasis by conjugating IAA to various amino acids (Staswick et al. 2005). Several *GH3* genes have been found to be upregulated during clubroot development (Siemens et al. 2006; Jahn et al. 2013). In *B. rapa* L., IAA-amino acid conjugates were hydrolysed more readily in *P. brassicae* infected roots compared with controls, also contributing to the free IAA levels in galls (Ludwig-Müller et al. 1996). However, an Arabidopsis *ilr1* (conjugate hydrolase gene) mutant did form clubroot galls comparable to those on wild type plants (Siemens et al. 2002).

1.5.2 Cytokinins

Compared to the work on auxin involvement in clubroot gall formation, cytokinins have been less well studied. The levels of both free and conjugated cytokinins increase during clubroot disease progression and subsequent gall formation in brassica species and Arabidopsis (reviewed in Ludwig-Müller and Schuller 2008; Ludwig-Müller et al. 2009). This increase is partially a result of the synthesis of small amounts of zeatin by secondary plasmodia of *P. brassicae* (Ludwig-Müller and Schuller 2008; Ludwig-Müller et al. 2009) as well as plants contributing by inducing endogenous cytokinin biosynthesis, or by repressing degradation (Ando et al. 2005, 2006; Devos et al. 2005; Siemens et al. 2006). Devos et al. (2005) showed that the amount of active cytokinins such as zeatin riboside was greater in infected *B. rapa* roots than in healthy control roots, and that *iso*pentenyl adenine (IPA) increased in clubroots at 21 dpi. In Arabidopsis, only the *iso* pentenyl-type cytokinins accumulated during early stages of infection (Devos et al. 2006). The transcription of two genes encoding root-specific cytokinin oxidase/dehydrogenases (*CKX*) was reduced in Arabidopsis during disease progression and plants overexpressing *CKX* genes were found to be more tolerant to *P. brassicae* infection (Siemens et al. 2006). However, since these plants also show a dwarf phenotype, this strategy cannot be used to control clubroot disease. Proteome analysis of both Arabidopsis and Chinese cabbage showed that the protein expression of adenosine kinase (*ADK*), involved in interconverting cytokinin ribosides to corresponding ribonucleotides, was downregulated during early infection (Devos et al. 2005, 2006). Downregulation of *AtADK* and *AtCKX* during *P. brassicae* infection maintains a high steady-state level of active cytokinins.

1.5.3 Abscisic acid

Some observations have led to the assumption that during the later developmental stages of a clubroot gall, as the vascular tissue of the root is impaired and water supply to the aerial part is

restricted, drought stress signalling might be important for above-ground clubroot disease symptoms. Drought-response transcripts such as *RAB18* (responsive to ABA), *RD20* and *RD22* (responsive to dehydration) were strongly upregulated with pathogen establishment and secondary infection in Arabidopsis roots at 21 dpi (Siemens et al. 2006). In late stage infected *B. rapa* roots, ABA concentrations over four times those of control roots have been measured at 21 dpi (Devos et al. 2006). As these responses are restricted to late stage infection, they could be a consequence of dehydration rather than signals contributing to the development of clubroot galls.

1.5.4 Jasmonic acid and ethylene

Generally, the jasmonic acid (JA) and ethylene (ET) pathways are commonly required for resistance to necrotrophic pathogens that kill plant cells before colonizing them, whereas salicylic acid (SA) signaling positively regulates plant defenses against biotrophic pathogens, that feed on living cells of their host in order to complete their life cycle (Glazebrook 2005). However, it has been reported that both JA and SA pathways are involved in resistance to *P. brassicae* (Lemarié et al. 2015). The biosynthesis of both SA and ET was repressed by *P. brassicae* infection in susceptible Arabidopsis wild type Col-0, whereas the biosynthesis of JA was induced during early stage infection and in developing clubroot galls at 21 dpi (Siemens et al. 2006; Agarwal et al. 2011; Gravot et al. 2012). Moreover, the expression of lipoxygenase genes, involved in the biosynthesis of JA, was found to be down-regulated in the partial resistant Arabidopsis ecotype Bur-0 at two dpi and 7 dpi (Jubault et al. 2013). A positive crosstalk between JA accumulation and auxin biosynthesis has been reported (Hentrich et al. 2013). JA accumulation in susceptible Arabidopsis may be involved in the regulation of IAA biosynthesis by the up-regulation of nitrilase, myrosinase, and tryptophan oxidase and enzymes in the auxin biosynthesis pathways (Grsic et al. 1999). However, treatment with JA after *P. brassicae* inoculation was found to reduce gall formation in susceptible Arabidopsis Col-0, but not the partially resistant ecotype Bur-0. A strong downregulation of the *JASMONATE RESISTANT 1* gene (*JAR1*), a JA signaling gene, was reported in susceptible wild type Arabidopsis (Siemen et al 2006), in line with observations that *jar1* was more susceptible to *P. brassicae* (Siemens et al. 2002; Lemarié et al. 2015). Together, this evidence points to JA contributing a weak defense response to *P. brassicae* infection.

A role for ET in the host defense response to *P. brassicae* has yet to be clearly established (Knaust and Ludwig-Müller 2013). The biosynthesis of ET was found to be suppressed in the

susceptibility Arabisopsis Col-0, but active in a partial resistance response in Bur-0 (Siemens et al. 2006; Jubault et al. 2013). In susceptible Arabidopsis Col-0, decreased transcription levels of aminocyclopropane carboxylic acid (ACC), an intermediate in the ET biosynthesis pathway, have been shown in *P. brassicae* infected roots at the same time as the transcriptional level for *ACO2*, encoding ACC oxidase, was elevated (Devos et al. 2005; Siemens et al. 2006; Knaust and Ludwig-Müller 2013). Moreover, the Arabidopsis constitutive ethylene over accumulating mutant (*eto2*) showed a slightly reduced disease index and root fresh weight at 18 and 28 dpi (Siemens et al. 2006; Knaust and Ludwig-Müller 2013). Treatment with ethrel, an ET generator, did not reduce clubroot symptoms in Arabidopsis, whereas clubroot gall formation was reduced when infected *B. rapa* plants were similarly treated (Knaust and Ludwig-Müller 2013). The Arabidopsis ET receptor mutants, including *etr1-1*, *etr1-3*, *ein2-1*, *ein3-1*, *ein4-1*, *eir1-1*, *eto1*, *eto2* and *hls*, when tested with high infection pressure, did not show any different clubroot phenotype compared to the wild type (Siemens er al. 2002; Alix et al. 2007). However, at low infection pressure, they were clearly more susceptible to the clubroot pathogen than the wild type, suggesting that a functional ET signalling pathway is also needed to restrict root gall growth (Knaust and Ludwig-Müller 2013).

1.5.5 Salicylic acid

Salicylic acid (SA) is a key signaling molecule, activating both local and systemic defence responses to biotrophic pathogens (Hout et al. 2014). Biosynthesis of salicylic acid, in susceptible plants, is repressed by *P. brassicae* infection (Siemens et al. 2006; Agarwal et al. 2011; Jubaut et al. 2013; Lemarié et al. 2015; Ludwig-Müller et al. 2015) and treatment with SA early after inoculation reduced gall formation in Arabidopsis (Agarwal et al. 2011; Lemarié et al. 2015) and *B. oleracea* var. *italic* (broccoli) (Lovelock et al. 2013). Reduced gall size has also been reported in the Arabidopsis SA constitutive expressor mutants, *cpr1* (*constitutive expressor of PR genes*) and *dnd1* (*defense-no death 1*). Both mutants, with elevated SA levels and constant PR expression, showed reduced gall size, suggesting a role for SA in limiting clubroot development during the secondary infection stages of the *P. brassicae* life cycle (Lovelock et al. 2016).

Methyl salicylate (MeSA) is a biologically inactive form of SA in plants and high MeSA levels relative to SA levels, leads to increased plant susceptibility to *P. brassicae* infection (Chen et al. 2003; Koo et al. 2007). *P. brassicae* infection has been shown to induce both host plant and *P. brassicae* SA methyltransferase genes (Lovelock et al. 2016; Ludwig-Müller et al. 2015). However,

the inactive SA derivatives (MeSA) can be converted back to free SA by MeSA esterase (MES) and the expression of MES genes is induced in resistant *B. oleracea* during *P. brassicae* infection (Manoharan et al. 2016), thereby suggesting that increased expression of MES genes will contribute to increased disease resistence in host plants (Forouhar et al. 2005).

1.6 Clubroot management

Effective control of soil borne pathogens is hampered by: i) persistence in soil through the formation of survival structures (e.g., oospores, chlamydospores, and sclerotia), ii) often wide host range, and iii) the inefficiency of chemical and biological controls due to poor soil accessibility. Current approaches to combat *P. brassicae* rely on genetic resistance, while biofungicide control has been approved for working under green house conditions (Peng et al. 2011; Lahlali et al. 2011; Lahlali et al. 2014).

1.6.1 R genes or QTLs

Over the past few decades, concentrated efforts have been made to identify clubroot resistance (CR) genes and to introgress them into cultivated varieties of brassicas. To date, nine major dominant CR loci contributing to clubroot resistance have been mapped on five different chromosomes of *B. rapa*, including *CRa* (chromosome A03) (Matsumoto et al, 1998), *CRb* (A03) (Piao et al. 2004; Zhang et al. 2014), *Crr3* (A03) (Hirai et al. 2004), *Crr1* (A08) and *Crr2* (A01) (Resistance requires both resistance alleles at both loci; Suwabe et al. 2003 and 2012), *Crr4* (A06) (Suwabe et al. 2006), *CRc* (A02), *CRk* (A03) (Sakamoto et al. 2008), and *Rcr1* (A03) (Chu et al. 2014). With the exception of *Rcr1*, which lacks a clear resistance source, the *CR* genes were all derived from European fodder turnips (*B. rapa* subsp *rapa*). *Crr1a* and *CRa*, have been cloned and identified as classical resistance genes containing Toll-interleukin receptor (TIR)-nucleotide-binding (NB)-leucine-rich repeats (LRR; Ueno et al. 2012; Hatakeyama et al. 2013), but the response mechanisms to *P. brassicae* infection associated with these two *CR* genes have yet to be fully elucidated.

Resistance to *P. brassciae* in *B. oleracea* and *B. napus* can be quantitative, controlled by numerous genes or quantitative trait loci (QTLs) (Lee et al. 2015; Nagaoka et al. 2010; Rocherieux et al. 2004; Hasan and Rahman 2016; Manzanares-Dauleux et al. 2000; Werner et al. 2008; Tomita et al. 2013). In *B. rapa*, CR is controlled in both a qualitative and quantitative manner dependent

on the genotypes, whereas genetic studies suggest that CR is controlled by many minor QTLs in *B. oleracea* (Rocherieux et al., 2004; Nagaoka et al., 2010; Lee et al., 2015). For example, a total of nine QTLs were detected for clubroot resistance to four single-spore isolates and one field isolate in the progenies of the cross C10 (resistant kale) by HDEM (susceptible broccoli) (Rocherieux et al. 2004). Among these nine QTLs, *Pb-Bo1* had effects on all five isolates, with a major effect on three isolates and a weaker effect on the two other isolates, while five of the QTLs had only minor effects on single isolates (Rocherieux et al. 2004). The major QTL, pb-*Bo(Anju)1*, derived from cabbage Anju, identified in F2 plants from the cross between a cabbage double haploid (DH) line (resistant) and a broccoli DH line of *B. oleracea* (Nagaoka et al. 2010), while the QTL (*Pb-Bo(GC)1*) was derived from the susceptible broccoli GC. Five genes involved in glucosinolate biosynthesis were also mapped in this study. The presence of the major QTL (*Pb-Bo(Anju)1*) or multiple minor QTLs does not impart strong clubroot resistance in *B. oleracea*; however, *Pb-Bo(Anju)1* together with two to three minor QTLs can confer moderate resistance, while all five minor QTLs including *Pb-Bo(Anju)1* produce the strongest resistance to multiple *P. brassicae* isolates. Two QTLs (*CRQTL-GN_1* and *CRQTL-GN_2*) for resistance to the GN isolate (Race 9) and one QTL (*CRQTL-YC*) for resistance to the YC isolate (Race 2) have also been mapped in cabbage (Lee et al. 2015).

In *B. napus*, the CR gene *Pb-Bn1* (on chromosome N03), with additional minor QTLs identified on chromosomes N12 and N19, was first shown to contribute to resistance to the two *P. brassicae* isolates belonging to pathotypes 4 and 7 (Manzanares-Dauleux et al. 2000). More recently, nineteen QTLs have been detected on chromosomes N02, N03, N08, N13, N15, N16 and N19 of *B. napus* L., providing resistance to seven different field isolates from Sweden and Germany (Werner et al. 2008). A single gene or cluster of genes, in a single genomic region on chromosome A8 in rutabaga (*B. napus* var. *napobrassica*), provides resistance to the five pathotypes 2, 3, 5, 6, and 8 (Hasan and Rahman 2016).

Until 2009, all canola cultivars in Western Canada were highly susceptible to *P. brassicae* (Strelkov et al. 2006). Since then, more than 20 registered clubroot resistant (CR) canola cultivars have been released in Canada, most of which carry a single dominant *CR* gene (‘45H29’, ‘Mendel’, ‘Mendelsson’, ‘Cracker’, ‘Andromeda’, ‘SY Alister’; Rahman et al. 2014; Strelkov et al. 2018). Seven *CR* genes have been identified at AAFC Saskatoon from six closely related brassica species, including three from *B. rapa* (*Rpb1* on chromosome 3 of *B. rapa* (A3), *Rpb3* on chromosome 3 of

B. rapa (A3), *Rpb4* on chromosome 8 of *B. rapa* (A8)), two from canola (*B. napus*) breeding lines, one from *B. nigra*, *Rpb2* on chromosome 5 of *B. nigra* (B5) and one from *B. oleracea* (http://www.agwest.sk.ca/kaizen/CIM-AGCI/CIM2015). *Rpb1* (*Rcr1*) was previously described by Chu et al. (2014). The resistance mechanism associated with *Rcr1* is mainly based on the up-regulation of the genes involved in jasmonic acid/ethylene and callose biosynthesis pathways. A single R gene on chromosome N3 of *B. napus*, corresponding to A3 in *B. rapa*, has been mapped (Zhang et al. 2016), and this has led to the suggestion that the *CR* loci in canola may have originated from *B. rapa*.

The breeding of resistant cultivars is one of the most efficient ways to control clubroot. However, the planting of oligogenic clubroot-resistant varieties can impose strong selection pressure on *P. brassicae* populations, favoring strains capable of overcoming the single gene resistance. Many pathogen:host examples exist where the effectiveness of major resistance genes has been broken down, including clubroot resistance (Osaki et al. 2008; Matsumoto et al. 2012; Diederichsen et al. 2014; Strelkov et al. 2016), therefore, new modes of resistance are needed to control clubroot. Through molecular marker-assisted breeding, three clubroot resistance genes (*CRa*, *CRk*, and *CRc*) have been pyramided in four Chinese cabbage lines making these lines highly resistant to six isolates of *P. brassicae* (Matsumoto et al. 2012). Other genes involved in defense responses (such as the production of antimicrobial compounds, cell wall strengthening, callose formation, lignification, the oxidative burst) or genes encoding metabolic enzymes could also be used in conferring quantitative resistance (Loarce et al. 2016).

1.6.2 Biocontrol agents

Biological control has been defined simply as the utilization of natural enemies, chiefly insects, parasites and pathogens, to reduce the damage caused by noxious organisms to tolerate levels. Biocontrol agents (BCAs), or just their elicitor molecules, could also be used to prime the defence response of a plant by triggering systemic acquired resistance (SAR) or induced systemic resistance (ISR) (Conrath et al. 2001).

Antagonistic bacteria that can contribute to the control of clubroot include *Bacillus subtilis* (Peng et al. 2011; Lahlali et al. 2011; Guo et al. 2013), *Lysobacter antibioticus* (Zhou et al. 2014), *Streptomyces sp.* (Joo et al. 2004), as well as various actinomycetes, including *Microbispora rosea ssp. rosea* and streptomyces species such as *S. olivochromogenes* (Lee et al. 2008), *S. griseoviridis*

and *S. lydicus* (Peng et al. 2011). Under environmentally controlled growth conditions, *B. subtilis* strain QST713 in its commercial product (Serenade®) reduced clubroot severity by more than 80% (Peng et al. 2011; Lahlali et al. 2011). This effect has been attributed to the suppression of root hair and cortical infection by *P. brassicae* as well as induced expression of genes involved in phenylpropanoid, jasmonic acid (JA), and ethylene (ET) pathways (Lahlali et al. 2011; Lahlali et al. 2014). A different *B. subtilis* strain, XF-1, that also suppresses *P. brassicae* activity, does so through the synthesis of chitosanase, suggesting that chitin in the resting spores would be the target (Guo et al. 2013). Other bacteria including *S. griseoviridis* and *S. lydicus* have also shown some potential control against clubroot (Peng et al. 2011).

Endophytic fungi, that are able to live inside host tissues without causing apparent disease, are present in almost all higher plants (Azevedo et al. 2000). The endophytic fungus, *Acremonium alternatum*, has been shown to be effective in controlling clubroot disease, in Arabidopsis and Chinese cabbage (*B. rapa*), by delaying disease development (Doan et al. 2010; Jäschke et al. 2010), whereas the effect was not so prominent with oilseed rape (*B. napus*) (Auer and Ludwig-Müller 2014). *A. alternatum* induced defence-related genes in the JA and SA signalling pathways (Ludwig-Müller 2016). Clubroot resistance in canola, induced by the fungus *Heteroconium chaetospira,* could be related to the induction of plant defence pathways via JA, ET and auxin, but not via SA (Lahlali et al. 2014). The commercial product Prestop®, containing the biocontrol agent *Clonostachys rosea*, also reduced clubroot symptoms via induced host resistance to root hair and/or cortical infection through the phenylpropanoid pathway and JA and ET signaling, but not SA (Lahlali and Peng 2014). The fungus *Gliocladium catenulatum* may also be useful in reducing clubroot severity (Peng et al. 2011).

Initial plant trials with potential BCAs were all carried out under controlled environmental conditions, i.e., in a growth chamber or greenhouse, where not only the environment but also the inoculum density were rigorously controlled. In field-trials, the effect of BCAs is much harder to evaluate (Peng et al. 2014). Many of the current commercial BCAs, including Serenade® (*B. subtilis*), Prestop® (*C. rosea f. catenulate*), Mycostop® (*S. griseoviridis*), and RootShield® (*Trichoderma harzianum Rifai*), have still to be tested agaist *P. brassicae* infection (Peng et al. 2014).

1.6.3 Liming, pH, and Ca^{2+}

P. brassicae pathogenesis requires a slightly acidic soil, therefore, increasing the pH of the soil by liming is a recommended treatment to decrease disease development in the field (Dixon 2014). Higher calcium ion levels also directly affected *P. brassicae* growth and calcium cyanamide, which reduced resting spore germination and the motility of primary zoospores, was an effective soil treatment of *P. brassicae* infection and clubroot disease progression (Donald et al. 2004; Niwa et al. 2008; Dixon 2014). However, the current debate is to whether the reduction in clubroot symptom is a result of calcium cyanamide increasing the alkalinity of the soil or Ca^{2+} acting as a stress transducer (Lecourieux et al. 2006; Takahashi et al. 2002). The application of salts that simultaneously increase Ca^{2+} and pH had a stronger effect on reducing clubroot symptoms than salts that only raised the pH (Dixon 2014). Other studies have suggested that the Ca^{2+} and Mg^{2+} in lime have additional effects on disease control, independent of pH (Murakami et al. 2002). Alkaline pH, by itself, does not eliminate clubroot in the field if other conditions are still conducive for infection (Gossen et al. 2015). A soil treatment with boron slowed down the development of *P. brassicae* in root hairs and cortical cells as well as decreasing the incidence and severity of the disease on canola (*B. napus*) (Deora et al. 2011). In addition, fertilizer treatments can potentially alter soil microbe populations and diversity, some of which may be antagonistic to *P. brassicae*, resulting in an indirect beneficial effect of this treatment on biocontrol agents (Dixon 2014).

1.7 Statement of objectives

The overall goal of my research was to investigate the host plants-*P. brassicae* interactions during *P. brassicae* infection and clubroot disease development. *P. brassicae* pathotype 3 which is predominant in canola growing region in Western Cananda, was used to inoculate host plants Arabidopsis and canola grown in Petri dishes and soil in an controlled environmental conditions to study plant-pathogen interactions. The pathogen infection structures and host responses to the infection was evaluated to explore the mechanisms that govern the infection initiation and pathogenesis. However, many puzzles and mysteries still remain in the *P. brassicae* life cycle, which hinder the *P. brassicae*-plant host interactions, and a better understanding of *P. brassicae* infection cycle can facilitate identifying critical steps where pathogenesis is initiated and host resistance is switched on to interfere the pathogen development in resistant plants.

The objectives of the studies presented in this thesis was to better understand the *P. brassciae* infection cycle and clubroot disease progression during Arabidopsis-*P. brassciae* interaction, and to finally link this information with the recently published *P. brassicae* genome to develop an understanding of the molecular mechanisms that govern the pathogenesis of *P. brassicae* during its infection cycle. This was addressed through the following studies:

1) Develop a dual culture system to monitor the *P. brassicae* life cycle in Petri dishes.
2) Establish live cell imaging protocols for specifically labelling *P. brassicae* since there is currently no technology available for the transformation of this pathogen.
3) Visualize the *P. brassicae* life cycle using a combination of transmission electron microscopy and confocal microscopy.
4) Link the cellular biology of the *P. brassicae* infection cycle with the recently published *P. brassicae* genome to identify stage-specific gene markers and molecular mechanisms that govern pathogenesis.
5) Address a single question – Does the auxin transporter play a role in clubroot symptom development.

Chapter 2 Materials and Methods

2.1 Plant materials

Arabidopsis thaliana wild-type Col-0 was in the collections of the Bonham-Smith lab. The mutant lines *pin1*, *pin2*, *pin3*, *pin4*, *pin7* and *aux1* were obtained from the Arabidopsis Biological Resource Center (ABRC) and each were described on The Salk Institute Genomic Analysis Laboratory website: http://signal.salk.edu. The Arabidopsis accessions and mutants used in this study are summarized in Table 2.1. All mutant alleles were created in Arabidopsis ecotype Col-0 background, which was used as the wild type. Canola, *Brassica napus* cv. 'Westar' used in this study to maintain the pathogen and generate clubroot galls was kindly provided by Dr. Gary Peng (AAFC, SK, Canada).

2.2 Inoculum and inoculation

2.2.1 Pathogen strain and gall propagation

Inoculum was prepared from air-dried clubroot galls collected from infested canola fields in central Alberta and kindly provided by Dr. Gary Peng (AAFC, SK, Canada). The pathogen population from these collections may represent a mixture of pathotypes, but pathotype 3 would predominate (Strelkov et al. 2006, 2007). To extract resting spores, about 10 g of air-dried galls were soaked in 200 mL distilled water for 2 h to soften the tissue and then ground in a mortar and pestle. The resulting slurry was filtered through seven layers of cheesecloth and the spore concentration was estimated using a haemocytometer and adjusted to 5.0×10^7 spores/mL for use as inoculum.

Table 2.1 *Arabidopsis* auxin transporter mutant lines used in this study.

Gene	Accession No.	Mutant line	Insert position	Genotype	Mutagen	Source
PIN1	At1g73590	SALK_097144	5th exon	homozygous	T-DNA insertion	Salk Institute
		SALK_047843	intron	heterozygous	T-DNA insertion	Salk Institute
PIN2	At5g57090	SALK_102916	promoter	heterozygous	T-DNA insertion	Salk Institute
		SALK_054455	5 ' UTR	heterozygous	T-DNA insertion	Salk Institute
		SALK_087188	5 ' UTR	heterozygous	T-DNA insertion	Salk Institute
		SALK_122916	1st exon	homozygous	T-DNA insertion	Salk Institute
		SALK_144447	3rd exon	homozygous	T-DNA insertion	Salk Institute
		SALK_091142 (cs859601)	5th exon	homozygous	T-DNA insertion	Yuan et al. 2013
PIN3	At1g70940	SALK_005544 (CS9364; *pin3-5*)	5 ' UTR	homozygous	T-DNA insertion	Friml et al. 2003 Rakusovà et al. 2011
		SALK_036969	1st exon	heterozygous	T-DNA insertion	Salk Institute
		SALK_113246	1st exon	homozygous	T-DNA insertion	Salk Institute
		SALK_038609 (CS9363; *pin3-4*)	1st exon	homozygous	T-DNA insertion	Friml et al. 2003 Willige et al. 2013
PIN4	At2g01420	CS9368 (*pin4-3*)	3rd exon	homozygous	Transposon insertion	Guenot et al. 2012
PIN7	At1g23080	SALK_044687	3rd exon	homozygous	T-DNA insertion	Haga and Sakai 2012
		SALK_048791 (*pin7-101*)	1st exon	homozygous	T-DNA insertion	Haga and Sakai 2012 Willige et al. 2013
		SALK_062056 (*pin7-102*)	1st exon	heterozygous	T-DNA insertion	Willige et al. 2013
		SALK_112516	promoter	heterozygous	T-DNA insertion	Salk Institute
AUX1	At2g38120	CS8040 (*aux1-7;axr4-2*)			axr4-2: γ ray mutagen	Marchant et al. 2012

2.2.2 Establishment of callus culture

The callus culture system was established according to Bulman et al. (2011) with minor modifications. Canola seeds were sown in a soilless potting mixture consisting of fine peat moss, vermiculite, gypsum, dolomitic limestone and starter nutrient (Sunshine Mix #3; pH 5.8-6.2; Sun Gro Horticulture Canada Ltd., Canada) in 13 cm diameter plastic pots. Five-day-old canola seedlings were inoculated by pipetting 5 mL of 5.0×10^7 spores/mL resting spore suspension to the base of the seedling shoots, where it meets the soil ('pipette' method). Plants were grown at 22°C with a 16 h/8 h light/dark photoperiod of 675 μmol photons/s/m^2 in a growth chamber (Conviron, UAS) and watered with tap water adjusted to pH 6.3 with acetic acid. At 35 days post inoculation (dpi), large root galls were harvested for inoculum preparation.

Canola clubroot galls were harvested at 35 dpi. After washing thoroughly in tap water, the epidermal layer of the large root galls was peeled off and the galls were surface-sterilized with 70% ethanol for 1 min, 30% bleach with 0.05% tween (~1.4% sodium hypochlorite) for 20 min, followed by three washes in sterile distilled water. After washing, galls were cut into medium-sized sections of 2-3 cm in length, which were sterilized with 70% ethanol for 1 min, 2% chloramine-T (Sigma-Aldrich, Oakville, Canada) for 20 min, followed by three washes in sterile distilled water. After this second sterilization, the sections were cut into ~0.5 cm segments and were placed on a medium consisting of Gamborg B5 basal medium (Sigma-Aldrich, Oakville, Canada) plus 3% sucrose, 300 mg/L timentin (Gold Biotechnology, St. Louis, US), and 1.5% agar. Lateral root segments of non-inoculated plants were used as controls, because the mature main roots were inflexible and too difficult to cut into small segments.

After two weeks in the dark at 23°C, gall segments demonstrating callus growth on the cut edges were transferred to fresh medium minus timentin. At the same time, a thin piece of section was removed from each cultured segment, divided into two, with one half placed into Luria-Bertani (LB) liquid medium and the second half placed onto Potato Dextrose Agar (PDA) medium to confirm that the gall/callus section was free of any endophytic bacteria and fungi. These thin sections were observed for three days to confirm no bacterial or fungal growth. Endophytic microbe-free calli were used to inoculate host seedlings grown in Petri dishes.

2.2.3 Inoculation of canola and Arabidopsis grown in Petri dishes

To test if the resting spores of *P. brassicae* in induced calli remain infectious, both canola and Arabidopsis plants were inoculated with the resting spore suspension prepared from

uncontaminated callus tissues. Canola seeds were surface-sterilized for 1 min in 70% ethanol, followed by 20 min in 30% bleach and four washes in sterile water. Seeds were plated on half-strength MS medium (Sigma-Aldrich, Oakville, Canada) with 1% sucrose, 0.8% agar (plant cell culture-tested), pH 5.7-5.8 in 100×100×15 mm square Petri dishes (Fisher scientific, Ottawa, Canada) and stratified at 4°C for two days in darkness before being transferred to a growth chamber at 23°C with a 16 h/8 h, light/dark photoperiod (light intensity 120 µmol m^{-2} s^{1}). After four days, each seedling was inoculated with 400 µl of 5.0×10^{7} spores/mL resting spore suspension, freshly prepared from callus, by pipetting the suspension onto the roots. Petri dishes were sealed thoroughly with Parafilm (Sigma-Aldrich, Oakville, Canada) to maintain the internal environment and incubated vertically in the dark at 23°C. The inoculation procedure in Arabidopsis was similar with one difference. The time for bleach sterilization of the seeds was reduced to 5 min. The infection process was observed under transmitted light microscopy (AxioPlan; Zeiss).

2.2.4 Inoculation of Arabidopsis in soil and disease assessment

Arabidopsis wild type plants, Columbia-0 ecotype, were grown in small pots filled with professional growing mix soil (section 2.2.1). Each 12-day old seedling, at the two- to four-leaf rosette stage was inoculated with 500 µL of 5.0×10^{7} spores/mL resting spore suspension pipetted to the base of its stem where it met the soil. Three independent biological replicates (20-24 plants each replicate) were carried out at two different spore concentrations (5×10^{6} and 5×10^{7} spores/mL) for each mutant and Col-0 plants. Controls, mock-inoculated plants of the same age, were treated with 500 µL water instead of spore suspension.

Plants were evaluated for clubroot resistance at 21 dpi. The extent and severity of clubroot symptoms were assessed qualitatively on the basis of a disease index (DI) as described by Siemens et al. (2002) as well as Hatakeyama et al. (2013) with a small modification. Disease symptoms were scored on a scale: 0, no visible clubbing or swelling; 1, very small swellings confined to lateral roots that do not impair the main root; 2, small swellings covering the main root and a few lateral roots; 3, moderate swelling on lateral root and main root, but 1/3-2/3 of fine roots are still present; 4, severe swelling on all roots, fine roots completely destroyed, and 5, big club on main root and hypocotyl, leading to degradation of the root, plant growth is affected severely and plants are dying (Fig. 2.1). The disease index (DI) was calculated using this six-grade scale according to the formula:

$$DI = \frac{\Sigma[(\text{class No.})\,(\text{No. of plants in each class})]}{(\text{total No. plants per sample})\,(\text{No. class-1})} \times 100$$

Student's t-test was used for all statistical analysis. Error bars on all figures represent the standard error of the mean of three replicates.

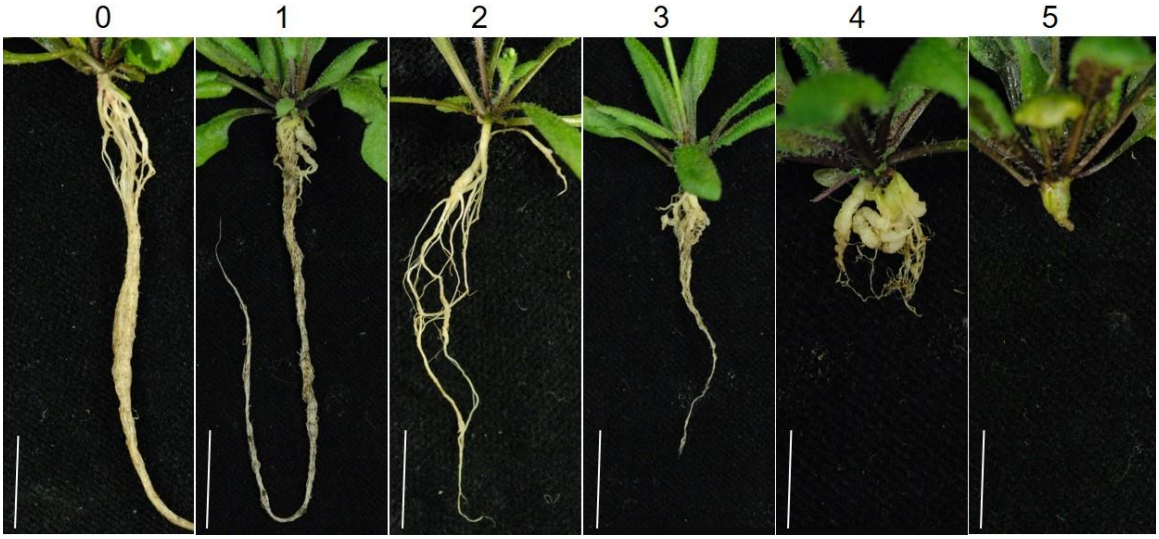

Figure 2.1 Typical root symptoms of *Arabidopsis* wild type (Col-0) inoculated with *P. brassicae*.

Disease responses were evaluated at 21 dpi. Root symptoms were graded as: class 0, no visible symptoms; class 1, very slight swelling confined to lateral roots that do not impair main root; class 2, slight swelling on lateral roots and a few later roots; class 3, moderate swelling on all roots 1/3-2/3 fine roots still remain; class 4, severe swelling on all roots, fine roots completely destroyed, and class 5, big club on main root and hypocotyl, leading to degradation of the root, plant growth is affected severely and plants are dying.
Scale bar indicates 1.0 cm.

2.3 Sample preparation for microscopy and gene expression analysis

To observe the *P. brassicae* life cycle and to link pathogen gene expression to the corresponding developmental stages and subsequently identify pathogen developmental stage specific molecular markers, Arabidopsis seedlings were inoculated, at the higher concentration of 5×10^7 spores/mL as described in section 2.2. In this way, the representation of pathogen mRNA in the early time point samples was increased. Mock-inoculated plants were treated with 500 µL water. All plants

were watered with all-purpose fertilizer once a week (Plant Products, 20-20-20 Plant Prod) as recommended by the manufacturer. Roots of inoculated and mock-inoculated Arabidopsis were sampled at 0, 2, 5, 7, 10, 14, 21, and 28 dpi. At early time points (0, 2, and 5 dpi), 24 plants were randomly selected for each treatment (inoculation and mock). At middle time points (7 and 10 dpi), 12 plants were randomly selected for each treatment and at later time points (14, 21 and 28dpi), four plants were randomly selected per treatment. Roots were washed with tap water, flash-frozen in liquid nitrogen and stored at -80ºC prior to RNA extraction. For microscopic observation of the life cycle, Arabidopsis roots of inoculated plants were also sampled at 0, 2, 5, 7, 10, 14, 21, and 28 dpi. Arabidopsis roots were harvested from soil, washed carefully with running water to remove as many soil particles as possible and stained with fluorescent dyes as described in the following section 2.4.

2.4 Microscopy techniques

2.4.1 Live cell staining of *P. brassicae*

During the first step axenic culture, a Nile red (9-diethylamino-5*H*-benzo[α]phenoxa phenoxazine-5-one, Sigma-Aldrich, Oakville, Canada) and calcofluor white (CFW, Sigma-Aldrich, Oakville, Canada) double staining technique was used to observe pathogen development in calli. Stock solutions of Nile red, 10 mg/mL in DMSO, were prepared. Calli were incubated in a final solution of 1 µg/mL Nile red, diluted in sterile water, for 10 min in the dark. After a wash with sterile water, calli were incubated in two drops of calcofluor white (CFW) (Sigma-Aldrich, Oakville, Canada) for 5 min in the dark following the supplier's procedure. After a wash with sterile water, calli were mounted on glass slides for observations.

During the second step axenic culture, double staining with Nile red and DAPI (4′,6-Diamidine-2′-phenylindole dihydrochloride, Sigma-Aldrich, Oakville, Canada) was used to distinguish pathogen structures from plant host organelles during the primary infection of Arabidopsis plants grown in Petri dishes. A 10 mg/mL stock solution of DAPI was prepared in methanol. At the appropriate time points, DAPI staining of inoculated Arabidopsis roots on a glass slide was carried out with a working solution of 1 µg/mL DAPI in sterilized distilled water for 20 min in the dark, followed by a wash with sterile water. Where appropriate, 1 µg/mL Nile red was added for 5 min and the roots were covered with coverslips for observation by confocal laser-scanning microscope (LSCM, Zeiss 510).

Double staining of the roots of soil-grown Arabidopsis was also carried out using Nile red or FM4-64 (Sigma-Aldrich, Oakville, Canada) and DAPI. A 10 mM stock solution of FM4-64 was prepared in DMSO. At the appropriate time-points, Arabidopsis roots were harvested from potting mixture and washed carefully with running water to remove soil particles. Infected roots were incubated in 1 μg/mL DAPI on a glass slid for 20 min at room temperature, washed three times with sterile water, followed by 1 μg/mL Nile red or 25 μM FM4-64 staining for 5 min prior to the roots being covered with coverslips. Images of stained roots were viewed and captured with LSCM (Zeiss 510).

2.4.2 Laser scanning confocal microscopy

Lipid detection through Nile red staining had previously used an excitation wavelength of 480-490 nm to identify neutral lipids and 510-560 nm to identify polar lipids. In this study, an excitation wavelength of 488 nm, with emission recorded with a 585-615 nm filter set, was used to observe neutral lipids. For polar lipids, an excitation wavelength of 543 nm was used, and emission recorded with a >650 nm filter set. For CFW and DAPI stained samples the excitation wavelength was 408 nm with emission measured between 420 and 480 nm. FM4-64 signals were detected using excitation/emission wavelengths of 488/>650 nm. All observations were obtained from at least three independent experiments. After acquisition, images were analyzed and processed with LSM Image Browser and Adobe Photoshop (Adobe Systems). Contrast and brightness levels were optimized.

2.4.3 Transmission electron microscopy

Infected Arabidopsis roots for life cyle observation were sampled at 7, 10, 14, 21 and 24 dpi. Material was fixed in a freshly prepared solution of 2% glutaraldehyde (SPI supplies, West Cheste, USA), in 0.1 M phosphate buffer (PB) at pH 7.4, overnight at room temperature, washed three times in fresh PB for 30 mins each and post-fixed for 4 h in 1% osmium tetroxide (SPI supplies, West Cheste, USA) freshly prepared in 0.1 M PB. After three washes in distilled water for 30 mins each, the tissue was dehydrated with a gradient series of ethanol (25%, 50%, 75%, 95%, 100%) and left overnight in 100% ethanol. After dehydration, samples were incubated twice in Propylene oxide (SPI supplies, West Cheste, USA) for 8-12 h each time and then embedded in Epon 812 resin (SPI supplies, West Cheste, USA) by increasing serial changes (8 h each) of mix with propylene

oxide 1:2, 1:1, 2:1 and eventually 100% resin overnight. Finally, samples were embedded in a mold in 100% resin and incubated at 60°C for 72 h for polymerization.

Ultra-thin sections (60 nm) were cut with a Microstar diamond knife (Huntsville, US) on a Reichert-Jung microtome (Reichert microscopic service, Depew, US) and captured onto single slot copper grids coated with Formvar or 100 naked mesh copper grids. The sections were post-stained with 2% uranyl acetate for 30 min in the dark and Reynold's lead citrate solution for 10 min prior to being observed with a Hitachi HT7700 transmission electron microscopy.

2.5 *P. brassicae* sequence analysis and primer design

Literature on meiosis tool kit (Ramesh et al. 2005; Schurko and Logsdon 2008; Weedall and Hall 2015) and keyword searches of the National Center for Biotechnology Information (NCBI) protein database identified 29 meiosis-related proteins and nine meiosis-specific protein orthologs from various eukaryotic organisms. The nine meiosis-specific protein sequences (amino acid and nucleotide) were used as queries for BLASTp and tBLASTn searches of the NCBI non-redundant protein and nucleotide collection database against the *P. brassicae* genome (https://blast.ncbi.nlm.nih.gov/Blast) and the *P. brassicae* genomic database (http://protists.ensembl.org/Plasmodiophora_brassicae/ Info/Index) for the identification of *P. brassicae* orthologous sequences. Putative *P. brassicae* orthologues of meiosis specific gene sequences were retrieved. Based on the gene sequences, RT-PCR primers were designed using ApE software and primer specificity was checked with primer-BLAST searches against the Arabidopsis Refseq mRNA database (http://www.arabidopsis.org/).

2.6 RNA isolation and RT-PCR assays of *P. brassicae* genes

Total RNA was isolated from root tissues of inoculated and mock-inoculated Arabidopsis seedlings harvested from different time points (0, 2, 5, 7, 10, 14, 21 and 28 dpi) following the procedure of Missihoun et al. (2011). Final concentration of total RNA was determine using a Thermo Scientific ND-1000 Nano Drop spectrophotometer. The quality of the RNA was verified by optical density (OD) absorption ratio OD_{260nm}/OD_{280nm} between 1.80 and 2.11 and OD_{260nm}/OD_{230nm} ranging from 2.00 to 2.48 and the integrity of the RNA was evaluated by gel electrophoresis. cDNA was generated from 1µg of total RNA using the QuantiTect Reverse Transcription Kit (Qiagen, Mississauga, Canada) according to the manufacturer's instructions.

For *P. brassicae* gene expression analysis, semi-quantitative RT-PCRs were carried out using primers specific for each gene (Table 2.2). Amplification of constitutively expressed *RIBOSOME PROTEIN S17* and *ACTIN1* genes from *P. brassicae* and *ACTIN7* gene from Arabidopsis were used as loading and RT controls. *P. brassicae* gene primers were tested for specificity to the *P. brassicae* genome, rather than other soil microorganisms or plant host tissues, in the cDNA from mock-inoculated root samples. Due to the low representation of pathogen biomass in the early time points samples, semiquantitative RT-PCR assays were conducted to test the expression of selected pathogen genes at plateau stage for 36 cycles. PCR products were visualized after electrophoresis on 1% agarose gels and staining with ethidium bromide.

Table 2.2 Primers for analysis of *P. brassicae* gene expression.

Accession No.	Gene name	Primer sequence (5' - 3')	Tm (°C)	PCR amplicon (bp)
AT5G09810	*AtACTIN7*	F: CATACATGGCAGGGACATTGA	60	562
		R: ACTCGTTTCGCTTTCCTTAGTG	60	
AY452179	*PbACTIN1*	F: AGCTGGCGTACGTGGCGCAG	70	342
		R: CCTTGACGCGCATCGACGAC	65	
AF539801	*PbCC249*	F: TACGCAGGAGTAGGGGACTC	59	274
		R: GTTGATGAGGTCGCCATTGT	61	
AJ605576	*PbCC243*	F: CCGGGCAGGTACTAAGATGT	50	200
		R: GGTACGCGGGGTATATTTAATG	45	
PBRA_008131	*SPO11*	F: TCGACGAACAGATTATGACGTGC	61	462
		R: TGCACGGCCATCATCGAAAC	61	
PBRA_002842	*MND1*	F: AATGGTCTTGGCATTGCTCTC	59	462
		R: ACCTATTCGTTTCCGCAGGTC	60	
PBRA_001543	*HOP1*	F: ATGCGTCAGAAGGTCGAGGAACAG	64	453
		R: AACCTGGGTTGCTTCCTTCCTG	62	
PBRA_000515	*HOP2*	F: TTTCGATGCCGAGACGTTCCTG	63	563
		R: TACATCTGGTGGTGGCAGGTTAG	62	
PBRA_008811	*RAD21-1*	F: ATGGCAAAGTCGAAGTCCAG	58	478
		R: TCTTCTCGTCGCTGCTGTTC	60	
PBRA_002411	*RAD21-2*	F: TGCAGTTTGATGGTGGAGATCG	61	355
		R: AAATCATCATCACCACCGGCAG	61	
PBRA_007671	*RAD51-1*	F: TTATCACAGGCAGGTCGCTATC	60	283
		R: AATTATGGGAGTGGCTGTGCATC	61	
PBRA_000359	*RAD51-2*	F: TTGCCTATGTAAACGGCTTCACC	61	316
		R: TCGAGTGCATCATTAGCCTGTG	61	
PBRA_002628	*RAD51-3*	F: AAGCGTTCCTGATGGGTTTCG	61	583
		R: ACACAAATGCGATGCTCACG	60	
PBRA_000023	*RAD51-4*	F: AATGGAGGAGGACAAGGCAAG	60	506
		R: TGAGGTAGCAAAGAGACGGAATG	60	
PBRA_001343	*RAD51-5*	F: TTACGATGATCGGTGTTGTGTG	59	461
		R: TTTCCCTGCTGACATCCATCG	60	
PBRA_000211	*RAD51-6*	F: ATGCGGCCTACAAGATCATCGAC	63	313
		R: TCCTCACAGCATCAAGCCCAAAC	63	
PBRA_000929	*RAD51-7*	F: AGCCTTTGTTATGTTGTGCGTC	60	503
		R: TGAGCGACACCATTTAGCAG	58	
PBRA_009486	*MSH4*	F: ATTGCCCTGCTCGATATGATCGTC	62	601
		R: TTCGTCAATCAGGACAAGGCTGG	63	
PBRA_002186	*MSH5*	F: ACGAATGCAGACACTTGCTGG	62	601
		R: ACCAGTAAGGAAGATGGGCTCG	63	

Table 2.2 cont.

Accession No.	Gene name	Primer sequence (5' - 3')	Tm (°C)	PCR amplicon (bp)
PBRA_001485	*MSH2*	F: TCATTGATGAGCTGGGAAGAGG	62	558
		R: TTATGCAGAGAGCAACGTGGAG	61	
PBRA_005360	*MSH6*	F: TCGAACTGTTTCGCCATTGCTTCC	64	738
		R: ACTCTACTCCGGCAAACCTGTC	62	
PBRA_000197	*MER3-1*	F: TTCCTGGTGTTGATTCCTGACG	60	430
		R: ACAGCGTCTTTGGGACCTCATTAG	62	
PBRA_008782	*MER3-2*	F: TGTCGCAGATGGTGATCCAG	60	512
		R: ATGCACGATCAGACGAAACAGG	61	
PBRA_006359	*MER3-3*	F: TAAAGGGTGGAGGTTGACACCAAG	62	642
		R: TCACAAAGAACAGTAAGGCAGCAC	62	
PBRA_000175	*SPEF2*	F: ATTGCCTTTGTGTCCCTGCTG	62	430
		R: TCACAAACGACCCGAACTTGG	62	
PBRA_000434	*IFT172*	F: TGCAACAAGTTCCCGTCAAAGTC	62	526
		R: ATGCGAAGCTCACGAACTGATGG	63	

2.7 Screening the Arabidopsis auxin transporter mutant lines

Homozygous SALK T-DNA insertion lines (ABRC) were genotyped by PCR using gene specific primers (Table 2.3) and a T-DNA left border primer, 5′-ATTTTGCCGATTTCGGAAC-3′, as described by Krysan et al. (1999). For transposon insertion lines, the exact insertion sites were confirmed using gene-specific primers and the primer annealing at the insertion borders, 5'-TGCAGCAAAACCCACACTTTTACTTC-3', as described by Guenot et al. (2012), which also enabled PCR-based genotyping of homozygous lines. Knockout confirmation of homozygous lines was carried out by semi-quantitative RT-PCR and/or mutant phenotyping. Primers used for semi-quantitative RT-PCR to comfirm lack of expression in homozygous mutants were as follows:

PIN4: forward primer: 5-TAGTGGAGAGGGAGAAAGAGAG-3

reverse primer: 5-TCACCTTCCACTCTTTCCCAC-3;

PIN7: forward primer: 5-ACTCCTCGTCCGTCTAATCTC-3

reverse primer: 5-TACCCTCTCCGACTCTTCTTC-3.

Table 2.3 Gene specific primers for confirmation of homozygosity of auxin transporter mutant lines in *Arabidopsis*.

Gene	Accession No.	Mutant line	Primer sequence (5' - 3')
PIN1	At1g73590	SALK_097144	F: AACTGGCTTCACAGCAGAAAG R: TCAACAAAAAGGGCATTGTTC
		SALK_047843	F: TGATCGAAAAGATCCAAACTTG R: TGCCATTGAACTTTAAAACCG
PIN2	At5g57090	SALK_102916	F: TAAGGTGTTCGATGAATTGCC R: GGTCCATAATTTTTCGAAGTGC
		SALK_054455	F: CCAATTGCCAATGTCTTTGAC R: CATTGGTCCGGTGTGAATATC
		SALK_087188	The same primers for SALK_054455
		SALK_122916	F: GCAAAAAGGAATCCCAAAATG R: TTCAAATGTCCAACGATCCTC
		SALK_144447	F: AAAAACCTAAGAGTTTTGGAAGTG R: TTTGTTCAAATTAACGGACCG
		SALK_091142 (CS859601)	F: TATGGTCAGTTCCGTCGTACC R: AACCCTGCTACTGATTTTCCG
PIN3	At1g70940	SALK_005544 (CS9364; pin3-5)	F: CCCATCCCCAAAAGTAGAGTG R: ATGATACACTGGAGGACGACG
		SALK_036969	The same primers for SALK_005544
		SALK_113246	F: TGCCACCTTCAATTCAAAAAC R: TGATTTTCTTGAGACCGATGC
		SALK_038609 (CS9363; pin3-4)	The same primers for SALK_113246
PIN4	At2g01420	CS9368 (pin4-3)	F: CAACGCCGTTAAATATGG R: TTCCCACTACAATTATTCC
PIN7	At1g23080	SALK_044687 (CS859789)	F: CTCTTTTGCAAACACAAACGG R: GGTAAAGGAAGTGCCTAACGG
		SALK_048791	F: TGGTACATAAATTAGGGGAAAGC R: TACCACCACCACCGTAAAAAG
		SALK_062056 (CS174830)	F: CGTTAGGCACTTCCTTTACCC R: TTCTCACCAGACCAATGTTCC
		SALK_112516	F: TCGTGCCATGTGATCATATTG R: CCGACAACAACAACGAAAAAC

2.8 Gravitropic and hypocotyl phototropic bending

Arabidopsis wild type (Col-0) and mutant seeds were surface-sterilized with 70% ethanol for 1 min and then for 5 min in 30% bleach. Seeds were washed three times with sterile water and plated on 100×100×15 mm square Petri dishes (Fisher scientific, Ottawa, Canada) containing half Murashige and Skoog (MS) medium, 1% sucrose, 0.8% agar (plant cell culture-tested), pH 5.7-5.8. Plates were sealed with Parafilm to prevent evaporation and incubated at 4°C for two days before transfering to a growth chamber at 22°C, 16 h day/8 h night, light intensity 120 µmol m^{-2} s^{1}. After seven days, seedlings were placed in a laminar flow hood with light from above. All plates were re-oriented clockwise by 90° for 12 h after which the gravitropic response of the roots was recorded. Root gravitropism assays were used to screen for homozygous *pin2* plants and lines with homozygous *pin2* alleles after crossing.

For hypocotyl phototropic bending experiments, plates of seeds were covered with aluminum foil to keep out the light. Four-day-old etiolated seedlings were exposed to low-intensity unilateral white light (fluorescent lamps) at room temperature for 12 h after which the hypocotyl phototropic response was recorded, as described by Ding et al. (2011). Hypocotyl phototropic beeding assays were used to screen for homozygous *pin3* plants and lines with homozygous *pin3* alleles after crossing.

Chapter 3 A Two-Step Axenic Culture System with Live Cell Staining for Studying the Early Infection of Arabidopsis with *Plasmodiophora brassicae*

3.1 Abstract

Plasmodiophora brassicae, a parasitic protist, induces club-shaped tumor-like growth of host Brassica roots and hypocotyls after infection. Due to its soil-borne nature, the biology of infection and early pathogenesis, especially during the primary infection stages, is difficult to observe. In this study, a new protocol, based on a two-step dual culture of *P. brassicae* with its hosts has been established, for easy and early observations *in vivo*. Firstly, *P. brassicae* was co-cultured with canola on growth-medium plates enabling the propagation of *P. brassicae* to provide pure inoculum and secondly, the pure inoculum was subsequently used for pathogenicity tests on both canola and Arabidopsis seedlings grown in Petri dishes. During the first dual culture process, a staining protocol by which the pathogen was fluorescently labeled with Nile red and calcofluor white was established, thus allowing *in planta* observation of pathogen development. In the pathogenicity assays, the results in this study showed that axenic cultures of *P. brassicae*, in calli, remains fully virulent and completes its life cycle in roots of both canola and Arabidopsis grown in Petri dishes. Combining the dual culture procedure with Nile red and DAPI staining I showed that primary plasmodia are uninucleate rather than multinucleate and contain lipid droplets. To conclude, the protocol established in this study is an improved procedure for investigating the early infection process of *P. brassicae* and its host plants.

3.2 Introduction

Clubroot, caused by the soil-borne obligate endo-parasite *Plasmodiophora brassicae*, is a serious, worldwide disease of the Brassicaceae. Infection by *P. brassicae* and subsequent disease progression, results in a transformation of the host root, at the site of infection, into a tumorous tissue, often restricting the uptake of water and nutrients. The above ground tissues become stunted, turn yellow, and often pre-ripen, resulting in significant yield and quality losses, accounting for a 10-15% yield reduction on a global scale in a susceptible crop (Dixon 2009). *P. brassicae* has three distinct stages to its life cycle: survival in soil as resting spores, primary infection of root hairs or occasionally an epidermal cell, where primary plasmodia, zoosporangia and secondary zoospores are formed, and secondary infection resulting from released secondary zoospores developing into multinucleate secondary plasmodia in the cortex and stele, resulting in cell hypertrophy and hyperplasy of the root (Kageyama and Asano 2009). During the secondary infection stages, the formation of galls resulting from pronounced cell enlargement and cell proliferation, is driven by substantial fluxes in phytohormone levels (Devos et al. 2005). Finally, cleavage of a secondary plasmodium produces numerous resting spores that are released into the soil, through infected tissue decay, where they can survive up to 20 years (Kageyama and Asano 2009). Although much effort has been expended to understand the infection process, many aspects of the *P. brassicae* life cycle still have to be elucidate.

Many studies on host plant-*P. brassicae* interactions have been performed under artificial conditions in growth chambers and greenhouses e.g., flooding potting mix with resting spore suspensions (Sharma et al. 2011a), growing the plant host in slurries of resting spores (Hwang et al. 2011) and using sand-liquid culture (e.g. Agarwal et al. 2009; Sharma et al. 2011b). However, observations of the infection process, especially during the early stages of infection and disease establishment, have proven difficult due to adherent soil and sand particles not easily removed by washing, subsequent root hair damage during root sample preparation and the presence of soil-borne bacterial, fungi and oomycetes on and/or inside host tissues, increasing the complexity of this system for elucidating the disease cycle. As well as inoculation in soil and sand, several so-called *in vitro* systems such as callus culture (Dekhuijzen 1975; Takahashi et al. 2001), hairy root cultures induced by bacteria (Asano et al. 2000 and 2006), suspension cultures (Asano and Kageyama 2006) and adventitious root culture (Takahashi et al. 2006) have failed to provide an

adequate system for the observation of the complete *P. brassicae* life cycle. The majority of this work used *B. napus* or *B. rapa* as the host species.

A. thaliana is a member of the family *Brassicaceae* that is host of *P. brassicae.* Its small physical size and short-generation time provide a potential model system for studying the pathogen life cycle, the infection process, the development of resistance and the response to infection in this host plant that is closely related to economically important crop plants such as turnip, cabbage, broccoli, and canola. Various histological methods have been used to study the *P. brassicae*-host plant interaction (Schuller and Ludwig-Müller 2016), but routine techniques for reliably differentiating between pathogen and host tissues are lacking, and in most cases selective staining of pathogenic structures has not been achieved. In some instances, pathogen structures have possibly been misidentified as host organelles or other soil microorganisms such as root pathogen oomycetes (Asano et al. 2000; Takahashi et al. 2006; Donald and Porter 2004; Sharma et al. 2011b; Hwang et al. 2011; Fei et al. 2016). Although the 24 Mb genome of *P. brassicae* was recently sequenced (Schwelm et al. 2015; Rolfe et al. 2016), allowing for the fluorescent tagging of pathogen proteins, the viewing of pathogen structures using these reporter genes, within host cells, is still very difficult. To differentiate *P. brassicae* structures from plant cell organelles and to remove soil microorganism contamination that can further confuse these observations, we have established a dual culture system and a live-cell imaging protocol, using fluorescent dyes, that specifically stain *P. brassicae* structures during the pathogen life cycle.

Electron-dense lipid droplets have been identified in *P. brassicae* secondary plasmodia and resting spores (William and McNabola 1967; Deora et al. 2013). These lipid droplets have a core of neutral lipids, mainly triacylglycerol (TAG) and sterol esters, which may act as substrates for energy metabolism, membrane synthesis, and the production of essential lipid-derived molecules. Nile red (9-diethylamino-5H-benzo[a]phenoxazine-5-one) is a hydrophobic and metachromatic dye with poor solubility and fluorescence in water and color emission varying from deep red to strong yellow gold in hydrophobic environments (Rumin et al. 2015). It has been successfully used to stain intracellular neutral lipids, such as sterol esters and oil bodies in Arabidopsis leaves and seeds with coupled wavelengths of 488/550-650 nm (Kopischke et al. 2013; Miquel et al. 2014). The detection of nonpolar lipid (excitation at 514 nm, emission at 520-560 nm) and polar lipid (excitation at 534 nm, emission at 600-700 nm) has been achieved with Nile red in Arabidopsis roots (Li et al. 2015). With an excitation at 488 nm and emission at 565-585 nm, Nile red has also

identified intracellular neutral lipid, predominantly triacylglycerol (TAG) in yeast and fungi (Kimura et al. 2004). In addition, using excitation/emission wavelengths of 554/605-623 nm, Nile red selectively identified cholesterol and lipid in the outer leaflet of bio-membranes (Kucherak et al. 2010) and has been used to study membrane heterogeneity at 570 nm excitation and 610 nm emission wavelengths (Ira 2001). Nile red has been widely and successfully used as a fluorescence probe for the semi-quantification measurement of lipid in microalgae using the two wavelength sets 480-490/570-625 nm or 530-560/575-615 nm (Simionato et al. 2011; Rumin et al. 2015). Also in microalgae, using wavelength sets of 488/580nm and 488/610nm, it has been used to estimate neutral and polar lipid fractions, respectively, by means of flow cytometry (Guzmán et al. 2010, 2011). In *Crypthecodinium cohnii,* a similar lipid analysis was carried out using wavelength sets of 488/560-640 nm for neutral lipids and 488/ >650 nm for polar lipids (De la Jara et al. 2003). In conclusion, short excitation wavelengths of 450 to 500 nm and yellow/gold emission wavelengths of ≤580 nm favor the detection of highly hydrophobic environments like neutral lipids whereas longer excitation wavelengths of 515 to 560 nm and red emission wavelengths of ≥590 nm favor a general fluorescence for polar lipids associated with membrane phospholipids. Here, we compared Nile red staining with the two sets of excitation and emission wavelengths 488/585-615 nm and 543/>650 nm for its ability to detect the intracellular lipid droplets of *P. brassicae.*

In this study, a two-step dual culture protocol has been established to obtain pure inoculum from canola galls and to use this inoculum to infect both canola and Arabidopsis on growth-medium plates to enable the observation of early infection stages during the life cycle of *P. brassicae*. I aimed to i) produce purified inoculum from canola galls; ii) establish live cell imaging using confocal microscopy by labeling the pathogen with fluorescent dyes; iii) provide protocols for the easy and early observations of the pathogen life cycle in the model plant, Arabidopsis. This is the first report of an *in vivo* culture system on growth-medium plates using an intact host plant for *P. brassicae* and will be a valuable tool for the future study of complex host-pathogen interactions at early infection stages.

3.3 Results

3.3.1 Dual culture of callus harbouring pure *P. brassicae*

To prevent other soilborne microorganisms from confusing the observation of the *P. brassicae* life cycle in *B. napus*, a modified Bulman dual culture system was established, taking care to remove all possible contaminating microorganism (Bulman et al. 2011). Five days after culture, even in the presence of 300 mg/L Timentin, some of the surface-sterilized sections of *B. napus* clubroot galls demonstrated either bacterial or fungal containmination on growth medium plates. However, non-inoculated *B. napus* lateral roots used as mock control show no contamination. Uncontaminated gall segments were transferred to fresh antibiotic medium. After a further two weeks of culture it became apparent that these transferred gall segments were free of obvious contamination. Abundant white/yellowish calli formed at the cut edge of the gall segments whereas the non-inoculated *B. napus* lateral roots did not produce calli (Fig. 3.1).

After two weeks culture on Gamborg B5 basal medium with antibiotics, uncontaminated calli were transferred to fresh B5 plates without antibiotics, and at the same time thin sections were cut from each callus and transferred to fresh liquid LB medium and solid PDA medium to double check whether calli were indeed free of contaminating bacteria and fungi. Approximately 25% of these calli-producing segments showing no contamination on antibiotic medium, were now discarded due to bacterial and fungi infection. Calli without further contamination were used in further inoculation experiments.

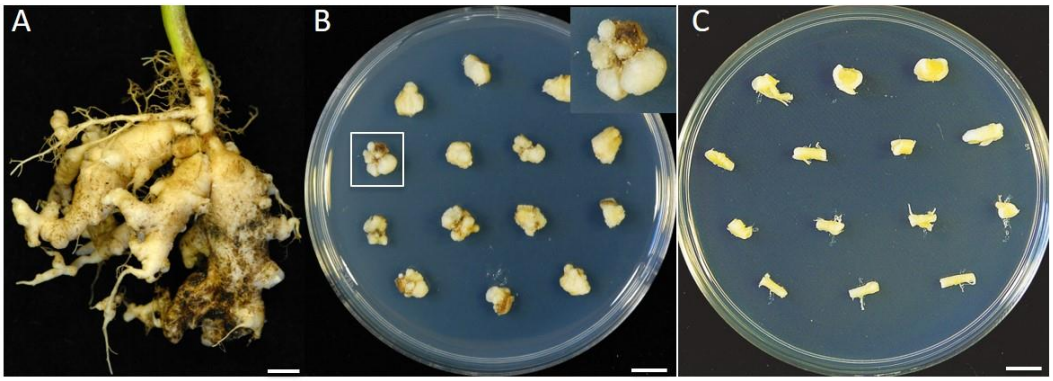

Figure 3.1 First step culture of canola clubroot gall segments on Gamborg B5 basal medium.

(A) Canola clubroot gall harvested 35 days post inoculation (dpi).
(B) Calli formed on the surface of clubroot gall segments after two weeks of culture on Gamborg B5 plates. Image on top corner is the higher magnification view of the boxed area.
(C) Un-inoculated canola roots cultured on Gamborg B5 plates for two weeks. Note that calli did not form on the surfaces of these canola root segments
Scale bars: 1 cm.

3.3.2 Optimization of intracellular lipid droplets staining with Nile red

To observe *P. brassicae* developmental stages in *B. napus* callus tissue, we employed the two fluorescence probes, Nile red and calcofluor white (CFW). Nile red, a lipophilic fluorescent marker, has been used to stain intra-cellular lipid droplets, abundant in secondary plasmodia and resting spores for TEM (William and McNabola 1967, Deora, et al. 2013). To develop an applicable staining method, optimization of the Nile red staining for fluorescent targets of lipids was studied. CFW, which selectively binds to β1-3 and β1-4 polysaccharides such as those found in cellulose and chitin, was used to label chitin in the cell walls of mature resting spores (Moxham and Buczacki 1983). Under light microscopy, the observed morphology of secondary plasmodia and resting spores in infected callus cells, were each similar to that observed in infected canola galls from soil. The abundant intracellular lipid droplets in secondary plasmodia (Fig. 3.2, top panels) and immature resting spores (Fig. 3.3, top panels) were readily observed after staining with Nile red and using an excitation/emission wavelength set of 488/585-615 nm rather than wavelengths 543/>650 nm. Using a 543/>650 nm wavelength set, the plasma membranes of host cells (Fig. 3.2 and Fig. 3.3, bottom panels) and cell membranes of mature resting spores (Fig. 3.4, bottom panel) were observed, but no intracellular lipid droplets were observed in either secondary plasmodia or

resting spores (Fig. 3.2, Fig. 3.3 and Fig. 3.4, bottom panels).

When viewed with either wavelength set, intracellular lipid droplets could not be observed in mature resting spores after Nile red staining (Fig. 3.4), even though lipid droplets were apparent in mature resting spores by TEM (William and McNabola, 1967 and our unpublished data). Using the wavelength set 543/>650 nm, cell membranes of mature resting spores were observed after Nile red staining (Fig. 3.4, bottom panel). The ability to differentially observe the membranes of immature and mature resting spores by Nile red, using the wavelength set 543/>650 nm, suggests that there is a change in membrane lipid composition during resting spore maturation. Both mature resting spore walls and host cell walls stained with CFW (blue colour) were observed at 420-480 nm after excitation at 408 nm.

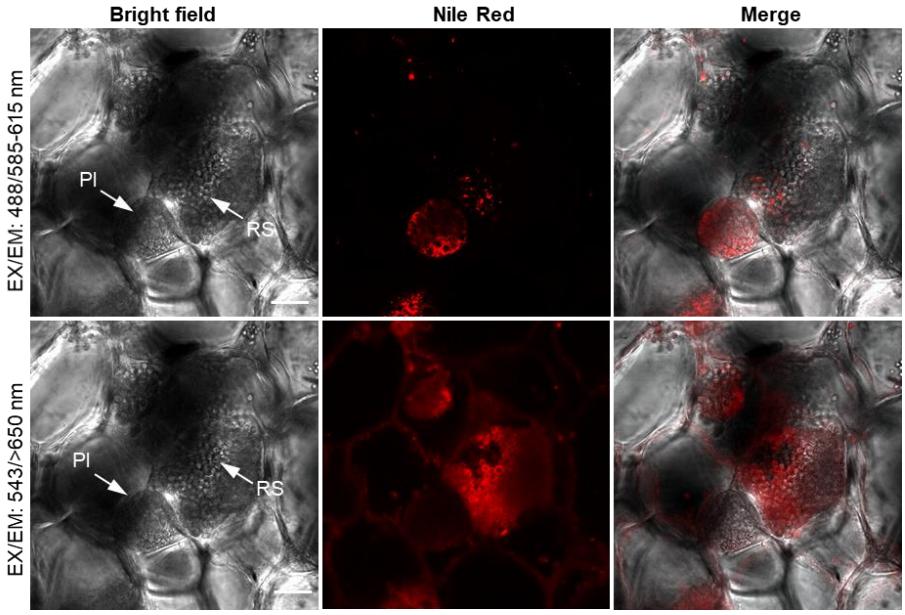

Figure 3.2 A secondary plasmodium and resting spores in the same callus cells induced from canola gall segments.

(A) Intracellular lipid droplets in secondary plasmodium stained with Nile red were observed at 585 to 615 nm after excitation at 488 nm.
(B) Membranes of resting spores and the infected host cells stained with Nile red were observed with the alternative wavelengths >650 nm after excitation at 543 nm.
PL, secondary plasmodium; RS, resting spores. scale bar: 20 μm.

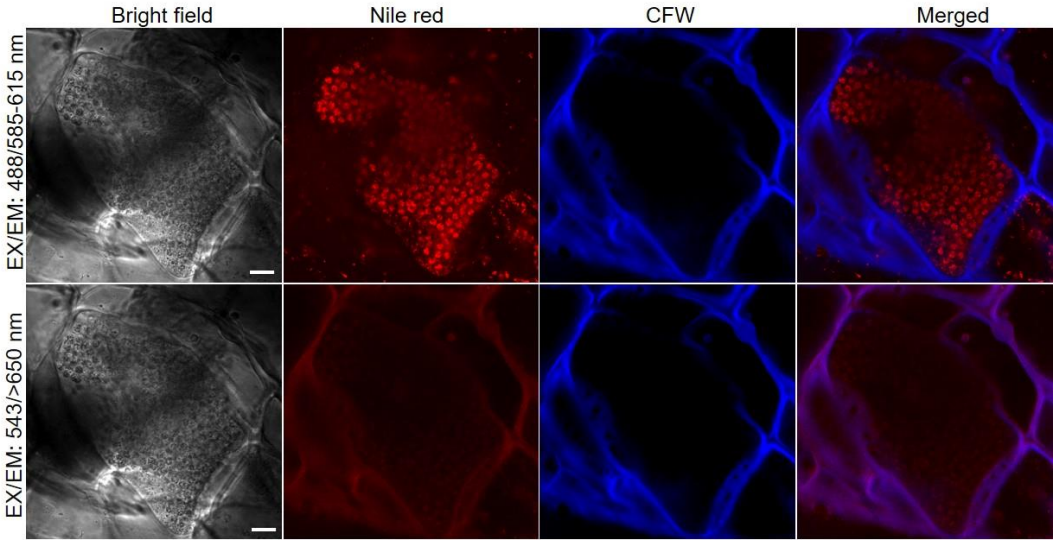

Figure 3.3 Immature resting spores in callus cell of infected canola segments.

(A) Intracellular lipids of immature resting spores stained with Nile red were observed at emission 585-615 nm after excitation at 488nm (red colour).
(B) Membranes of callus cells stained with Nile red were observed at >650 nm after excitation at 543 nm (red colour).
Notes that the host cell walls stained with CFW (blue colour) were observed at 420-480 nm after excitation at 408 nm. Scale bars: 10 µm.

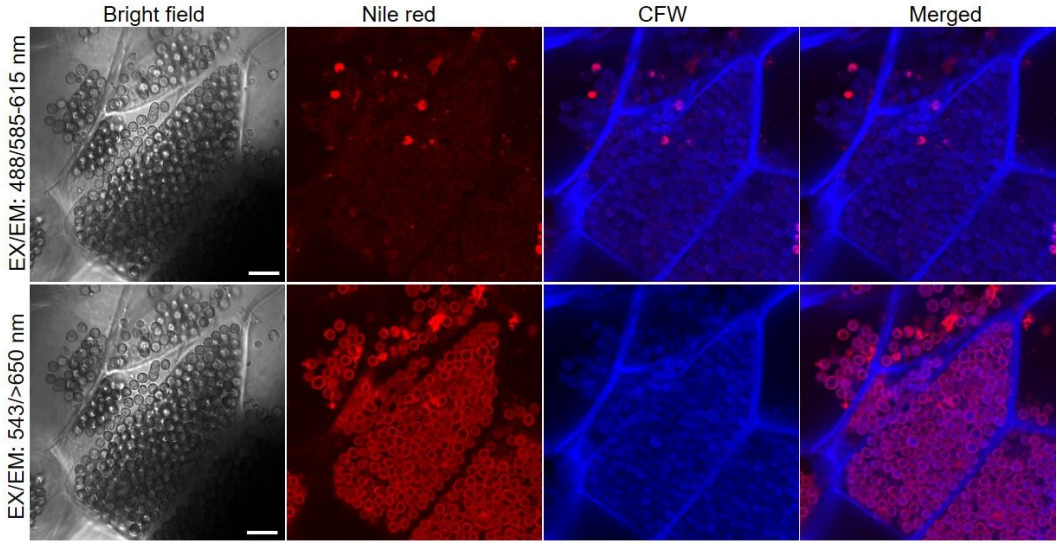

Figure 3.4 Mature resting spores in callus cell of infected canola gall segments.

(A) Mature resting spores stained with Nile red were observed at emission wavelength 585-615 nm after excitation at 488 nm. Note the lack of Nile red staining of lipid droplets in the mature resting spores.
(B) Cell membranes of resting spores stained with Nile red were observed at >650 nm after excitation at 543 nm (red colour). Note membranes of callus cell with mature resting spores lack Nile red staining. Scale bars: 10 µm.

To confirm the Nile red staining pattern for the pathogen in callus cells was not an artifact of the tissue culture process we observed the staining pattern of resting spores in *P. brassicae* infected Arabidopsis root tissue harvested from soil. The intracellular lipid droplets of immature and mature resting spores were observed after Nile red staining with a wavelength set of 488/585-615 nm (Fig. 3.5, top panel). Like immature resting spores in callus cells, the plasma membrane of immature resting spores in soil-grown galls could not be detected using the 543/>650 nm wavelength set, however the cell membranes of mature resting spores were observed (Fig. 3.5, bottom panel). Why intracellular lipid droplets of mature resting spores in infected Arabidopsis roots showed a different Nile red staining with the wavelength set 488/585-615 nm compared with mature resting spores in infected canola calli is unclear. In conclusion, the confocal microscopy imaging protocol for Nile red stained intracellular lipid droplets of *P. brassicae* was optimized at a wavelength set of 488/585-615 nm. In both infected callus cells (Fig. 3.3 and Fig.3.4) and Arabidopsis cells (Fig. 3.5), immature resting spores and mature resting spores were differentiated by CFW staining of cell wall deposition during resting spore maturation. This observation demonstrates the completion of the *P. brassicae* life cycle in callus cells.

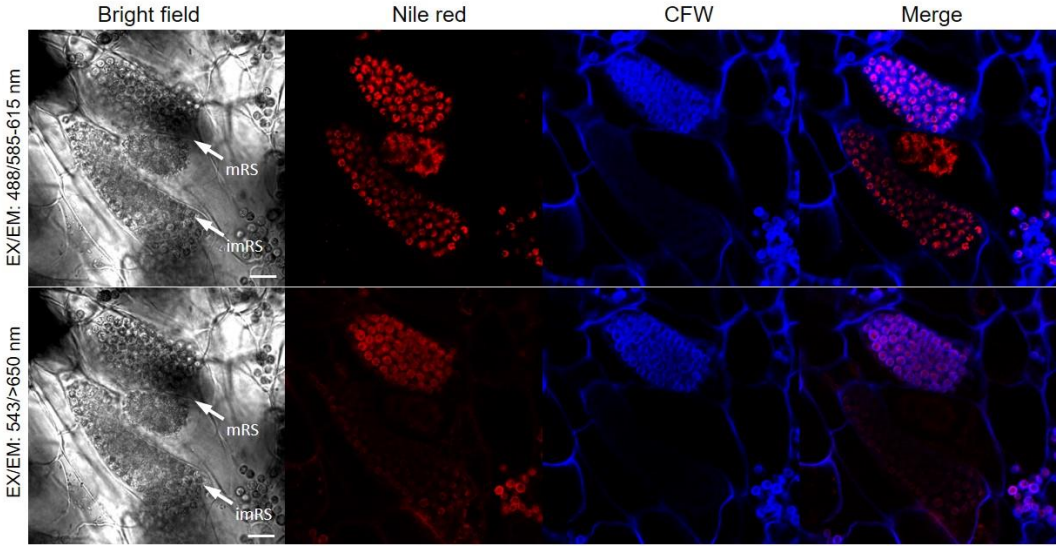

Figure 3.5 Resting spores in infected *Arabidopsis* root grown in soil at 28 dpi.

(A) Intracellular lipid droplets of both immature and mature resting spores stained with Nile red were observed at 585 to 615 nm after excitation at 488 nm.
(B) Cell membranes of mature resting spores observed at >650 nm after excitation at 543 nm. Both mature resting spore walls and host cell walls stained with CFW (blue colour) were observed at 420-480 nm after excitation at 408 nm.
imRS: immature resting spores; mRS: mature resting spores; Scale bars: 10 µm.

3.3.3 Infectivity of callus-grown *P. brassicae* mature resting spores

Resting spore suspensions of *P. brassicae* from calli were used to infect Arabidopsis seedlings growing in Petri dishes and proliferation of the pathogen was observed by microscopy. With a high inoculation pressure (5×10^7 to 10^8 spores/ mL), Arabidopsis epidermal cells of the root elongation zone were filled with multiple primary plasmodia at three dpi (Fig. 3.6), and inoculated Arabidopsis roots were shorter than control roots. *P. brassicae* primary plasmodia were spherical, approximately 5 μm in diameter and showed identical morphology in both infected Arabidopsis and canola roots grown in soil (unpublished data). To confirm these spherical structures as pathogen rather than host cell organelles, infected Arabidopsis roots were double stained with Nile red and DAPI. Nile red stained intracellular lipid droplets were observed at 585-615 nm after excitation at 488 nm (Fig. 3.6, top panel), whereas the endomembranes of primary plasmodia were observed at >650 nm after excitation with 543 nm (Fig. 3.6, bottom panel). The nucleus of each primary plasmodium was fluorescently labeled blue with DAPI, indicating primary plasmodia were uninucleate rather than multinucleate as previously reported (Kageyama and Asano 2009) (Fig. 3.6). Like other eukaryotic cells, primary plasmodia contain complex cellular components, including nuclei, lipid droplets and an endomembrane system.

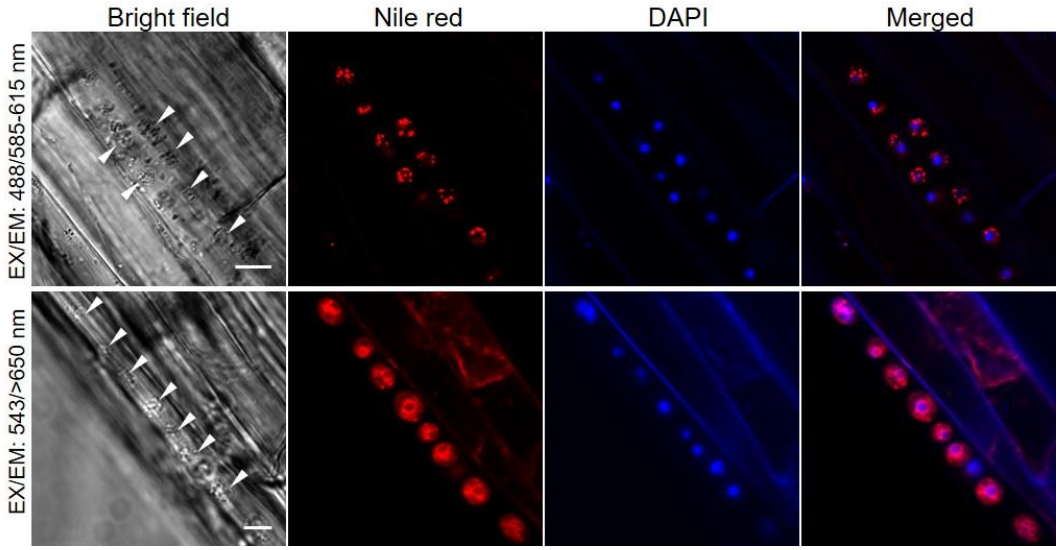

Figure 3.6 Primary plasmodia in two infected root epidermal cells of *Arabidopsis* plants grown in Petri dishes at three dpi.

(A) Intracellular lipid droplets of primary plasmodia stained with Nile red were observed at 585 to 615 nm after excitation at 488 nm (red colour) and nuclei in primary plasmodia stained with DAPI were observed at 420-480 nm after excitation at 408 nm (blue colour).
(B) Endomembrane of primary plasmodia stained with Nile red was observed at >650 nm after excitation at 543 nm (red coclour) and DAPI stained nuclei were observed at 420-480 nm after excitation at 408 nm (blue colour).
Arrows: primary plasmodium; Scale bars: 10 μm

Approximately six weeks post inoculation, small galls, emerging from epidermal cells in the elongation zone of Arabidopsis roots, were visible under light microscopy (Fig. 3.7A and B). Mature resting spores, stained with CFW for cell wall deposition, were observed at 60 dpi (Fig. 3.7C and D). However, the number of resting spores in root galls of Arabidopsis plants growing in Petri dishes was much less than that found in galls of Arabidopsis roots grown in soil. Although only a small number of resting spores were produced in this *in vivo* dual-culture method, it did support the complete life cycle of *P. brassicae*, that is primary plasmodia to mature resting spores. The ability of the pure *P. brassicae* inoculum to infect roots of canola (*B. napus*) growing in Petri dishes was also investigated. About 30 dpi, small galls in the elongation zone of canola roots were observed under light microscopy (Fig. 3.7E). Sporulating plasmodia (SP) undergoing sporulation to resting spores (i.e. plasmodia at an early stage in resting spore formation) and resting spores (RS), were observed in these galls (Fig. 3.7F). These galls became visible to the eye about 45 dpi of canola roots (Fig. 3.7G).

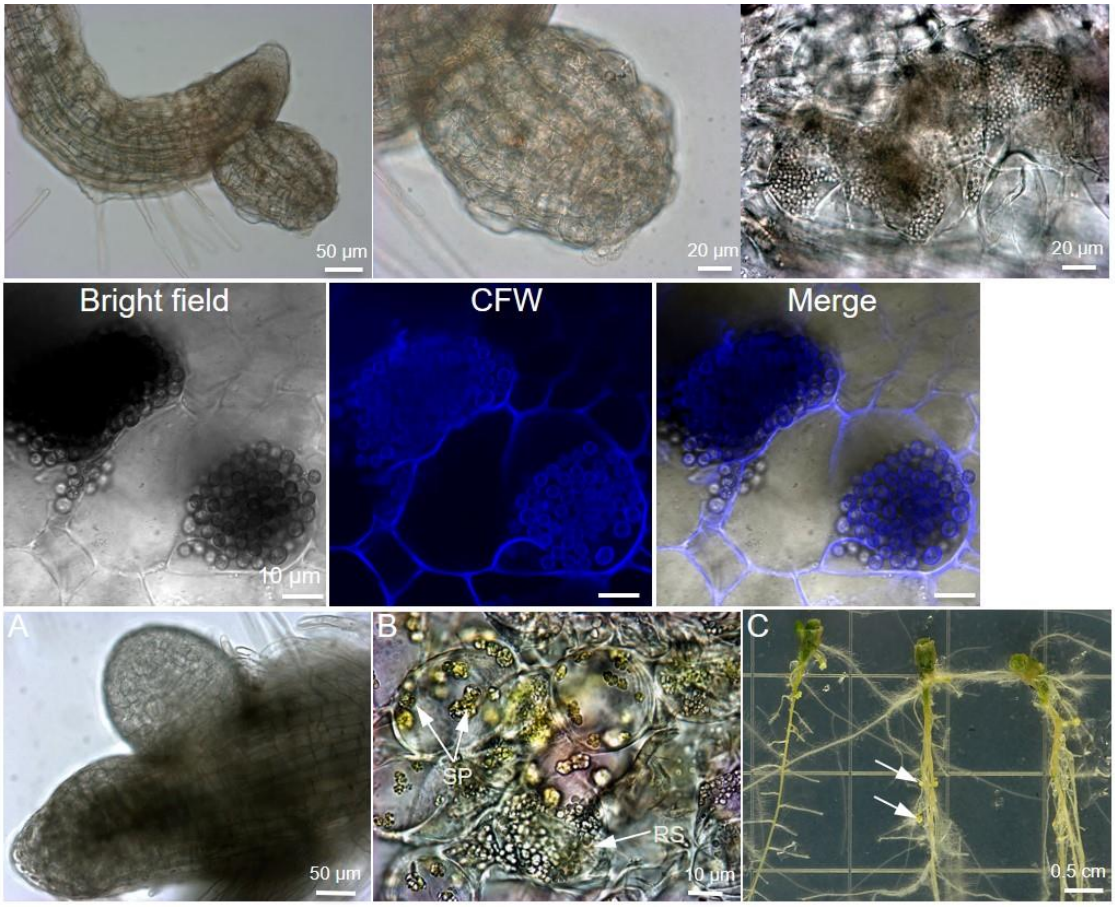

Figure 3.7 *P. brassicae* complete life cycle in the roots of Petri dish-grown *Arabidopsis* and canola plants.

(A) A small gall emerging from epidermal cells in the elongation zone of Arabidopsis roots at 45 days post inoculation (dpi).
(B) Enlarged image of the small gall in (A).
(C) Resting spores (RS) in host cells of the infected roots of Arabidopsis at 60 dpi.
(D) Cell walls of mature resting spores in infected Arabidopsis roots stained with calcofluor white (CFW) (blue color) at 60 dpi.
(E) A small young gall emerging from epidermal cells in the elongation zone of a canola root at 30 dpi.
(F) Sporulating plasmodia (SP) and resting spores (RS) of *P. brassicae* in infected canola roots at 30 dpi.
(G) Typical clubroot gall symptoms developed on canola roots at 45 dpi. Arrows indicate small clubroot galls on canola roots.

3.4 Discussion

3.4.1 Dual culture of *P. brassicae* with canola

The aim of this study was two-fold: i) to develop a new two-step dual culture system and ii) to use this system for early and easy *in vivo* observations of the *P. brassicae* primary infection process and subsequent disease progression in intact host plants. In developing this dual culture system, a mothod modified from Bulman et al. (2011) was followed, in that a 'callus cleaning' step was added to ensure that final calli were free of any and all bacterial and fungal contamination. The Bulman et al. (2011) study lacked this step and the gall segments were only surface sterilized and may have been compromised by the inter- or intracellular presence of bacterial or fungal microorganisms that surface-sterilization alone would not have removed.

During the life cycle of *P. brassicae,* a number of its developmental forms are difficult to differentiate from host organelles. Methods have yet to be identified for the selective staining of the pathogen in infected host cells, that is, to observe the infection and differentiated developmental stages of *P. brassicae* simultaneously. Using TEM, intracellular lipid droplets have been observed in secondary plasmodia and resting spores (William and McNabola 1967; Deora et al. 2013). Nile red, which is able to bind to intracellular neutral lipids, was used in this study for the labeling of the intracellular lipid droplets of *P. brassicae*. Using excitation and emission wavelengths of 488 nm and 585-615 nm, respectively, the neutral lipid droplets in *P. brassicae* secondary plasmodia and immature resting spores, in callus cells, were readily observed, suggesting that Nile red is a useful stain in the study of *P. brassicae* development during primary and secondary infection stages. Calcofluor white (CFW), previously described in studies of the morphological diversity of chytrids (Rasconi et al. 2009; Gerphagnon et al. 2013), binds to the β1-4 polysachharides found in the chitin of fungal cell walls and *P. brassicae* mature resting spore walls. As the excitation and emission wavelengths of 408 nm and 420-480 nm, respectively, are quite different to those for Nile red, both CFW and Nile red staining of *P. brassicae* was combined to observe the complete life cycle. This procedure identified two main differences between mature and immature resting spores: (i) cell wall deposition and (ii) plasma membrane lipid composition. The double staining procedure made it possible to visualize the chitin cell wall of mature resting spores at the same time as the intracellular lipid droplets of immature resting spores in infected Arabidopsis cells (Fig. 3.5) and did not interfere with the identification of host cell structures. The ability to differentially detect the membranes of immature and mature resting spores by Nile red, using the wavelength set

543/>650 nm, suggests that there is a change in membrane lipid composition during resting spore maturation. Why mature resting spores in infected calli were defective for intracellular lipid staining is not clear and out of scope of this current study. Possibly, it is the result of a thick cell wall deposition and plasma membrane component changes that prevents Nile red from penetrating the cell wall and plasma membrane.

3.4.2 Dual culture - stage two

Although there have been numerous efforts to develop a dual culture method for *P. brassicae* with its host (Asano et al. 2000; Takahashi et al. 2006; Asano et al. 2006; Asano and Kageyama 2006), this is the first report of a dual culture system with intact host plants. Without selective staining, small vacuoles or other host organelles have been previously misidentified as pathogen structures during the early stages of infection (Asano et al. 2000; Takahashi et al. 2006; Sharma et al. 2011). Using DAPI, with a wavelength set of 408/420-480 nm, the same as that used for CFW fluorescence, nuclei in both *P. brassicae* and host cells were observed. By double staining with Nile red and DAPI, multiple small spherical uninucleate primary plasmodia, in individual infected epidermal cells of Arabidopsis roots, were observed. With this improved staining procedure, it is suggested that previously identified multinucleated primary plasmodia in root hairs were in fact condensed cytoplasm resulting from the sample preparation (Asano et al. 2000; Kageyama and Asano 2009; Sharma et al. 2011). It has been confirmed, by DAPI staining in live cells, that the primary plasmodia are uninucleate rather than multinucleate. Uninucleate primary plasmodia (previously called uninucleate amoebae) were previously observed by TEM in cabbage root hair (Aist and Williams 1971). The inoculated Arabidopsis roots were shorter than mock-treated roots at three dpi. However, whether the effect on roots is the result of infection of *P. brassicae* or toxin produced by *P. brassicae* infection is still unknown.

While it was not possible to observe *P. brassicae* structures during the secondary infection stages using this two-step dual culture method and live cell imaging, the large number of primary plasmodia observed in epidermal cells at three dpi suggests that this two-step dual culture method has value for studying primary zoospore attachment and penetration of host root hairs and epidermal cells, and subsequent amplification during primary infection stages, both of which are extremely difficult to observe in soil grown plants. The production of resting spores in the two-step dual culture system indicates that secondary infection did occur. However, the level of secondary

infection was much lower than that observed in soil grown plants. This discrepancy could be as a result of : (1) As an intracellular pathogen, *P. brassicae* feeds on the contents of its host cell during the secondary infection stages (see section 4.3.3), therefore, development and final population size of the pathogen will be closely dependent on host cell contents. *P. brassicae* also has a long-life cycle which means that after three weeks of culture on a Petri dish, when the host plant is starting to senesce because of nutrient limitation, secondary infection is limited and fewer pathogen resting spores will be produced, (2) *P. brassicae* is a natural soil borne pathogen and exposure to light during Petri dish culture may block pathogen development by inhibiting some light-sensitive processes, (3) Other soil microorganisms may induce the host plant to produce a chemical substance that attracts *P. brassicae* infection. In the first stage of dual culture of *P. brassicae* with canola calli, it was found that after surface sterilization, the culture of lateral roots from mock plants was free of contamination, however, microorganism contamination quite often was observed on root gall segments. The dual culture system produced calli containing *P. brassicae* resting spores free of any soil microorganism and as such, host plants may have been less attractive for *P. brassicae* infection and proliferation.

Using the combined dual-culture and dual-staining strategies reported herein, Nile red labeled *P. brassicae*, coupled with other dyes, in both primary and secondary infection stages was accomplished and pathogen developmental structures were observed using confocal microscopy. One current drawback to the use of Nile red is that not only does Nile red have a broad emission range, but also its excitation range significantly overlaps with other widely used fluorescent reporters such as GFP (488 nm) and mCherry (543 nm), hindering the use of most ready-made Arabidopsis fluorescent reporter lines for plant-pathogen interaction experiments.

3.4.3 Epidermal cells in the root elongation zone are more sensitive to infection

Surprisingly, in this study, it was observed that epidermal cells of the hairless root elongation zone and root hairs close to this region are the most sensitive to pathogen penetration. Epidermal cells of the root elongation zone at three dpi were filled with primary plasmodia (Fig. 3.6). Moreover, at later stages of disease development, galls emerged from epidermal cells of the elongation zones in both canola and Arabidopsis roots (Fig. 3.7). These observations are consistent with previous reports that many root hair deficient mutants, including the hairless mutants *rhd4-1* and *axr1-12*, are as susceptible to *P. brassicae* infection as wild type Arabidopsis plants (Siemens et al. 2002).

Compared to cells in other zones of the root, cells in the elongation zone may be more prone to penetration by *P. brassicae* as a result of the breakage of cell wall polysaccharide links, during the extension of the cellulose cell wall, occurring during the rapid increase in length with negligible change in radius of these cells.

This is the first report of infectious *P. brassicae* propagation in canola calli and the complete life cycle of *P. brassicae* in cultured whole canola and Arabidopsis plants. We further used a combined Nile red and DAPI dual-staining methodology to identify primary plasmodia and to investigate very early primary infection stages, both of which are extremely difficult to do in soil-grown plants. The dual-culture and dual-staining systems provide a useful methodology for propagating pure *P. brassicae* inoculum as well as providing an easy means of observing the infection process and host response to early infection by *P. brassicae*, thus contributing to a greater understanding of primary infection by this pathogen.

Chapter 4 The Life Cycle of *Plasmodiophora brassicae*: Morphogenetic Events and their Implications for Pathogen Biology

4.1 Abstract

Plasmodiophora brassicae, a protist parasite, induces club-shaped tumor-like growths on host brassica roots (clubroot) and hypocotyls after infection. Due to its soil-borne obligate parasitic nature, infection biology such as the parasite life cycle and details of pathogenesis remain in doubt and subject to debate. As the genome sequence projects of *P. brassicae* were completed recently, two major challenges are becoming urgent: to interpret the plethora of data in terms of pathogen biology, and use this information effectively in the control of the pathogen. The life cycle of *P. brassicae* in the plant host was described in the last century, but comparatively few details are available, despite the fact that it is probably one of the most serious and widespread pathogens in the cruciferous family. Understanding the life cycle of pathogens is fundamental to understanding their pathogenicity.

Cell biology approaches including confocal fluorescence imaging and transmission electron microscopy (TEM), together with transcript analysis of putative stage specific genes, were used to investigate the *P. brassicae* life cycle. A haploid-diploid sexual life cycle was suggested by the alternation of haploid primary infection stages and diploid secondary infection stages. The first recorded developmental stage of *P. brassicae* in root hair and epidermal cells was uninucleate primary plasmodia, which were detected at two days post inoculaiton (dpi). The presence of young uncleaved zoosporangia, appearing two days later than primary plasmodia, was confirmed in root hair and epidermal cells. Zoosporogenesis was described in detail from five dpi to 12 dpi for the production of mature secondary zoospores. In cortical cells with secondary infection, development of *P. brassicae* started from a myxamoeba stage with pseudopodium-like structures and rapidly proliferated into numerous haploid resting spores by endomitosis and endomeiosis followed by final cytoplasmic cleavage. To fuel the rapid growth and divisions of the secondary infection stages, the pathogen internalized and degraded large amounts of host cytoplasm, using three independent processes.

In this study a haploid-diploid unisexual life cycle of *P. brassicae,* with an alternation between haploid and diploid phases, was suggested. During the life cycle, *P. brassicae* undergoes multiple nuclear divisions without cytokinesis to produce multinucleate structures preceding the final cytoplasmic cleavage. The results of this study provided the first detailed analysis of membrane development during cytoplasmic cleavage in the multinucleate stage of the *P. brassicae* life cycle, including multinucleate zoosporangia and sporulating plasmodia stages. The timing and sequential events during the lifecycle of *P. brassicae* have been mapped by confocal and TEM. The good correlation of microscopic observation with the expression of molecular marker genes provides a fast and easy disease diagnostic technique. These data sets also provide a platform that will be of use for post genomic analyses of *P. brassicae* cell biology in relation to differentiation, infection and disease control.

4.2 Introduction

Clubroot, caused by the soil-borne obligate endo-parasite *Plasmodiophora brassicae*, is a serious disease of Brassicaceae worldwide, including economically important brassica crops and vegetables, as well as the model plant Arabidopsis. Infection by *P. brassicae* can result in significant yield and quality losses in a susceptible crop, accounting for a 10-15% yield reduction on a global scale (Dixon 2009). Due to the scale of the problem and the limited range of effective chemical control options, disease control is difficult in an agricultural setting. Development of sustainable control measures for future management of *P. brassicae* will require a comprehensive understanding of the cellular and molecular basis of pathogen development and pathogenicity. In order to fully analyze the molecular mechanisms that govern *P. brassicae* pathogenesis, a rigorous quantitative description of the cellular changes that occur to the cell during the life cycle is needed. Understanding the biology, and particularly the life cycle, of this parasite will be an important step in combating the disease it causes.

Since the first discovery of *P. brassicae* by the Russian scientist Woronin in 1878, many efforts have been made to elucidate its lifecycle (Fig. 4.1; Aist and Williams 1971; Ingram and Tommerup 1972; Kageyama and Asano 2009). The pathogen has three distinct stages in its life cycle: i) survival in soil as resting spores, ii) primary infection occurring inside host root hairs and epidermal cells, during which primary plasmodia, zoosporangia and secondary zoospores are formed, and iii) secondary infection, producing multinucleate secondary plasmodia in the root cortex and stele, ultimately resulting in cell hypertrophy and hyperplasty.

The lifecycle initiates within the soil with the release of a haploid primary zoospore from a haploid resting spore in the vicinity of host roots. The zoospore moves through water in the soil via capillary motion and when encountering a root, encysts on the exterior surface of a host cell where it forms a cytoplasm extension, an adhesorium. A dense organelle, the satchel, is within the adhesorium and is injected ahead of the contents of the encysted zoospores through the host cell wall and cell membrane into the host cell (Aist and William 1971). Inside the host cell, the contents of the zoospore appears as a small spherical amoeba (Aist and William 1971). The amoeba enlarges, and a number of nuclear divisions occur synchronously leading to the formation of a primary multinucleate plasmodium, followed by cleavage into zoosporangia (Ingram and Tommerup 1972; Kageyama and Asono 2009). The zoosporangia form clusters in the root hair and epidermal cell. In each zoosporangium, 4-16 secondary zoospores are formed and after being released, the empty

zoosporangia remain in the root hair or epidermal cell (Ludwig-Müller and Schuller 2008; Kageyama and Asano 2009).

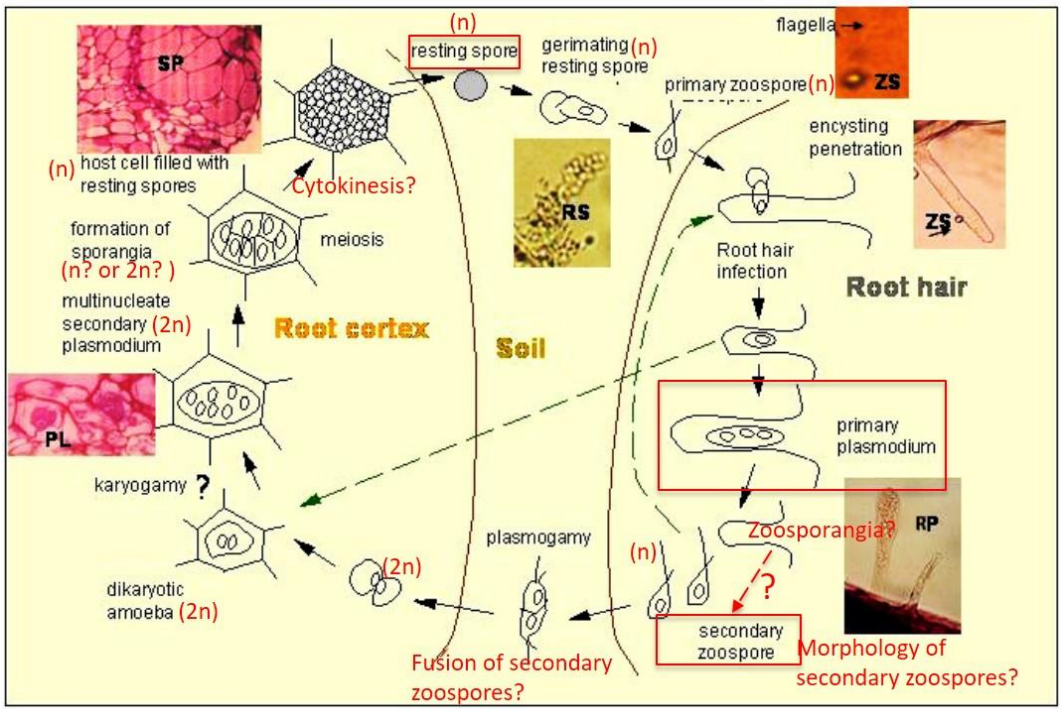

Figure 4.1 Life cycle of *P. brassicae* illustrated by microscopic pictures of characteristic developmental stages of the pathogen in the development of root gall on brassica host plant species.

The developmental stages during which cell divisions and hypertrophy occur are marked. Abbreviations as they appear from the top panel: ZS, zoospore; RP, multinucleate primary plasmodium; PL, multinucleate secondary plasmodium; SP, sporulating plasmodium. (adapted from Ludwig-Müller and Schuller 2008)

Released secondary zoospores penetrate the cortical tissues of the main roots, a process called cortical infection or secondary infection. Initial colonization by *P. brassicae* of cortical cells has been characterized by the presence of bi-nucleate secondary plasmodia or myxamoeba containing numerous, prominent lipid droplets (Deora et al. 2013). Secondary plasmodia proliferate and are associated with cellular hypertrophy, followed by gall formation in root tissues. The bi-nucleated

secondary plasmodia undergo a number of mitotic nuclear divisions to produce multinuclear secondary plasmodia (Ingram and Tommerup 1972; Garber and Aist 1979a). Meiotic nuclear division occurs following the cessation of mitosis of the multinucleate secondary plasmodium to produce numerous haploid resting spores that, as infected tissues decay, are released into the soil where they can survive harsh environments for up to 20 years (Garber and Aist 1979b; William and McNabola 1967). Despite considerable research over the past 50 years to describe the major structures of at least six successive developmental forms: primary zoospores, primary plasmodia, zoosporangia, secondary zoospores, secondary plasmodia and resting spores, in the complex life cycle of *P. brassicae*, there are still many open questions and puzzles concerning specific stages of development and subsequent colonization of its host by this pathogen. For example, how to differentiate the complex developmental stages of the pathogen? How do the uninucleate primary plasmodia (see section 3.3.3) develop into multinucleate zoosporangia? The ploidy of the primary and secondary infections? Is there a sexual life cycle for *P. brassicae*? As an intracellular parasite, how does *P. brassicae* obtain nutrients to feed itself?

The soil-borne, obligate intracellular nature, as well as the multi-stage life cycle of the pathogen makes microscopic observation of the infection process difficult. In order to fully understand the molecular mechanisms that govern *P. brassicae* pathogenesis, a rigorous quantitative description of the pathogen life cycle is needed. The 24 Mb genomes of different *P. brassicae* pathotypes were recently sequenced (Rolfe et al. 2016; Schwelm et al. 2015), however, *in vivo* genetic manipulation techniques for *P. brassicae* have yet to be developed. Against this background, examination, by transmission electron microscopy (TEM) combined with confocal fluorescence imaging with several dyes specific for molecules or cell components in the pathogen and/or host cell, was conducted to produce a detailed time course of the development of *P. brassicae* in *A. thaliana*. The aim of this study was to describe the complete life cycle of *P. brassicae* in *A. thaliana* and attempt to re-evaluate and record the stage-dependent characteristics previously reported for other brassica crops.

Due to its small size, mode of parasitism and the limited number of infected host cells in a primary infection, there has been no detailed description of pathogen development through zoosporogenesis. In this study, detailed pathogen development during primary infection is described. Obligate intracellular parasites must live within cells in order to survive. The loss of key biosynthetic pathways is a common feature of parasitic protists, making them heavily dependent

on scavenging nutrients from their hosts. In this study, the description of three independent feeding processes, distinguishable temporally and morphologically, which were utilized by the pathogen to internalize and degrade massive amounts of cytoplasm from host cortical cells, is provided. These feeding processes are essential for pathogen development, survival and pathogenesis. Here molecular and morphological evidence of meiosis in secondary plasmodia prior to or at the same time as the final cytoplasmic cleavage is presented. By mining the *P. brassicae* genome database, orthologues of eukaryotic meiosis-specific genes and flagella-related genes were identified. Further, it is shown that meiosis-specific genes were expressed around the same time as meiosis occurs in sporulating plasmodia (SP). Expression profile of flagella-related genes had two peaks, one around zoosporogenesis and another around meiosis of SP. Identifying the unique features of *P. brassicae* that govern its pathogenesis in host cells will provide possible targets for clubroot disease control.

4.3 Results

4.3.1 Live cell imaging

To differentiate *P. brassicae* from plant cell organelles and other root microorganisms, I established live-cell, fluorescent dye staining, imaging protocols to study and document, in detail, the life cycle of *P. brassicae* at set time intervals after inoculation of the model plant, *A. thaliana* by Laser Scanning Confocal Microscopy (LSCM). Lipid droplets are storage organelles with a core of neutral lipids, mainly triacylglycerol (TAG) and sterol esters, that may be used for energy metabolism, membrane synthesis, and/or the production of essential lipid-derived molecules. Electron-dense lipid droplets have been previously identified in secondary plasmodia and resting spores (William and McNabola 1967; Deora et al. 2013). Nile red, a hydrophobic and metachromatic stain for intracellular TAG, was used to stain lipid droplets in *P. brassicae*. 4′,6-diamidino-2-phenylindole (DAPI), a membrane permeable dye that binds strongly to A-T rich regions in DNA, was used to label nuclei of both *P. brassicae* and host cells. The fluorescent, lipophilic styryl dye, FM4-64, that is rapidly incorporated into the outer leaflet of the plasma membrane, only enters the cell through an active, time-dependent endocytosis or invagination of the plasma membrane. FM4-64 was used as a general membrane marker to highlight cytokinesis. Previously it had been used to study cytoplasmic cleavage of *Allomyces macrogynus* zoosporangia (Fisher et al. 2002).

4.3.2 *P. brassicae* development during primary infection

4.3.2.1 Primary plasmodium

After germination, resting spores release active zoospores, which in order to avoid adverse soil conditions quickly penetrate a host root hair cell or epidermal cell. Penetration by primary zoospores occurs so rapidly that very few cells exhibit the penetration process under microscopic observation. In this study, the first LSCM observed developmental stage of *P. brassicae* was the uninucleate primary plasmodia in both root hairs and epidermal cells of infected Arabidopsis root samples between two and five dpi (Fig. 4.2). Primary plasmodia were spherical ranging from 2.69-6.63 μm (n = 38, mean ± s.d. = 4.89 ± 1.00 μm) in diameter.

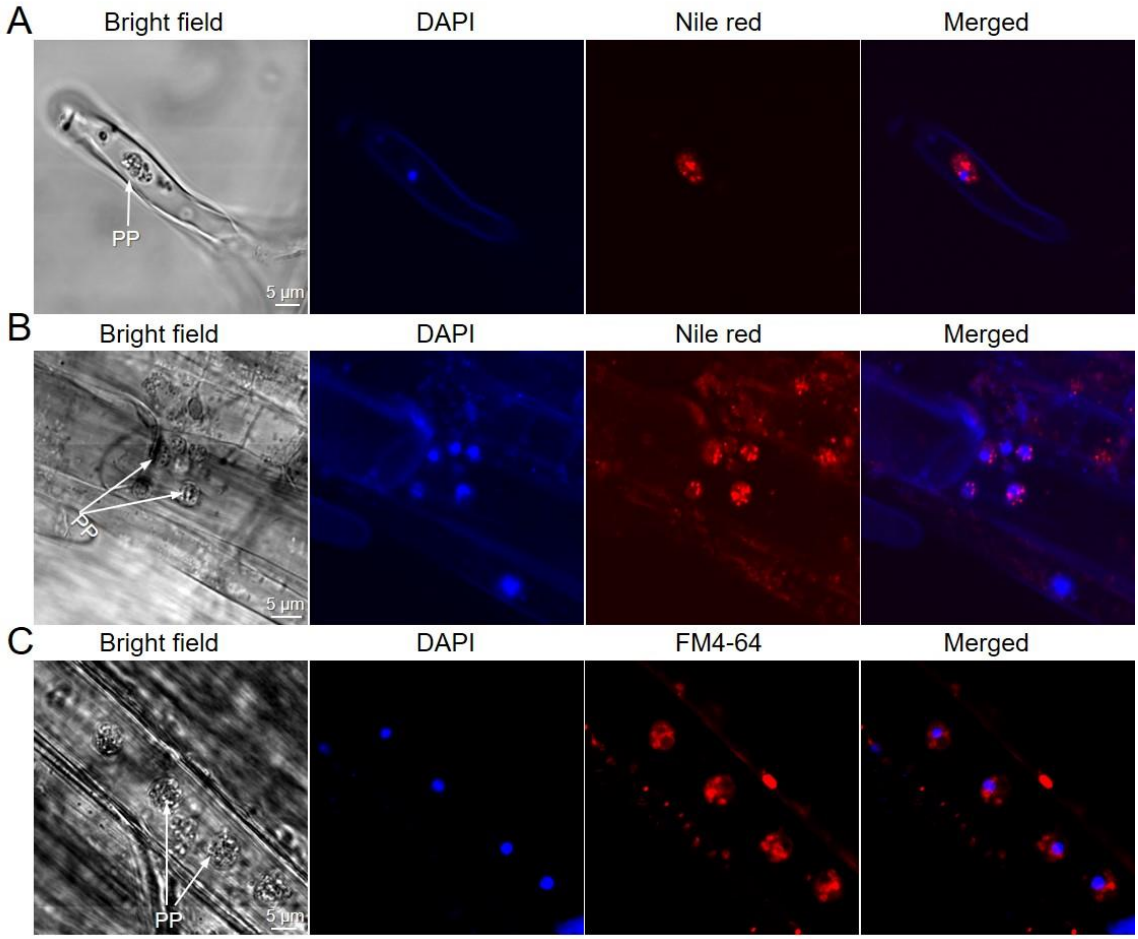

Figure 4.2 Uninucleate primary plasmodia in *Arabidopsis* hair and epidermal cells during primary infection stages.

(A) A primary plasmodium (PP) in a root hair stained with Nile red (red color) to label lipid droplets and with DAPI (blue color) to detect the nucleus of *P. brassicae* by LSCM at two dpi.
(B) Primary plasmodia (PP) in a epidermal cell stained with Nile red (red color) to label lipid droplets and with DAPI (blue color) to detect nuclei of *P. brassicae* by LSCM at two dpi
(C) Primary plasmodia (PP) in an epidermal cell stained with FM4-64 to label membranes (red colour) and with DAPI (blue color) to detect nuclei of *P. brassicae* by LSCM at two dpi.

The central, large nuclei of primary plasmodia were intensely stained by the intercalating dye DAPI, thereby confirming primary plasmodia were uninucleate cells (Fig. 4.2), which was also reported in dual culture system in Petri dishes (see section 3.3.3). The cytoplasm of each plasmodium was packed with lipid droplets stained with Nile red (Fig. 4.2). As a result of host cellular uptake, FM4-64 stained whole plasmodia fluorescent red. Under light microscopy, individual early primary plasmodia were morphologically indistinguishable from young uncleaved zoosporangia. In contrast to previous observations of primary plasmodia in *B. rapa* (Ingram and Tommerup 1972), multi-nucleate primary plasmodia were not observed during the primary infection stage except during the later stage cell divisions to form zoosporangia (Fig. 4.3 and Fig. 4.4).

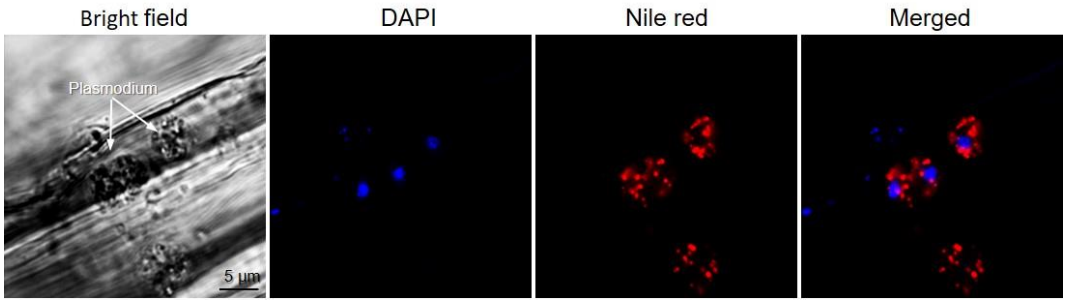

Figure 4.3 Binucleate stage of primary plasmodia during cell division at three dpi.

Binucleate primary plasmodia in inoculated Arabidopsis roots were stained by Nile red (red color) to label lipid droplets and DAPI (blue color) to detect nuclei by LSCM.

4.3.2.2 Amplification of primary plasmodium

The number of pathogen cells within host root hairs or epidermal cells increased rapidly to form a cluster of multinucleate zoosporangium at six dpi from a few individual primary plasmodia at two dpi. Moreover, the apparance of bi-nucleate primary plasmodium structures in epidermal cells at three dpi (Fig. 4.3) prompted the question, is the increasing number of primary plasmodia a reflection of cell division? FM4-64 staining of primary plasmodia membranes and DAPI staining of nuclei provided visualization of these cell divisions. Primary plasmodia in infected epidermal cells were observed undergoing cell division as early as three dpi (Fig. 4.4). Similar to cell division in mammals, after nuclear division, cytokinesis resulted in two daughter cells formed by a cleavage furrow of the primary plasmodium. However, Laser Scanning Confocal Micoscopy (LSCM) counld not provide enough resolution to study cell division in details, the delails of uninucleate primary plasmodium amplificaiotn still remain to be elucidated. During the uninucleate primary plasmodium stage, FM4-64 stained the general membranes of *P. brassicae* by rapidly internalized through endocytosis, resulting in the whole plasmodium fluorescing (Fig. 4.3, 4.4).

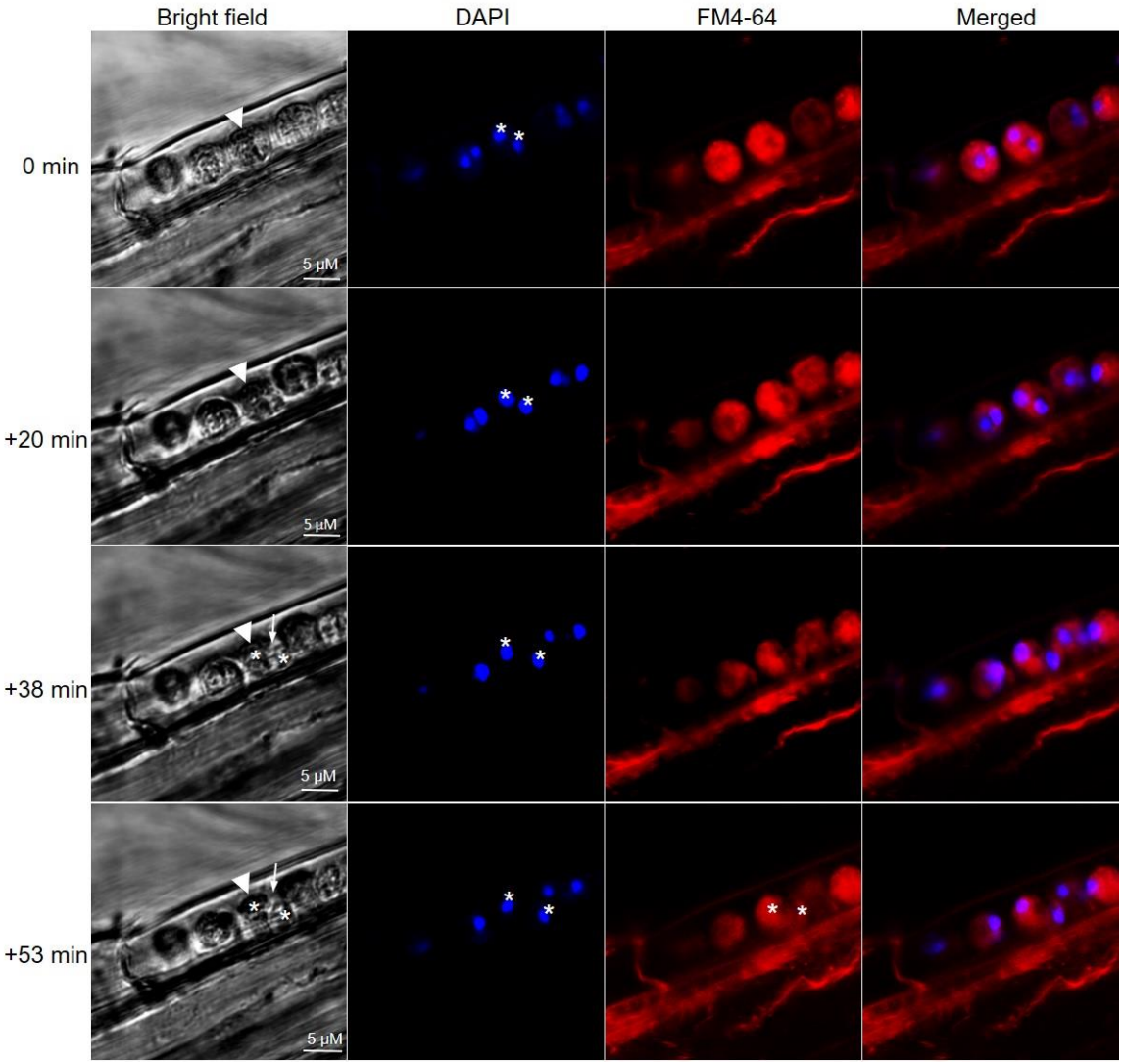

Figure 4.4 Times-lapse LSCM of primary plasmodium division in an infected *Arabidopsis* epidermal cell at three dpi.

Arrowhead: a primary plasmodium with two nuclei, note that the distance between two nuclei (asterisks) in the starting circular increased in one plasmodium along with the time series. Arrows: the distance between the two nuclei, Red color is parasite-derived internal membranes.

4.3.2.3 Zoosporogenesis

By five dpi, the development from primary slightly enlarged plasmodia to young uncleaved multinucleate zoosporangia was complete (Fig. 4.5). Nuclear division of each uninucleate primary plasmodia to multinucleate zoosporangia was too rapid to observe with TEM. However, the development of primary plasmodia into zoosporangia could be distinguished by the development of thin cell walls surrounding the zoosporangia and the formation of daughter nuclei *in situ*. Uninucleate primary plasmodia are amoeboid and lack cell walls (Aist and William 1971). Zoosporangia are surrounded by thin walls and the degradation of these walls between contact zones of adjacent zoosporangia results in a chain arrangement (Fig. 4.5A, B). Cell wall fusion occurred before zoosporangia cleavage and its initiation probably preceeds nuclear division in zoosporangia. Two rounds of mitotic divisions in each primary plasmodium give rise to a tetranucleate zoosporangium. Uncleaved tetranucleate zoosporangia are globose amoeba-like, approximately 3-5 μm in diameter and contain bean-shaped electron-dense nuclei without nucleoli, mitochondrion, lipid droplets and electron translucent small vesicles (Fig. 4.5D, E, F). After the first mitotic division, an axoneme profile of four axonemes, was found between the two daughter nuclei (Fig. 4.5D). Transversely sectioned flagellar axonemes were also seen in the tight space formed between the cell wall and the invagination of the plasma membrane (Fig. 4.5D, E). Following the second mitotic division, assembled flagella were observed completely within the cytoplasm of the cell, coiled around the nucleus (Fig. 4.5E).

Over the next seven days from five dpi to 12 dpi, zoosporangia undergo zoosporogenesis, where tetranucleate zoosporangium are compartmentalized into four mature biflagellate secondary zoospores ready for release (Fig.4.5, 4.6, 4.7). Uncleaved zoosporangia contained large numbers of small electron translucent vesicles (Fig 4.5D, E, F), that may contribute to the membrane cleavage system. The earliest sign of transformation into flagellate zoospores is the appearance of the non-membrane-bound flagellar axonemes near the nuclei and longitudinally sectioned flagella in young zoosporangia, preceding cytoplasmic cleavage (Fig. 4.5D, E, F). These observations suggest that *P. brassicae* axoneme assembly occures completely within the cytoplasm. This is followed by a cleavage of the entire contents of the zoosporangia and maturation into biflagellated zoospores.

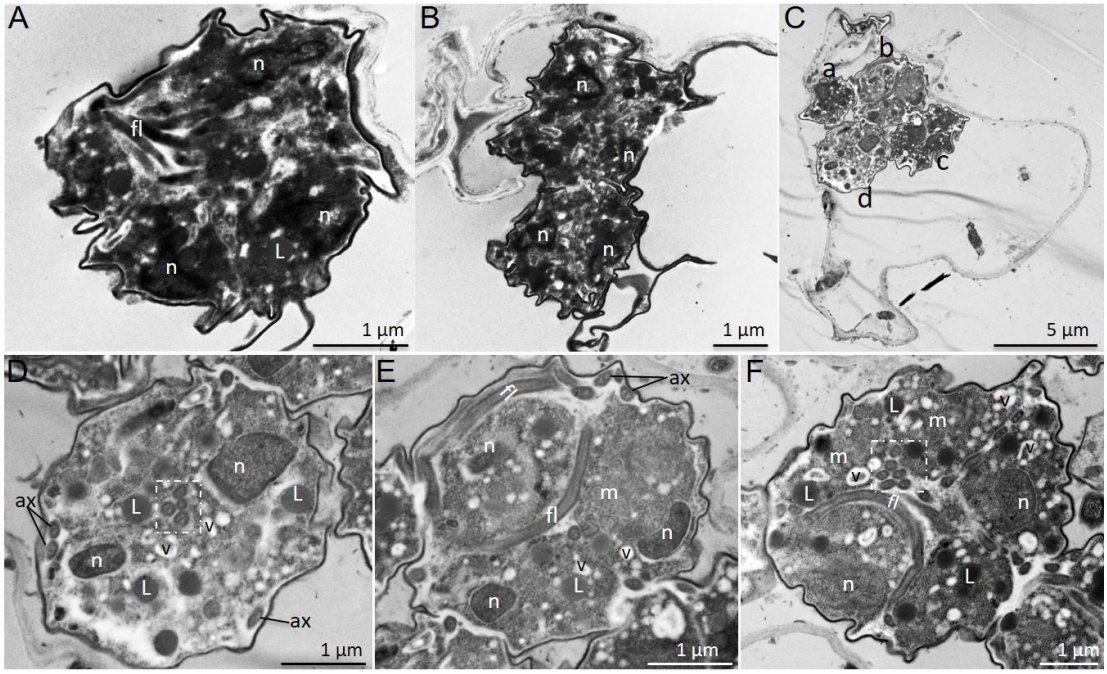

Figure 4.5 TEM micrographs of uncleaved zoosporangia and developing secondary zoospores of *P. brassicae* in infected epidermal cells and root hairs of *Arabidopsis* roots at five dpi.

(A) and (B) young zoosporangia in infected epidermal cell. Each zoosporangium cell is multinucleate (n), but the cytoplasm has not yet divided. Flagella (fl) are already assembling prior to cytoplasmic cleavage. L: lipid droplet.

(C) Cross section of an infected root hair with four zoosporangia (a, b, c, d). Note the fusion of the cell walls between the four zoosporangia at contact points.

(D) Enlarged image of zoosporangium (d) in (C). Transversely sectioned flagella profiles (dashed white box) of non-membrane bound axoneme are located between two nuclei (n) in the cytoplasm and an axoneme (ax) was also located in the tight space between the cell wall and invaginated plasma membrane .

(E) Enlarged image of zoosporangium (b) in (C). Longitudinally sectioned flagella coil (fl) in the cytoplasm around a nucleus. v: vesicle; m: mitochondrion.

(F) Cross section of a zoosporangium with cytoplasmic cleavage profile.

Cytoplasm of each tetranucleate zoosporangium separates into uninucleate zoospore initiates through cleavage resulting from infurrowing of the plasma membrane together with the fusion of small vesicles in the cytoplasm (Fig. 4.5E, F). The final compartmentalization of the contents of zoosporangia into zoospores results from the fusion of small vesicles to delimit each zoospore and to provide an external membrane. At the intermediate stage of cytoplasmic cleavage, each delimited zoospore initial contains one nucleus and a cluster of lipid droplets, mitochondrion and small vesicles (Fig. 4.5F). The plasma membrane of the mother zoosporangium is partitioned between the plasma membranes of the daughter zoospores. Secondary zoospore formation requires a growth phase, during which there are repeated nuclear divisions, followed by a differentiation phase when the nuclei move to the periphery of the zoosporangium and cytoplasmic cleavage occurs.

The zoosporangia stages were found exclusively in root hair and epidermal cells, occurring infrequently, with the majority of infected main root cells showing no sign of *P. brassicae* infection (Fig. 4.6A). Young, cleaved zoosporangia at seven dpi are typically spheroid with rigid cell walls and a diameter between 2.95 to 6.52 μm (n = 45, mean ± s.d. = 4.60 ± 0.84 μm) under TEM (Fig. 4.6), which is slightly larger than uncleaved zoosporangia. With the dissolution of the cell walls between adjacent zoosporangia, a chain of zoosporangia is formed in the root hair or epidermal cell, permitting the movement of zoospores from one zoosporangium to the other. Zoosporangia at the end of the chain and adjacent to the host cell wall abort (Fig. 4.6B, C, D, E). There is also dissolution of zoosporangium cell walls and the host cell wall at the point of contact (Fig. 4.6b, d). During this period the young zoosporangia become fully cellularised to immature resting spores. Vesicle fusion within zoosporangia produces space as they are maturing, in which numerous extracellular flagellum fragments in both longitudinal and transverse sections, can be seen (Fig. 4.6b, d, F). The flagellar axoneme consists of the regular microtubule nine doublet and central pair arrangement (Fig. 4.6G). Immature secondary zoospores during early development exhibit complicated intercellular aspects, similar to those seen in immature primary zoospores when undergoing germination from resting spores (Tanaka et al. 2001). The cytoplasm of each immature zoospore contains an electron dense oval nucleus minus a nucleolus, intracellular flagella and a few small visicles (Fig. 4.6b, F). Mitochondria and electron dense lipid droplets are dispersed throughout the cytoplasm. Compared to uncleaved zoosporangia, most small vesicles disappear as they form the internal cleavage furrows to delineate secondary zoospores (Fig. 4.6).

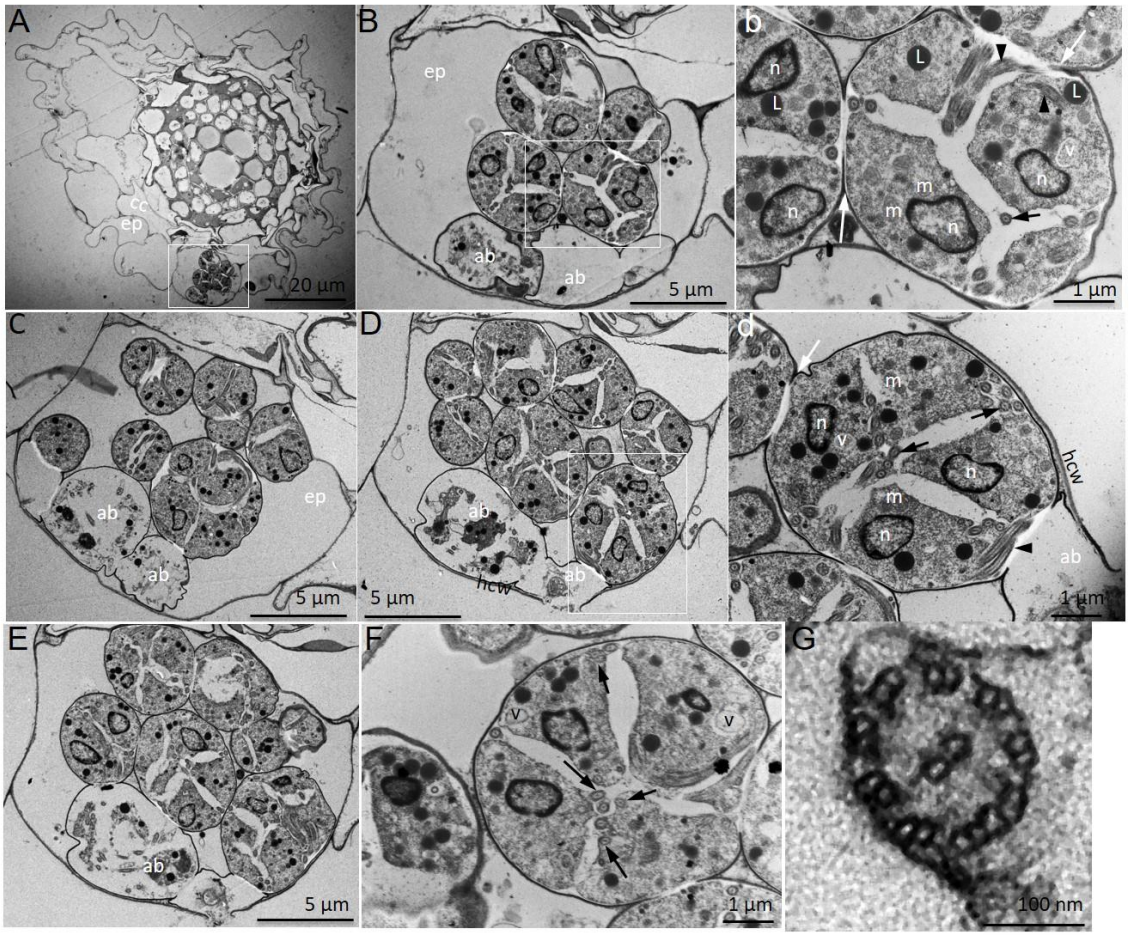

Figure 4.6 TEM micrographs of *P. brassicae* cleaved young zoosporangia at seven dpi.

(A) Cross section of Arabidopsis root with zoosporangia in an epidermal cell (ep). cc: cortical cell.

(B) – (E) Images of serial sections of the same infected epidermal cell in (A) filled with cleaved zoosporangia. Note the aborted zoosporangia (ab) adjacent to the host cell wall (HCW) for secondary zoospore discharge and fusion of aborted zoosporangium cell walls and the host cell wall at the point of contact for secondary zoospore discharge.

(b) Enlarged image of a zoosporangium in white square of (B) showing longitudinal sectioned intracellular and intercellular flagella (black arrowhead), cross sectioned intercellular axoneme (black arrow), lipid droplets (L), mitochondria (m) and nucleus for each immature zoospore. Note the fusion between two adjacent zoosporangia (white arrow).

(d) Enlarged image of a zoosporangium in white square of (D). Note the fusion of the aborted zoosporangium cell wall and the host cell wall (HCW) at the point of contact for secondary zoospore discharge.

(F) Cross section of a zoosporangium with intercellular and intracellular flagella axoneme (black arrow).

(G) Cross section of a flagellum axoneme.

This final stage of zoospore differentiation was associated with condensation of the secondary zoospore cytoplasm (contraction of cell body) and the development of a wide electron-lucent extracellular band of material within the zoosporangia and around the developing secondary zoospores (Fig. 4.7). Mature secondary zoospores had an irregular-shaped and fully condensed cell body, as has previously been described for mature primary zoospores germinating from resting spores (Tanaka et al. 2001) and germinated free primary zoospores attached to cabbage root hair walls (Aist and Williams 1971). During maturation of secondary zoospores and while surrounded by electron-lucent materials, initial intracellular flagella become externalized (Fig. 4.7A, B, E, F). Flagella appeared to be extruding from the periphery of the zoospore body and transverse flagellar axonemes were observed in the distal end of mature zoospores (Fig. 4.7C, D, G, H). Intracellular flagella were not observed in this stage. Mature secondary zoospores still had an electron-dense nucleus without a nucleolus and evenly dense ribosome-rich cytoplasm with lipid droplets, mitochondria and numerous central and peripheral vacuoles and vesicles, that were absent in immature zoospores (Fig. 4.7C, D, G). Vesicles were round bodied or irregular in shape and some peripheral vesicles possibly resembled secretory or pinocytotic vesicles leading to the exterior of the zoospore body (Fig. 4.7C, G). Aist and Williams (1971) report various types of vesicles associated with primary zoospores during attachment to host root hair walls.

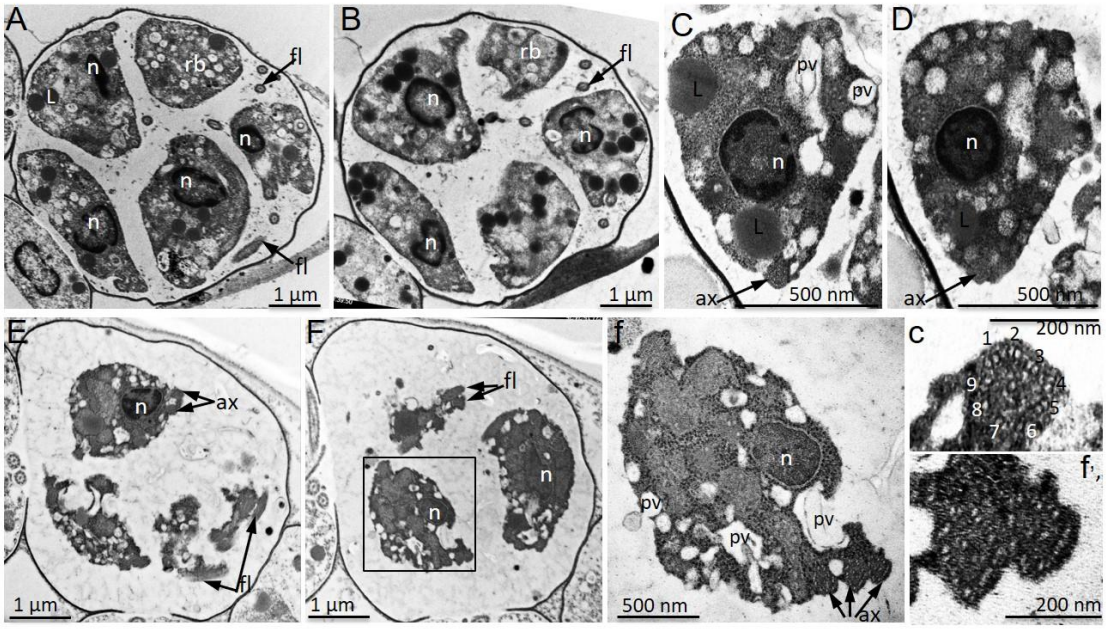

Figure 4.7 TEM micrographs of *P. brassicae* mature zoosporangia containing condensing zoospores and flagella fragments at 12 dpi.

(A) and (B) Serial sections of an intermediate-mature zoosporangium with four oval shaped intermediate-mature zoospores and a residual body (rb). fl: flagellum; n: nucleus.

(C) and (D) Serial sections of an intermediate-mature zoospore showing lipid droplets (L), nucleus and peripheral vesicles (pv) with a peripheral flagella axoneme (ax).

(E) and (F) Serial sections of a mature zoosporangium prior to zoospore release. The nuclei are electron-dense and irregularly shaped. Zoospores appear amoeboid and more condensed than intermediate-mature stage.

(f) Enlarged mature zoospore in (F) showing peripheral vesicles opened to the exterior of the zoospore body.

(c) and (f') Detailed transverse section through flagella showing microtubule doublets or singlet with central pair arrangement from (C) and (f) respectively.

The process of zoosporogenesis could also be followed by using LSCM with fluorescent dye staining. Nile red successfully labeled the lipid droplets of zoosporangia at all stages of zoosporogenesis (Fig 4.8A, a, Fig. 4.9A, a). In contrast, DAPI only stained nuclei in young zoosporangia (including uncleaved and cleaved zoosporangia), but not nuclei in mature zoosporangia (Fig.4. 8, Fig. 4.9). As a result of endocytosis, FM4-64 stained the whole young uncleaved zoosporangia brightly, while in young cleaved zoosporangia, FM4-64 only outlined the plasma membranes of both immature and mature secondary zoospores (Fig. 4.8B, Fig. 4.9B). FM4-64 labeling of the endomembrane was not observed after cleavage of zoosporangia, leaving the center of each daughter zoospore in a cleaved zoosporangium void of FM4-64 fluorescence (Fig. 4.8B, Fig. 4.9B). As zoosporangia matured they became lighter in color and homogeneous in content under light microscopy (Fig. 4.8 and Fig. 4.9, bight field channels) and nuclei could not be stained with DAPI. Lipid droplets in mature zoosporangia,containing fully formed secondary zoospores were still stained by Nile red (Fig. 4.9), showing a similar staining pattern to that of young cleaved zoosporangia.

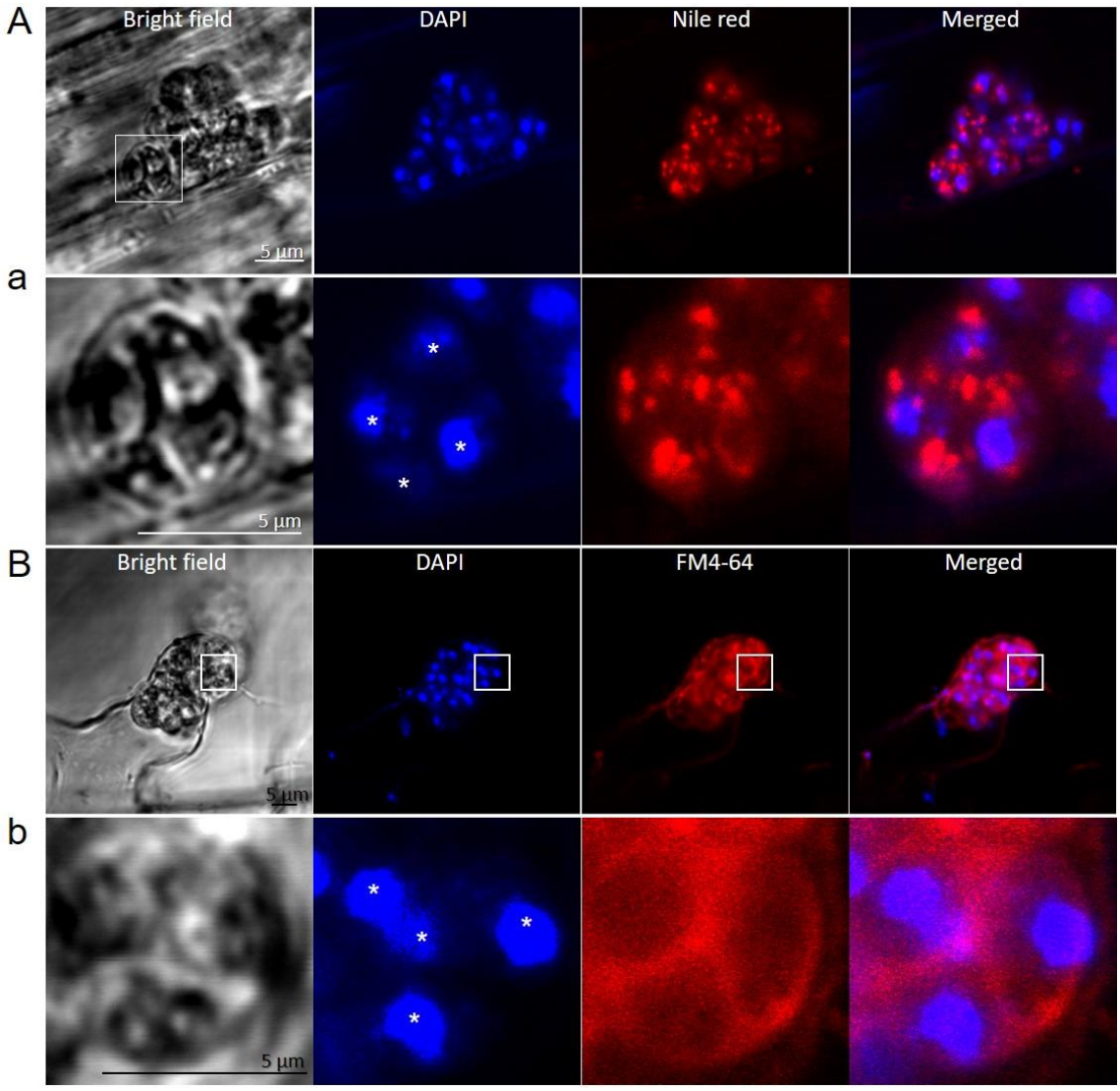

Figure 4.8 LSCM of cleaved young zoosporangia in an infected epidermal cell and root hair of *Arabidopsis* roots at seven dpi.

(A) Tetrads in a cleaved young zoosporangium; nuclei were stained with DAPI (blue color) and lipid droplets were stained with Nile red.
(a) Enlarged image indicated by the square in (A).
(B) Tetrads in a cleaved young zoosporangium; nuclei were stained by DAPI (blue color) and the membranes of each immature daughter zoospore were stained by FM4-64.
(b) Enlarged image indicated by the square in (B).
Asterisks: nuclei.

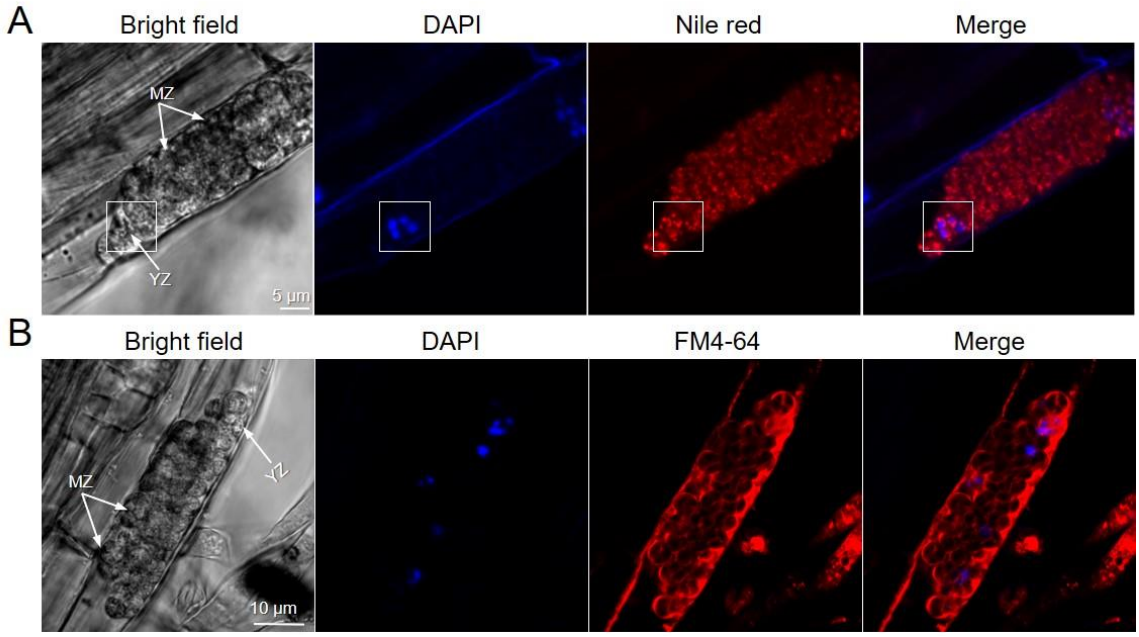

Figure 4.9 LSCM of young and mature zoosporangia in an epidermal cell of infected *Arabidopsis* roots at 10 dpi.

(A) Predominant mature zoosporangia (MZ) and a young zoosporangium (YZ) in an epidermal cell. Nuclei were stained with DAPI (blue color) and lipid droplets were stained with Nile red (red color).
(B) Mature and young zoosporangia stained with DAPI (blue color) and FM4-64 (red color).

4.3.2.4 Release of secondary zoospores

The final step of the primary infection is the release of invasive, mature secondary zoospores, from an zoosporangium in the infected host cell, for subsequent cortical infection. Escape of the invasive secondary zoospores is a fundamental step in the pathogenesis of *P. brassicae*, of which little is known. Release of secondary zoospores from infected host root hairs or epidermal cells could result from fusion of the mature zoosporangium wall and host cell wall and release of secondary zoospores into the soil; or by a rupture of the zoosporangium wall within the epidermal or root hair cell, from where secondary zoospores initiate cortical cell infection. Description of the dissolution of adjacent zoosporangium walls, and the dissolution of aborted zoosporangia walls and the host cell wall at the point of contact between them supports the first hypothesis, (Fig. 4.6B, C, D, E). The dissolution of adjacent zoosporangium walls also occurred between young uncleaved zoosporangia (Fig. 4.5) and empty zoosporangia (Fig. 4.10E) as well as movement of zoospores by flagella from one zoosporangium to the other (Buczacki and Clay 1984), suggesting the final release of mature secondary zoospores along the zoosporangia chain to the soil. Zoosporangia containing mature secondary zoospores with flagella, together with the presence of an exit pore formed by the dissolution of the zoosporangium wall and host cell wall, were first observed by TEM in root hairs of infected Chinese cabbage (Buczacki and Clay 1984). However, under light microscopy, before being discharged from an infected host cell, secondary zoospores swimming freely in epidermal and root hair cell lumen have been observed, following the disruption of the zoosporangium membrane at 12 dpi (Fig. 4.10A). After zoospores have been released, zoosporangia were clear, indicating that they were empty (Fig. 4.10B, E). The zoosporangium walls still remained in the infected cells but were deformed as they were empty. Empty zoosporangia were devoid of any DAPI, FM4-64 or Nile red staining (Fig. 4.10). The fate of secondary zoospores after discharge is the remaining major unknown feature of the life cycle of *P. brassicae*. Once secondary zoospores are released and move freely within the host epidermal cell or root hair, they may be discharged into the soil by a fusion of host cell membrane and cell wall, from where they infect cortical cells, or they may infect the inner root tissue from the base of the infected epidermal cells.

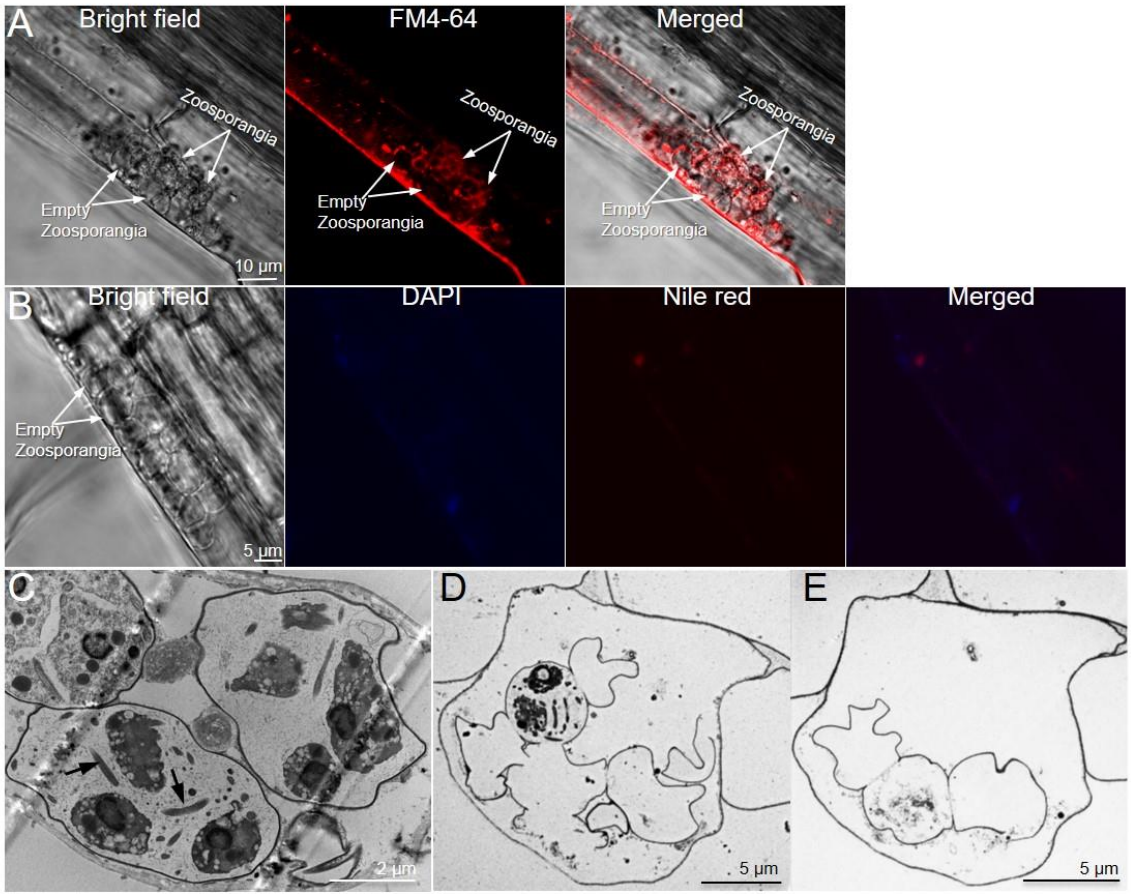

Figure 4.10 Egress of secondary zoospores from mature zoosporangia at 12 dpi.

(A) Secondary zoospores were released from zoosporangia into the host epidermal cell. Note that the membrane of mature zoosporangia with zoospores were stained with FM4-64, empty zoosporangia were not stained with FM4-64.
(B) Empty zoosporangia in an epidermal cell.
(C) Mature zoosporangia undergoing release of secondary zoospores. Note that the zoosporangia were shrunken during release of secondary zoospores. Arrow: flagellum profile
(D) and (E) Cross section of empty zoosporangia in an epidermal cell. Note the empty zoosporangia were shrunken and deformed.

4.3.3 *P. brassicae* development during secondary infection stages

Invasion and parasitism of host root cortical cells is central to the pathology of clubroot disease. Using transmission electron microscopy (TEM), in conjunction with confocal live cell imaging, of an Arabidopsis root disease series (14, 17, 20 and 24 dpi), the importance of *P. brassicae* life cycle development to clubroot disease progression has been identified.

4.3.3.1 Myxamoeba

The process by which secondary zoospores recognize, attach to, and invade a host cell is still largely unknown. In previous reports, the first pathogen structures observed during secondary infection stages were bi-nucleate myxamoeba in the cytoplasm of cortical cells (Kobelt et al. 2000), probably as a result of cytoplasm fusion of two secondary zoospores without nuclei fusion. However in this study, the earliest pathogen strucutures observed in the cortical cells were uninucleate myxamoeba and occasionally binucleate myxamoeba. Two sequential morphological stages of vegetative secondary plasmodia were identified by TEM (Fig. 4.11, Fig. 4.13), and through different nuclei labeling patterns with DAPI under confocal microscopy (Fig. 4.12A, C). For the earlier stage, between 14-17 dpi in cortical cells of infected roots, *P. brassicae* is in the myxamoeba stage with irregular pseudopodia-like extension structures. These uninucleate myxamoeba, of approximately 3-5 µm diam, are the earliest identified form of the pathogen residing within the cortical cell cytoplasm. They have simple cellular components, an electron-dense nucleus with prominent nucleoli and some cytoplasmic lipid droplets (Fig. 4.11A). Binucleate myxamoeba were occasionally present (Fig. 4.11B). A myxamoeba occupies the majority of an infected host cell before the host cell starts to expand (Fig. 4.11A). Unlike the nucleus in zoosporangia, the myxamoeba nucleus contains a nucleolus (Fig. 4.11A). When stained with DAPI and Nile red, nuclei and lipid droplets are visible (Fig. 4.12A). Myxamoeba were not commonly observed in each infected cortical cell. Infected cells were undistended in comparison to uninfected host cells, which were highly vacuolated and contained little cytoplasm and organelles. Infected cells appeared to have an increased volume of host cytoplasm and contained fragmented vacuoles, mitochondria and amyloplasts (Fig. 4.11). Pseudopodia-like protrusions of the myxamoeba form a cup, engulfing bulk host cytoplasm contents, resulting in food vacuoles containing host cytoplasm and organelles (Fig. 4.11A, C, D).

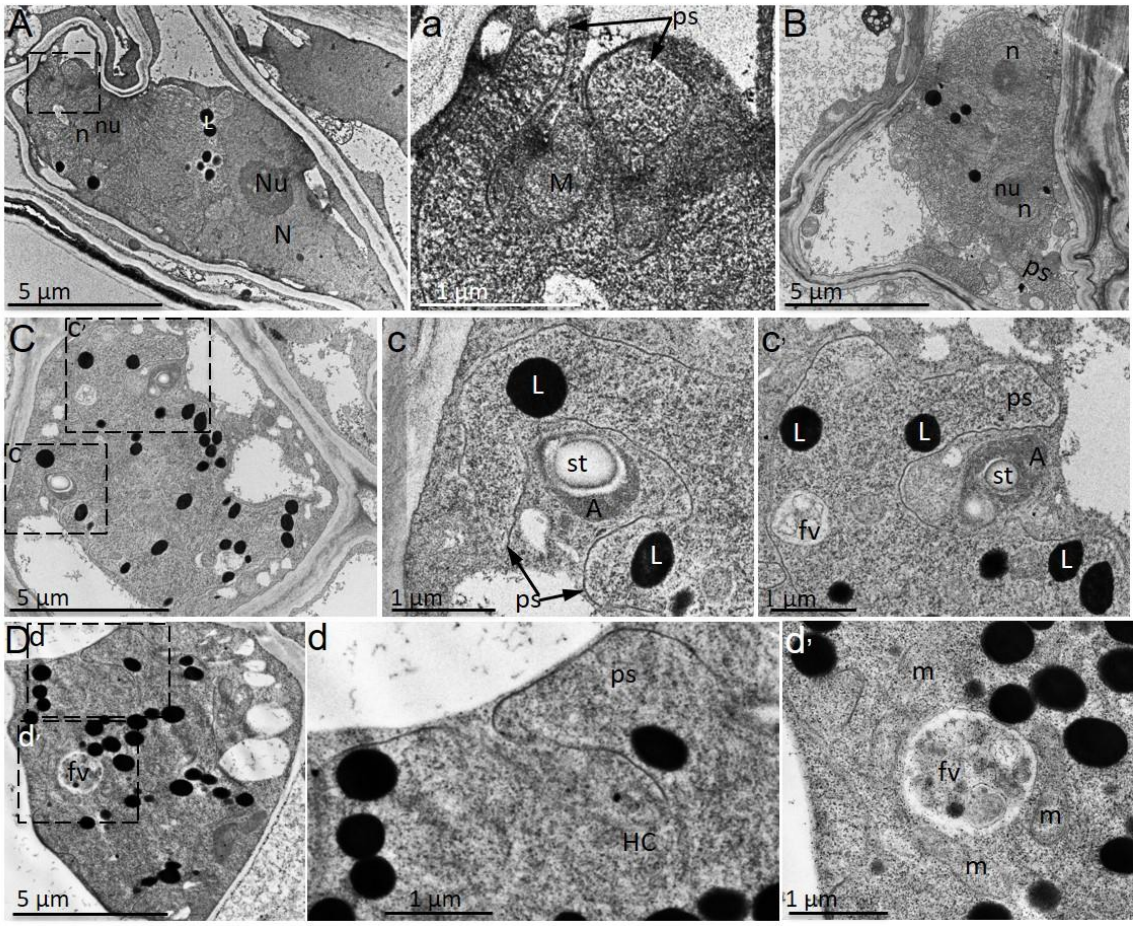

Figure 4.11 TEM micrographs of myxamoeba engulfing host cell contents by pseudopodia resulting in the formation of digestive vacuoles between 14 dpi to 17 dpi.

(A) A uninucleate myxamoeba engulfing host cell mitochondrion (M). The pathogen has a single nucleus (n) with prominent nucleolus (nu), and the cytoplasm contains few lipid droplets (L). (a) enlarged image of dashed square in (A) showing engulfment of host cell mitochondrion by pseudopodia (ps)-like strucutures.

(B) An intracellular binucleate myxamoeba with prominent nuclei and few lipid droplets.

(C) A myxamoeba engulfing host cell amyloplasts (A) with starch granules (st) to form digestive vacuole (dv). (c) and (c') enlarged images of dashed squares in (C).

(D) A myxamoeba engulfing host cell cytoplasm (HC) to form food vacuole. (d) and (d') enlarged images of dashed squares in (D). Note that pathogen mitochondria (m) are associated with digestive vacuole.

N: host nucleus; Nu: host nucleolus

4.3.3.2 Vegetative secondary plasmodium replication

Following the myxamoeba stage, the irregular myxamoeba round up to form vegetative plasmodia (secondary plasmodia). Within host cells, the vegetative plasmodia expand to twice the size of the original myxamoeba and contain a complex cellular arrangement, characterized by a thick plasma membrane, nuclei, ER, mitochondria and abundant lipid droplets (Fig. 4.13). An increased number of lipid droplets in vegetative plasmodia suggests increased lipid synthesis during the myxamoeba stage. However, there are no fatty acid synthase genes in the *P. brassicae* genome (Schwelm et al. 2015), therefore it is suggested that *P. brassicae* synthesizes fatty acids by elongation and modification of fatty acid precursors taken up from the host cell. In each infected cell, usually a cluster of plasmodia with well-defined plasma membranes are produced (Fig. 4.12C, D, Fig. 4.13). The nuclei of these vegetative plasmodia are unable to be stained with DAPI, or their plasma membane with FM4-64 (Fig. 4.12C, D). However, DAPI does stain the host nucleus and FM4-64 does stain host cell plasma membrane and endocytotic vesicles in non-infected host cells but not in infected host cells or pathogen cells (Fig. 4.12D). One possible explanation for the lack of FM4-64 fluorescence of plasmodia is that a *P. brassicae* infected host cell may have decreased endocytotic capabilities and as a result, the FM4-64 dye does not reach the intracellular pathogen. Early dye-loading experiments with FM4-64 documented tubular and round vesicles proliferating near non-infected host cell plasma membranes (Fig. 4.12D), suggesting that these are part of the endocytotic compartment of host cells. The vegetative plasmodia grow substantially in size to prepare for asexual replication and cell division.

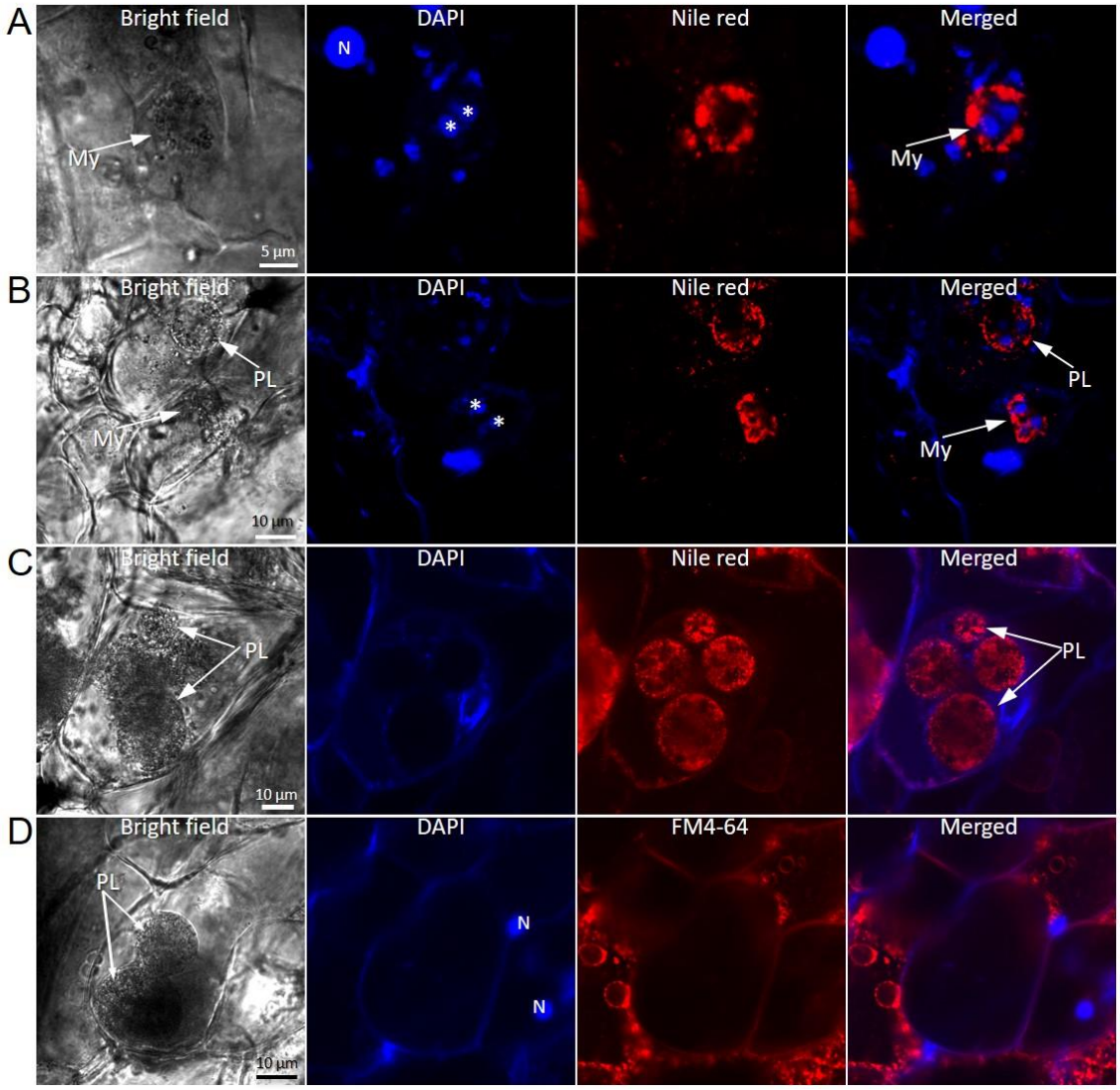

Figure 4.12 LSCM of vegetative plasmodia during secondary infection of *P. brassicae* in *Arabidopsis* cortical cells.

(A) A binucleated myxamoeba (My) in an infected cortical cell stained with DAPI and Nile red at 14 dpi; N: host cell nucleus, asterisk: pathogen nucleus.
(B) Two neighboring cortical cells infected with early stage myxamoeba (My) and spherically shaped plasmodium (PL) stained with DAPI and Nile red at 17 dpi. Note that the nuclei in the spherically shaped plasmodium is difficult to stain with DAPI.
(C) Four spherically-shaped late stage plasmodia (PL) in a cortical cell stained with DAPI and Nile red at 21 dpi. Note that nuclei in late stage plasmodia are not stained with DAPI.
(D) Multiple spherically-shaped late stage plasmodia (PL) in cortical cells stained with DAPI and FM4-64 at 21 dpi. Note that nuclei in late stage plasmodia are not stained with DAPI and plasma membrane and endocytosis of late stage plasmodia are not stained with FM4-64 but host cell nuclei (N) are stained.

The majority of plasmodia nuclei, during vegetative growth of the pathogen, were in interphase with a large centrally positioned nucleolus (Fig. 4.13B, F). At early cell division, the uninucleate plasmodia contain a pair of centrioles at opposite poles of the nucleus, clearly outside the nuclear envelope (Fig. 4.13B, C). Each pair of centrioles were closely aligned end-to-end (Fig. 4.13C; Garber and Aist 1979a). Centrioles in *P. brassicae* exhibit the typical 9x3 cartwheel configuration of microtubules (Garber and Aist 1979a). Microtubules radiated into the pathogen cytoplasm from electron-dense material at the periphery of the centrioles. These cytoplasmic microtubules also extend along the sides of the nucleus but never pass through the nuclear envelope (Fig. 4.13C). Cisternae of endoplasmic reticulum (ER) were frequently aligned with the cytoplasmic, centriole microtubules, and were also closely associated with the nuclear envelope (Fig. 4.13B, C, F).

Through multiple rounds of nuclear division, mirrored by an increase in transcription of DNA replication, repair and nucleotide metabolism genes, uninucleate, round, secondary plasmodia developed into multinucleate plasmodia (Schwelm et al. 2015). Daughter nuclei formed in secondary plasmodia underwent repetitive rounds of nuclear division without cytokinesis, resulting in the formation of a multinucleate cell with each nucleus surrounded by a double membrane (Fig. 4.13F). Unlike classical eukaryotic cell division, the nuclear cell membrane of *P. brassicae* appears to remain intact and the nucleolus persists throughout the cell cycle (endomitosis), a common feature in unicellular eukaryotes. At prophase, the nucleus has been described with irregularly shaped masses of chromatin around the nucleolus (Garber and Aist 1979a). At metaphase, chromatin aligns at the equator of the nucleus in a well-defined plate, and the persistent nucleolus is elongated parallel to the spindle and perpendicular to the plate of chromatin, thus foming a crosslink (cruciform) configuration when viewed from the side (Fig. 4.13D; Garber and Aist 1979a). The nuclear envelope is intact except at the poles, where the centrioles are embedded. Microtubules radiating from the centriolar region, previously observed only outside the nuclear envelope in prophase, at metaphase are visible inside the nucleus and pass through the chromatin masses from the polar regions (Fig. 4.13D). During anaphase the chromatin at the metaphase plate divides into two plates, that separate, and the nucleolus elongates along the spindle axis (Garber and Aist 1979a). Microtubules have been described within the interzonal space between the chromatin plates (Garber and Aist 1979a). Entering telophase, the nucleus is extremely long and near each pole is a densely packed mass of chromatin and nucleolar material, the nucleolus having finally broken apart (Garber and Aist 1979a). Completing telophase, two daughter nuclei are

formed as a result of the mitotic division of the parent nucleus (Fig. 4.13E).

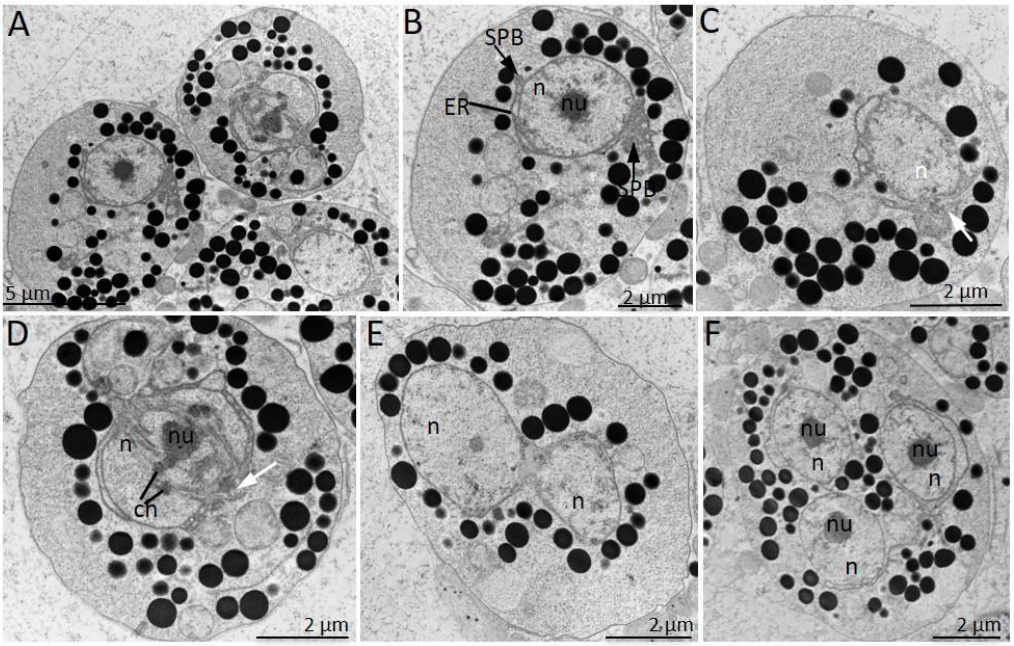

Figure 4.13 TEM micrographs of vegetative secondary plasmodia at 21 dpi.

(A) Three vegetative secondary plasmodia in an infected host cell.
(B) Vegetative secondary plasmodium with an interphase nucleus (n), nucleolus (nu) and spindle pole plaques (SPB) at each pole. The nucleus is partially surrounded by perinuclear endoplasmic reticulum (ER).
(C) Vegetative secondary plasmodium with centriole pair (white arrow) in longitudinal section showing close end-to-end paring at one pole of the nucleus.
(D) Vegetative secondary plasmodium with a metaphase nucleus, showing a paired centriole (white arrow) embedded in the nuclear envelope. ch: chromatin.
(E) Two daughter nuclei formed by fission of the parent nucleus after telophase.
(F) Vegetative secondary plasmodium with multiple nuclei in interphase.

This endomitotic asexual stage of DNA replication and nuclear division, while maintaining the nuclear membrane and in the absence of cytokinesis, occurs several times during the secondary plasmodium stage, resulting in polyploid secondary plasmodia (Fig. 4.13F). Repeated mitosis without cell division occurs within a secondary plasmodium to create a multinuclear cell. To fuel this tremendously fast replication and expansion of a vegetative secondary plasmodia a second process, and major contributor to nutrient uptake and pathogenesis occurs. A bulk ingestion, by the secondary plasmodium plasma membrane, of host cytoplasm and host cell organelles in the immediate vicinity of secondary plasmodia occurs (Fig. 4.14). Various host cell organelles including mitochondria, amyloplasts, vacuoles as well as cytosol were observed partly or wholly surrounded by plasmodial pseudopodia-like structures (Fig. 4.14). During this replication stage, *P. brassicae* degrade approximately 80% of the host cell volume to provide a source of fatty acids, amino acids and carbohydrate and to create sufficient space for pathogen growth and proliferation.

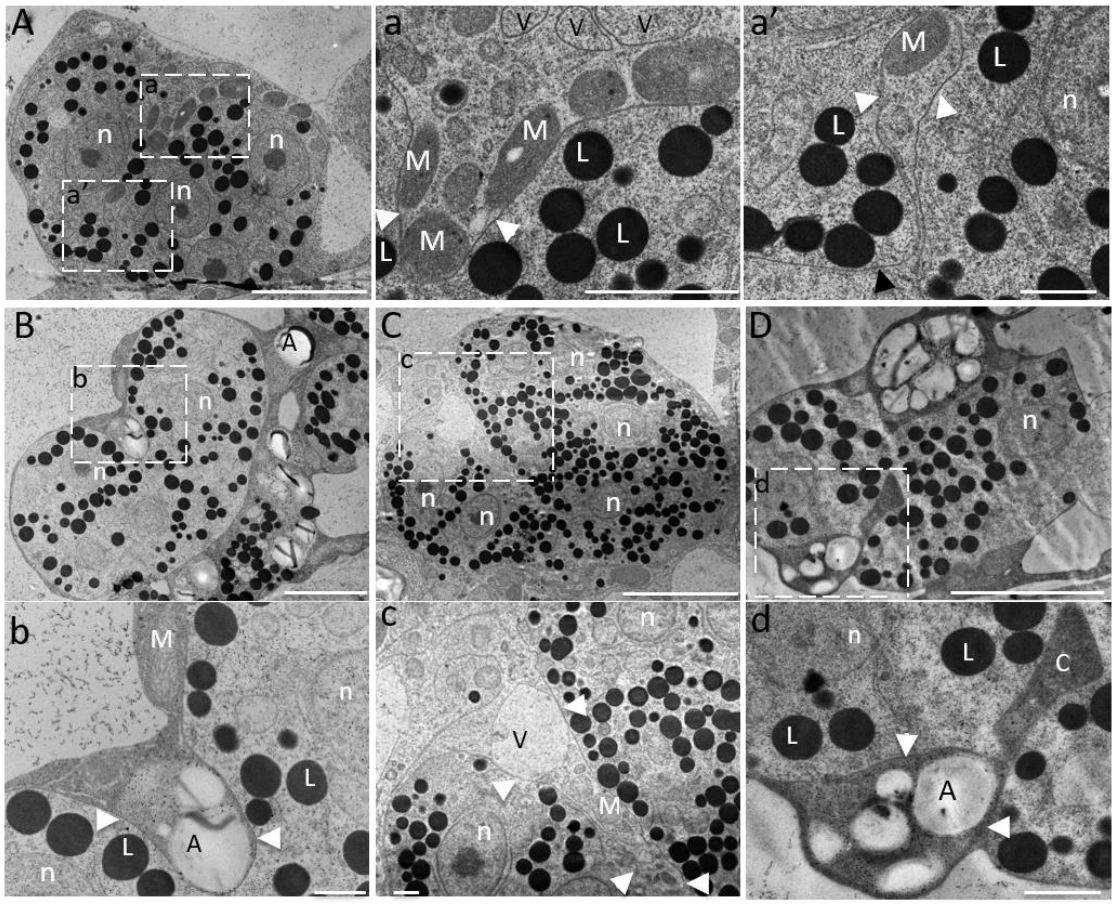

Figure 4.14 Morphology of second phagocytosis showing engulfment of host cell contents by the pathogen via invagination of the pathogen membrane during vegetative plasmodium stage at 21 dpi.

(A) Engulfment of host mitochondria (M) by multinucleate secondary plasmodium. (a, a') Magnified images of the highlighted areas in (A). Note that phagocytosis may occur from anywhere in the secondary plasmodium cell. Closing of the invagination can be seen (white arrowhead). n: plasmodium nucleus; L: lipid droplets in plasmodia.

(B) Engulfment of host amyloplast (A) with starch granules (st) by multinucleate secondary plasmodia. (b) Magnified image of the highlighted area in (B).

(C) Engulfment of host mitochondria (M) and vacuole (V) by multinucleate secondary plasmodia. (c) Magnified image of the highlighted area in (C).

(D) Engulfment of electron-dense host cytoplasm by multinucleate secondary plasmodia. (d) Magnified image of the highlighted area in (D). Note that invagination is closed off from the host cytosol.

Scale bar: 5 µm and 1 µm in insets.

4.3.3.3 Meiosis and cytoplasmic cleavage in sporulating secondary plasmodia

The first indication of a transitioning from vegetative growth to sporogenesis was the presence of synapses in the central region of nuclei, an indicator of prophase I of meiosis (Fig. 4.16A, B; Garber and Aist 1979b). There are also obvious morphology distinctions between vegetative secondary plasmodia and sporulating secondary plasmodia. Variable numbers and sizes of vacuoles/vesicles start to accumulate in sporulating secondary plasmodia (Fig. 4.15). These vacuoles may originate from ingestion of host vacuoles during the vegetative secondary plasmodia stage (Fig. 4.14C, c) or result from invaginations of the secondary plasmodial plasma membranes to produce plasmodial vacuoles (Fig. 4.15D, E, F). Second, abundant host amyloplasts and starch granules are present in sporulating secondary plasmodia (Fig. 4.15). Host amyloplasts with starch granules are present in the vicinity of vegetative secondary plasmodia stages (Fig. 4.14B, D). Third, thinning and fusion of the membranes of individual sporulating secondary plasmodia occurs to form larger sporulating secondary plasmodia (Fig. 4.15A, B, Fig. 16, Fig. 17, Fig. 4.18A, B). Fourth, nuclei of vegetative secondary plasmodia undergoing endomitotic division do not stain with DAPI (Fig. 4.12C, D), however, nuclei in sporulating secondary plasmodia do stain with DAPI (Fig. 4.18).

Once the pathogen moves into the sporulating secondary plasmodia stage, and undergoes meiosis and cytoplasmic cleavage, a third nutrient uptake process occurs. Onset of resting sporulation, correlates with a highly vacuolated appearance of the secondary sporulating plasmodia, with numerous vacuoles of different sizes and shapes. In sporulating plasmodia, food vacuoles containing the remains of starch granules, amyloplasts with starch granules, membrane fragments and electron-dense lipid droplets were observed (Fig. 4.15D-G, Fig. 4.16A). The vacuoles distributed in the periphery of the secondary sporulating plasmodia appeared to be the result of invagination of the plasmodia plasma membrane around host cytoplasm, as the electron-density of the food vacuole is similar to that of host cytoplasm (Fig. 4.15D-G).

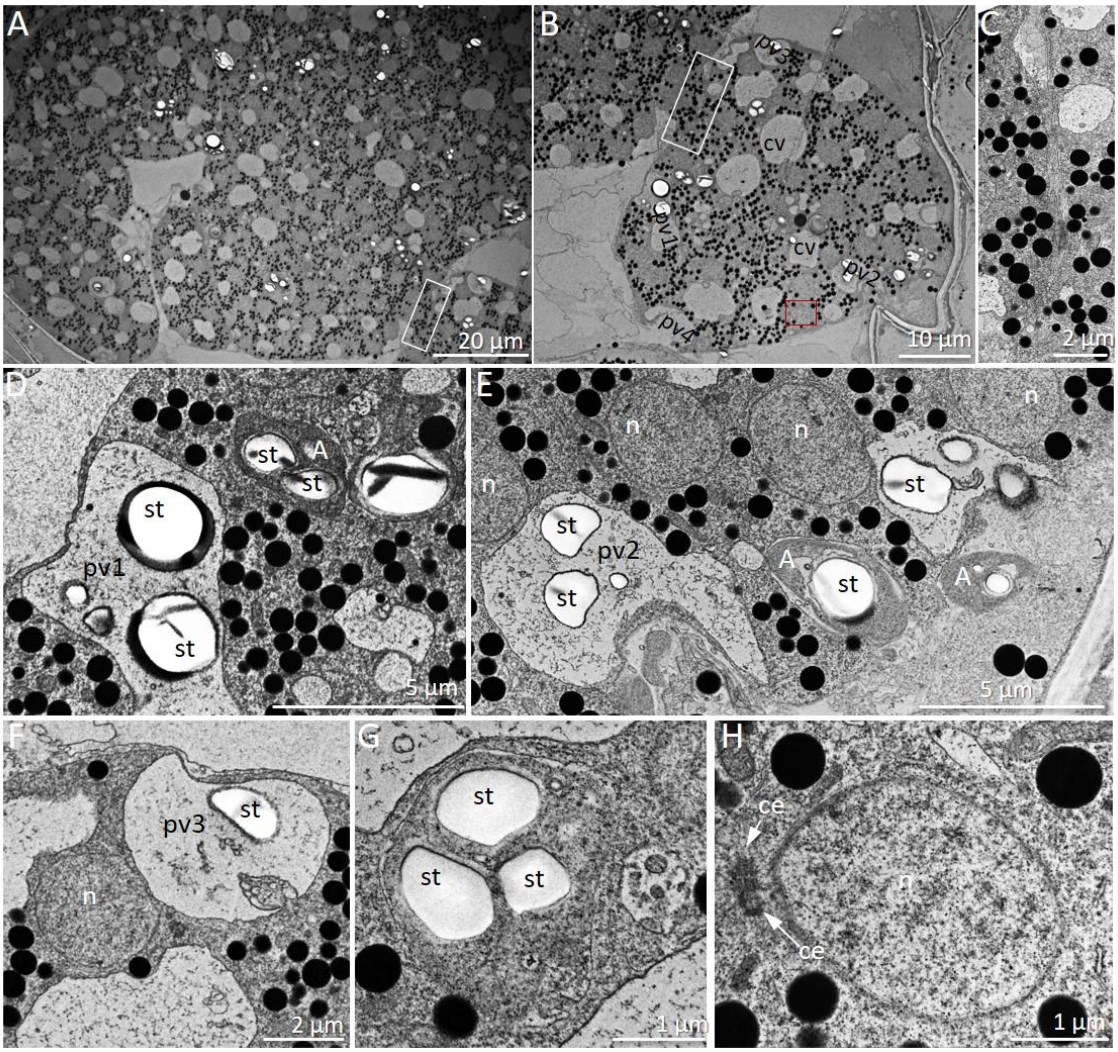

Figure 4.15 TEM micrographs of sporulating secondary plasmodia showing onset of resting sporogenesis and phagocytosis at 24 dpi.

(A) Sporulating secondary plasmodia fusing to form one larger sporulating secondary plasmodium.

(B) A sporulating secondary plasmodium from rectangle in (A) showing numerous vacuoles. Note that sporulating plasmodia were highly vacuolated with both peripheral vacuoles (pv) and central vacuoles (cv).

(C) Magnified images of the highlighted area in the white square in (A) and (B) showing membrane fusion between two sporulating secondary plasmodia.

(D) Details of peripheral vacuole 1 (pv1) in (B) containing degenerate host amyloplasts (A) with starch granules (st). Note the invagination of both the plasmodial membrane and vacuole membrane and the neighboring intact host amyloplast (A) with two starch granules (st).

(E) Details of peripheral vacuole 2 (pv2) in (B). Two peripheral vacuoles containing degenerated host amyloplasts. Note an intact host amyloplast was ingested by the plasmodium membrane adjacent to pv2 and another one was completely outside of

Figure 4.15 cont.

the sporulating secondary plasmodium. n: pathogen nucleus
(F) Details of peripheral vacuole 3 (pv3) in (B) with a degenerated host amyloplast and taking in plasmodial cytoplasm by vacuole membrane invagination.
(G) A degenerated amyloplast bounded by a double membrane.
(H) A nucleus in red square in (B) showing paired centrioles in meiosis I interphase or prophase. ce: centriole.

During sporogenesis, the meiotic nuclear divisions characterized by the formation of chromosome synapsis in prophase I were only observed in sporulating plasmodia either immediately preceding or during initiation of cleavage of the cell into future immature resting sporangia (Fig. 4.15H, 4.16A, B). Nuclei containing synapsis had a pair of centrioles, at each pole, that were tethered to one another in an end-to-end orientation (Fig. 4.15H, Garber and Aist 1979b). Like mitosis in *P. brassicae*, meiosis was also intranuclear with the pathogen nuclear envelope remaining intact during prophase I (Fig. 4.14, 4.15, 4.16). The second meiotic division was distinguished from the first division by the structure of the centrosomes. The centriole within the centrosomes did not remain paired throughout the second division (Fig. 4.17). A single centriole was associated with each nuclear pole at late prophase II and the microtubules were starting to radiate away from the centriole (Fig. 4.17A, a). The nuclear envelope was still intact. At metaphase II and thereafter, the nucleus elongated (Fig. 4.17B-D) and the chromatin was aligned in a distinct metaphase plate (Fig. 4.17B). The bipolar, unpaired centrioles became elongated and were oriented with their long axis nearly parallel with the spindle axis, rather than at right angles as was the case during meiosis I and prophase II (Fig. 4.17 B; Garber and Aist 1979b). Thus, re-orientation of the individual centrioles must occur between prophase II and metaphase II. The nuclear envelope was still present in metaphase II, although it was disrupted at the poles by centrioles and microtubules also penetrated the nuclear envelope at these regions (Fig. 4.17B, b). In anaphase II, the chromasomes at the metaphase plate divided and separated. The nucleolus was reformed at the equator and was not incorporated into the nucleus at telophase (Fig. 4.17C, c). During telophase II, a new nuclear envelope was formed within the confines of the old nuclear membrane, which was broken down (Fig. 4.17D, d).

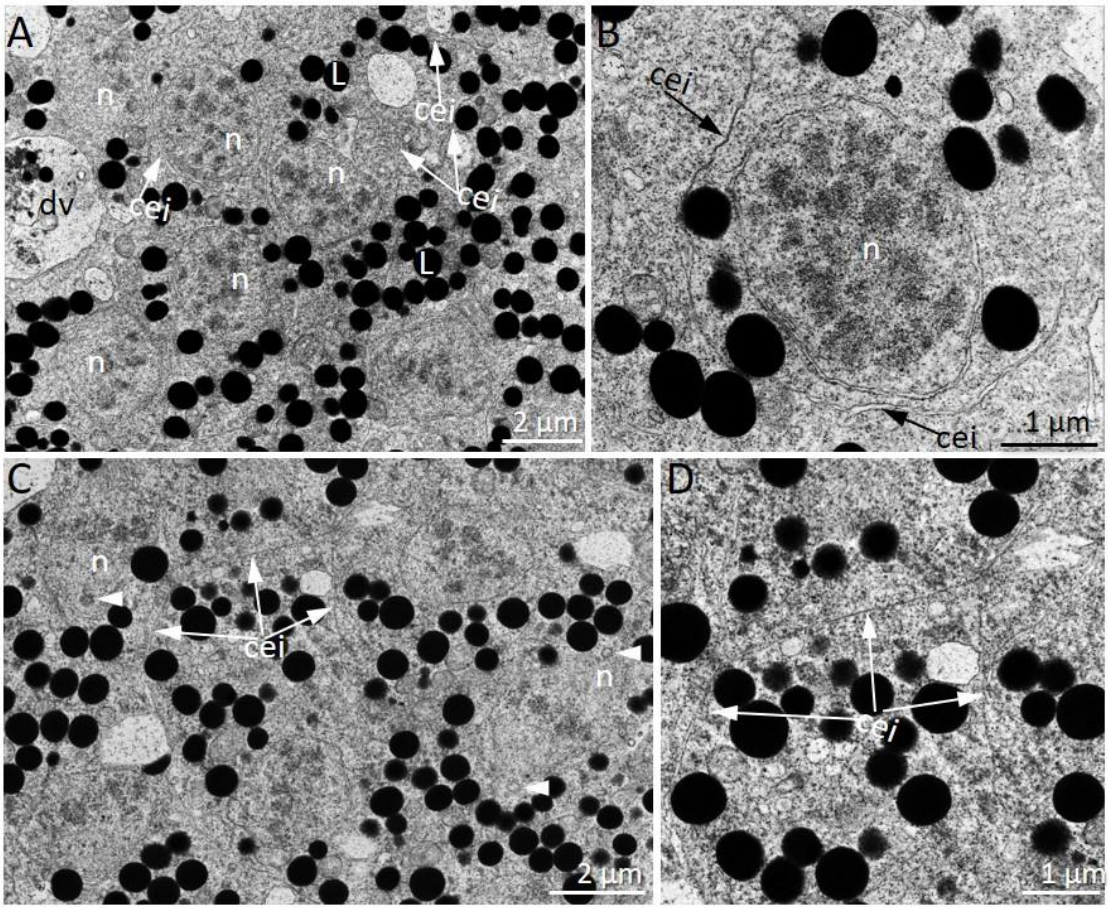

Figure 4.16 Cleavage element initials in sporulating secondary plasmodia undergoing meiosis I at 24 dpi.

(A) Cleavage element initials (CEI) starting to divide up the cytoplasm, in a sporulating secondary plasmodium undergoing meiosis prophase I. Note the digestive vacuole (dv) and large number of lipid droplets (L). n: nuclei in prophase I.

(B) Magnified image of cleavage element initial (CEI) associated with the nuleus (n) in prophase I, in the same sporulating plasmodium as seen in (A). Cleavage element initials are paired membrane sheets with an electron-lucent lumen. Note that the nucleus in prophase I shows dispersed chromatin masses.

(C) Cleavage element initials (CEI) in a sporulating secondary plasmodium undergoing meiosis metaphase I. n: nucleus in metaphase I showing chromasomes aligned on the metaphase plate. Arrowhead: centrosome at each nuclear pole.

(D) Magnified image of cleavage element initials in (C).

Each nucleus in sporulating secondary plasmodia completes meiosis to produce haploid immature resting spores (Garber and Aist 1979b; William and McNabola 1967). During meiosis I the spindles arise from a pair of centrioles at each pole while during meiosis II, the spindles arise from a single centriole at each pole, indicating that only a single round of centriole duplication takes place before prophase I. Centriole duplication likely accompanies DNA synthesis. In this study, the coordination of multiple cleavage elements with meiosis in sporulating secondary plasmodia is suggested.

In contrast to the lack of vacuolated areas in vegetative secondary plasmodia, vacuoles as well as cleavage element initials (CEIs) started to appear in sporulating secondary plasmodia in prophase I (Fig. 4.16A, B) and aligned around individual nuclei that were undergoing meiosis (Fig. 4.16, Fig. 4.17), where they defined the boundaries along which cleavage into resting sporangia will occur. Chromosome synapsis was observed either immediately preceding or during the initiation of cytoplasmic cleavage into future resting sporangia. CEIs are electron-lucent membranous bilayers, morphologically similar to a single array of perinuclear ER in the vegetative secondary plasmodia. CEIs were generally long and slender throughout the plasmodium cytoplasm in early stages of cytoplasmic cleavage. In the early stage of cytoplasmic cleavage, CEIs surround a nucleus domain as a ring. Cleavage element elongation was coincident with nuclear meiotic division, which formed extensions into the cytoplasm and became considerably branched in late stages of meiosis. There is no ultrastructural evidence supporting a prealignment of vesicles along the leading edge of the cleavage elements, as suggested by Williams and McNabola (1967). Cleavage as identified in this study, is more likely the result of progressive extension and expansion of the partitioning membrane, along future subdivision boundaries, without any observed prealignment of vesicles. Vesicles were identified in the preliminary cleavage process but never aligned along the future resting spore boundaries (Fig. 4.15, Fig. 4.16). As meiosis proceded, the cleavage network became increasing ordered. Cleavage progressed as the partitioning membranes continued to extend throughout the cytoplasm, interconnecting with each other to delineate the future resting sporangia (Fig. 4.16, Fig. 4.17). The vacuoles in early sporulating secondary plasmodia disappeared during the cleavage (Fig. 4.17). The fate of the vacuoles was not clear, but some of them will have fused with CEIs to form complete cleavage elements and some will have developed into digestive vacuoles for cleaning up residual bodies of the sporulating secondary plasmodia as well as host organelles (Fig. 4.16B, D, F, Fig.4. 17A), that were taken up by *P.*

brassicae. Resting sporangia were delineated by cleavage element activity resulting from expansion of the lumen between cleavage elements as well as membrane fusion with vacuoles and plasma membrane (Fig. 4.17D, d).

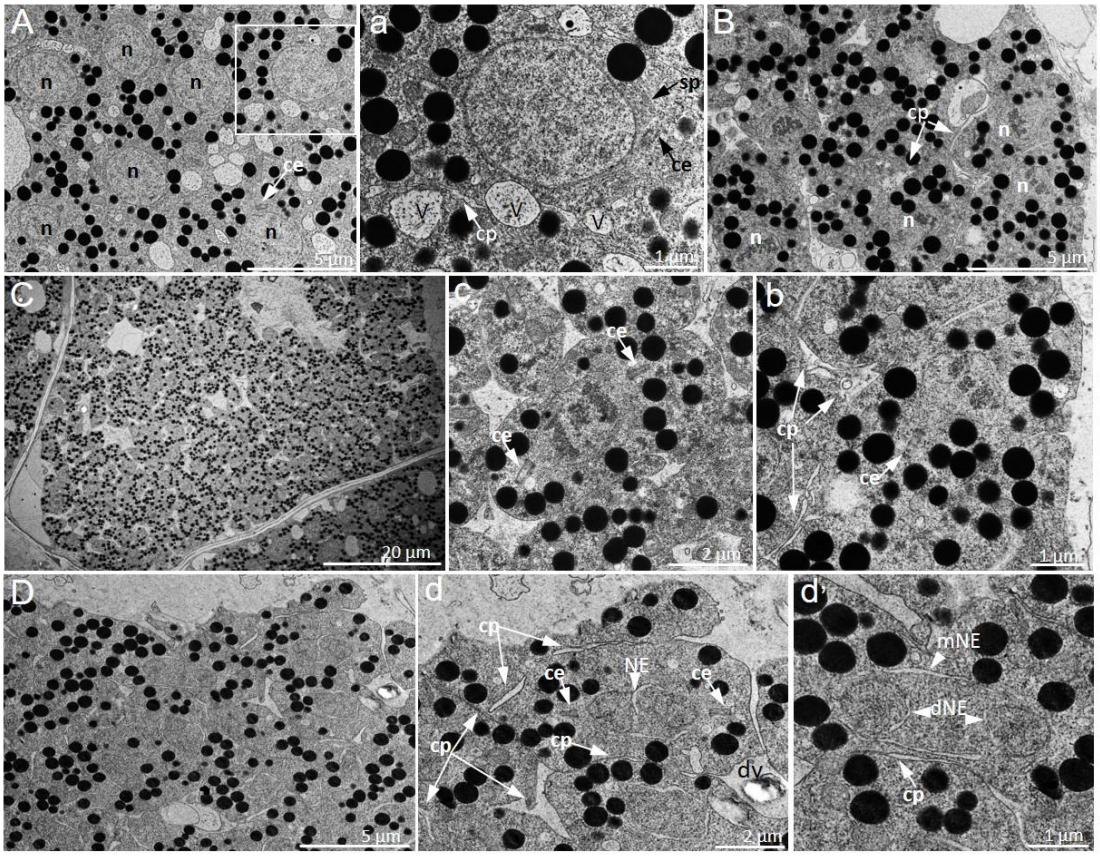

Figure 4.17 Sporulating secondary plasmodia with advanced cleavage elements in meiosis II at 24 dpi.

(A) Sporulating secondary plasmodium with nuclei (n) at various stages of meiosis II. (a) Magnified image of nucleus in white square in (A) with a single centriole (ce). Note that the cleavage plane (cp) was fused with vacuoles (V). sp: spindles

(B) Sporulating secondary plasmodium with nuclei (n) in metaphase II with internal cleavage planes (cp) fully organized and border uninucleate domains in metaphase II. (b) Details of internal cleavage planes (cp) and nucleus in metaphase II in (B).

(C) Sporulating secondary plasmodium with nuclei in anaphase II. Delimitation of resting sporangia into spindle-shaped cells was near completion in this sporulating plasmodium. (b) Magnified image of a nucleus in anaphase II in (C) showing cleavage planes were fully organized and border a uninucleate domain.

Fig. 4.17 cont.

(D) Sporulating secondary plasmodium with nuclei in late telophase II. (d) Detailed nucleus in (D) in late telophase II with cleavage planes surrounding it. Note the cleavage plane fused with both a digestive vacuole (dv) with degenerated amyloplast and plasmodial membrane. (d') Detailed nucleus in late telophase II with daughter nuclear envelope (dNE) formed within the confines of the old nucleus. mNE: mother nuclear envelope.

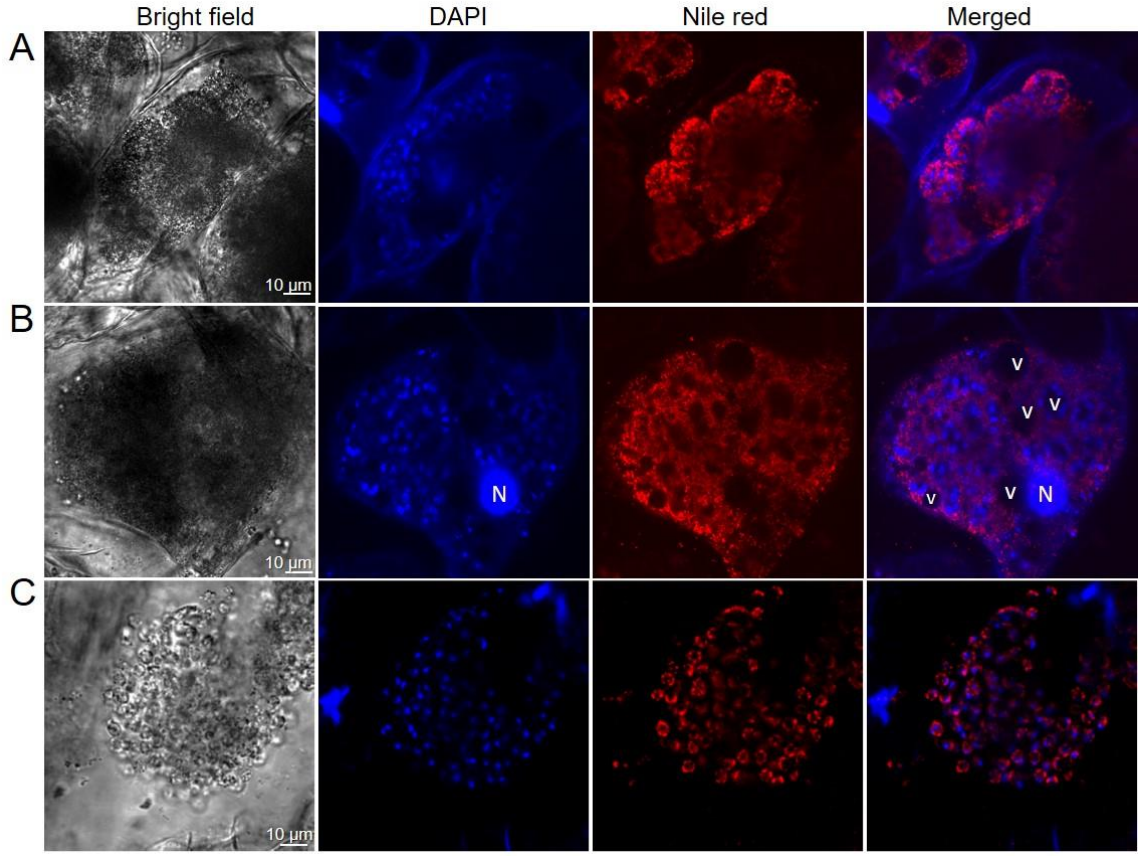

Figure 4.18 LSCM of resting sporogenesis in sporulating secondary plasmodia stained with DAPI and Nile red at 24 dpi.

(A) Multiple sporulating secondary plasmodia connected with each other at the membrane fusion stage (identified as the equivalents of membrane fusion stage observed by TEM of Fig. 4.15).
(B) Larger sporulating plasmodia labeled with DAPI and Nile red. The larger sporulating plasmodium were identified as the equivalents of meiosis stages of Fig. 4.16 and Fig. 4.17.
(C) Young resting sporangia after completion of meiosis in sporulating plasmodium.

4.3.4 Coupling of gene expression to pathogen morphology during the *P. brassicae* life cycle

In view of the cytological and morphological changes observed during the primary and secondary infections, differentially expressed genes (DEGs) used as markers to indicate different development stages during the *P. brassicae* life cycle, were expected to be indentified. The eight-time points: 0, 2, 5, 7, 10, 14, 21 and 28 dpi, corresponding to different clubroot development stages (see earlier), were chosen for this study.

A long-standing misconception in clubroot research has been that a multinucleate primary plasmodium develops from a uninucleate haploid primary zoospore by repetitive cruciform divisions and that the resulting multinucleate primary plasmodium then cleaves into many zoosporangia. This is not the case. Instead, I have confirmed that a uninucleate primary plasmodium undergoes nuclear division *in situ* to form a thin walled tetranucleate zoosporangium, that develops into a mature zoosporangium with four fully developed secondary zoospores (Fig. 4.4-Fig. 4.8). The presence of the tetranucleate zoosporangia in this chain-like arrangment suggests that the primary plasmodium has undergone either a single round of DNA replication followed by meiosis and cytokinesis, or two rounds of endomitosis (nuclear division without cytokinesis) followed by a final cytokinesis. If one round of meiosis is the case, the expression of meiosis-related genes should be detected during the primary infection stages between five dpi and 10 dpi.

Cellular studies above identified flagellar assembly during zoosporogenesis between five dpi and 12 dpi and suggested meiosis in sporulating secondary plasmodia between 24 dpi and 28 dpi. To support the observation of meiosis in sporulating secondary plasmodia, the full complement of known genes required for meiosis were identified in the *P. brassicae* genome (http://protists.ensembl.org/Plasmodiophora_brassicae/Info/Index; Schwelm et al. (2015)). Of these meiosis-related genes, nine are meiosis-specific (Ramesh et al. 2005; Schurko and Logsdon 2008; Weedall and Hall 2015; Table 4.1). To confirm meiosis in sporulating plasmodia, expression of the nine putative conserved meiosis-specific genes was analyzed during the pathogen life cycle.

Table 4.1 Putative meiosis specific genes in the *P. brassicae* genome.

Gene ID	Super Family	Conserved Domain	Protein Function	Name
PBRA_008131	TP6A_N&TOPRIM	cd00223	Transesterase; creates DNA double-strand breaks (DSBs) in meiosis I.	*SPO11*
PBRA_001543	HORMA	pfam02301	Binds to DSB and oligomerizes early during meiotic prophase, forming axial and lateral elements of the synaptonemal complex.	*HOP1*
PBRA_002842	Mnd1	pfam03962	Functions after meiotic DSB formation and is required for stable heteroduplex DNA formation and interhomolog repair.	*MND1*
PBRA_000515	TBPIP	pfam07106	Forms heterodimer with MND1, ensuring accurate and efficient homology searching.	*HOP2*
PBRA_000023	Rad51	PTZ00035	DMC1 and RAD51 co-localize during meiosis and cooperate during meiosis recombination. RAD51 is required for mitotic recombination, DNA damage repair, and in meiosis. DMC1 is a meiosis-specific homolog of RAD51 and is essential for meiotic recombination and normal synaptonemal complex formation. RecA is a bacterial enzyme which has roles in homologous recombination, DNA repair, and the induction of the SOS response. RecA couples ATP hydrolysis to DNA strand exchange and homologues to RAD51 and DMC1.	*DMC1/ RAD51*
PBRA_001343	Rad51	PTZ00035		
PBRA_000359	RecA_like NTPases	cd01123		
PBRA_007671	RecA_like NTPases	cd01123		
PBRA_000211	RecA_like NTPases	cd01123		
PBRA_000929	RecA_like NTPases	cd01393		
PBRA_002628	RecA_like NTPases	cd01393		
PBRA_008811	Rad21_Rec8_N	pfam04825	Holds sister chromatids together during mitosis and meiosis. REC8 is a meiosis-specific homolog of RAD21.	*REC8/ RAD21*
PBRA_002411	Rad21_Rec8_N	pfam04825		
PBRA_009486	MutS_III	COG0249	MSH4 and MSH5 form a heterodimer and have a role in meiosis recombination and Holliday junction resolution.	*MSH4*
PBRA_002186	MutS_III	COG0249		*MSH5*
PBRA_001485	MutS_III	COG0249	Forms heterodimer with MSH6, works in DNA mismatch repair.	*MSH2*[a]
PBRA_005360	MutS_III	COG0249	Forms heterodimer with MSH2, works in DNA mismatch repair.	*MSH6*[a]

Table 1. cont.

Gene ID	Super Family	Conserved Domain	Protein Function	Name
PBRA_000197	BRR2	COG1204	Meiosis-specific DEAD-box helicase that promotes Holliday junction resolution with crossover interference together with ZMM, including MSH4 and MSH5.	*MER3*
PBRA_008782	BRR2	COG1204		
PBRA_006359	BRR2	COG1204		

[a] indicate non-meiosis-specific gene

In-planta expression profiles of the meiosis-specific genes, over the *P. brassicae* life cycle in *A. thaliana*, were determined by RT-PCR using *AtACTIN7*, *PbACTIN1*, *PbCC249* (S17 ribosomal gene) and *PbCC243* (S17 ribosomal gene) as internal controls (Siemens et al. 2009). *P. brassicae ACTIN1* gene and S17 ribosomal genes (*PbCC249* and *PbCC243*) were expressed and detectable as early as two dpi when the pathogen was in the primary plasmodium stage and strongly upregulated during the secondary infection stages (Fig. 4.19). As such, all three genes were used as markers of pathogen biomass. The highest transcript accumulation for most meiosis-specific genes was detected at 28 dpi, except for genes PBRA_008811 (*Rad21-1*), PBRA_007671 (*Rad51-1*), that may be involved both in mitosis and meiosis. However, the expression profiles of the non-meiosis specific genes, PBRA_001485 (*MSH2*) and PBRA_005360 (*MSH6*), confirmed that the pathogen amplifies itself by nuclear division from very early developmental stages at two dpi. The expression pattern of meiosis-specific and non-specific genes confirmed that meiosis only occured during the late stages of the life cycle when resting spores were formed and suggested indirectly that tetranucleated zoosporangia were produced by two rounds of mitosis (Fig. 4.19).

A significant number of genes encoding hypothetical flagella assembly proteins have also been identified in the *P. brassicae* genome. Two were selected to confirm their *in-planta* expression profile: PBRA_000175 and PBRA_000434. The expression pattern of PBRA_000175, which encodes a hypothetical protein orthologue with central pair complex (CPC1/KPL2) in *Naegleria gruberi* (GenBank accession no. XP_002683128; e value: 1e-16) and the mouse sperm flagella protein 2 (SPEF2) (GenBank accession no. NP_072142; e value: 2e-11), correlated with the appearance of flagella in zoosporangia at seven to 10 dpi and resting sporangium formation at 28 dpi. PBRA_000434, encoding intraflagellar transport protein (IFT172), which in protists is thought to be important for flagellar assembly and maintaining flagella length, was highly expressed at very late, 28 dpi, infection stages. This expression pattern of IFT172 in resting spore formation stage rather than zoosporogangium stage suggested that flagella assembly during zoosporogenesis may occur in the cytoplasm, a rare phenomenon shared between the malaria parasite *Plasmodium* and *Chromera velia* classified in superphylum Alveolata, in which the canonical mode of flagellar assembly and intraflagellar transport is dispensed with (Sinden et al. 2010; Portman et al. 2014) or IFT172 have more than one function in intraflagellar transport (Taschner and Lorentzen 2017) . The differential expression of these genes during the infection process suggests their involvement in specific life cycle process of *P. brassicae*, therefore they could be used as *P. brassicae* stage

specific molecular markers.

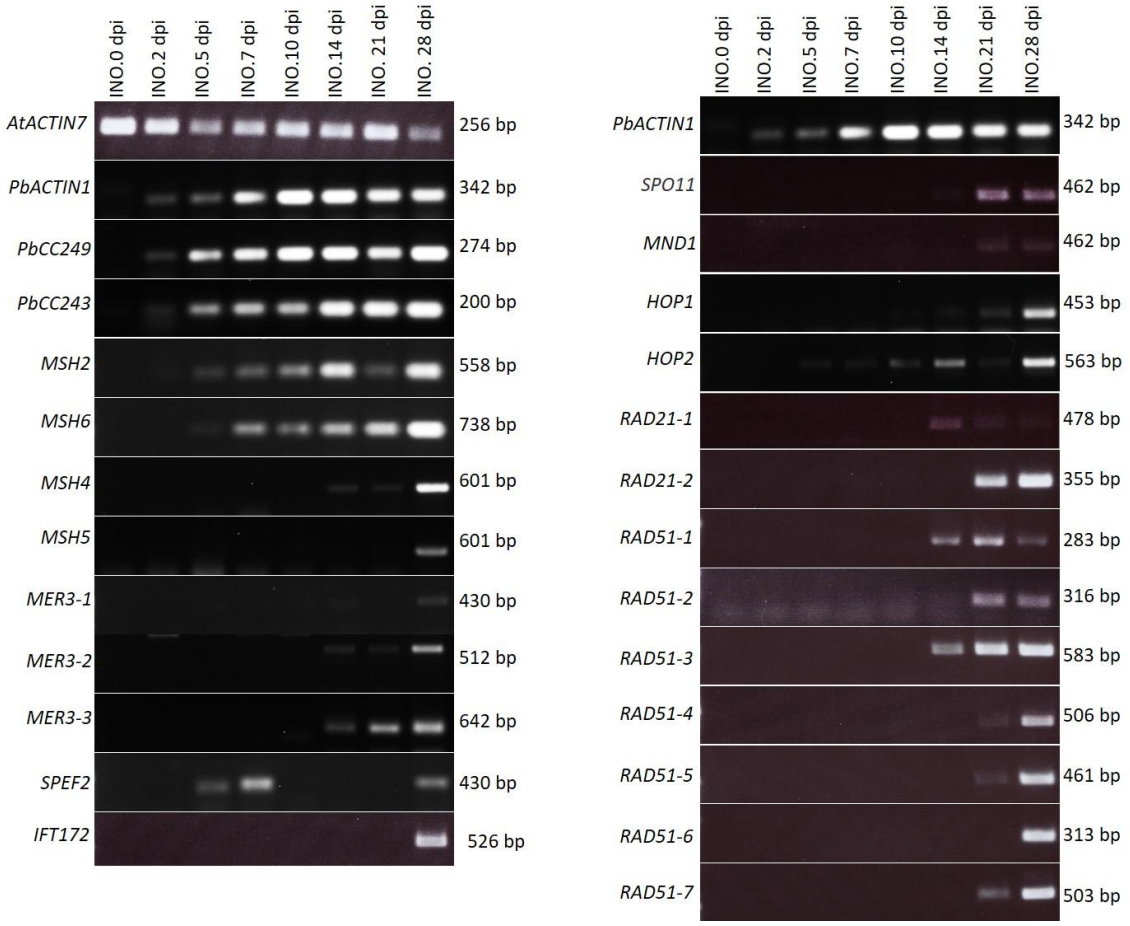

Figure 4.19 Expression of meiosis- and flagella-related genes during the *P. brassicae* life cycle.

Amplicons were visualized after electrophoresis on agarose gels and ethidium bromide staining. Arabidopsis *ACTIN 7* was used as an internal control of equal total RNA in all samples for RT-PCR. The *PbACTIN1* and S17 ribosome protein genes (*PbCC249* and *PbCC243*) were used as references to allow for variation in *P. brassica*e biomass. Each RT-PCR was performed three times using RNA samples from three independent experiments.
INO: inoculated. dpi: days post inoculation.

4.4 Discussion

4.4.1 The advantages of a combined microscopic approach

The aim of this study was to provide a timetable of *P. brassicae* development in terms of microscopically recognizable features, which can be related to clubroot pathogen diagnosis *in planta*. In this study we have combined the high resolution of electron microscopy providing the ultrastructure of the pathogen with the assessment of larger *P. brassicae* numbers by confocal live cell imaging to monitor and dissect the life cycle of *P. brassicae*. This combined approach was crucial to achieve reliable and complex data on the life cycle of *P. brassicae*. It is clear that throughout the *P. brassicae* life cycle the pathogen adopts many forms within host cells, that makes it extremely difficult to differentiate host cell organelles from the pathogen using standard light microscopy. This remains the single biggest impediment to furthering the understanding the pathology of this pathogen.

Preparation of the samples for TEM proved to be a challenge during the primary infection stage, due to the small number of infected host cells together with the small size of the pathogen. A breakthrough was achieved with the combination of TEM and confocal microscopy. During the primary infection stages, uninucleate primary plasmodia, young uncleaved zoosporangia, young cleaved zoosporangia and mature zoosporangia were morphologically very similar under light microscopy, but they could be distinguished by differential fluorescent dye staining. There was a major difference in FM4-64 staining patterns for primary plasmodia and zoosporangia. Whereas uninucleate primary plasmodia (one nucleus stained by DAPI) and uncleaved zoosporangia (multiple nuclei stained by DAPI) were brightly fluorescent as a result of internal FM4-64 staining, young cleaved zoosporangia (four nuclei stained by DAPI) and mature zoosporangia (defective in DAPI staining) were closely outlined by a thin layer of FM4-64 fluorescence and lacked internal FM4-64 fluorescence. DAPI stained the nucleus in primary plasmodia as well as nuclei in young zoosporangia except for the nuclei in mature zoosporangia. In TEM images, it is apparent that mature secondary zoospores in zoosporangium contain nuclei. The reasons for the loss of DAPI staining during zoospore maturation is unknown. It may be the result of nuclear changes during zoospore maturation or changes in membrane permeability during zoosporangium maturation, that inhibit DAPI reaching mature zoospores. Double staining with DAPI and FM4-64 of *P. brassicae* in the primary infection stages enabled visualization of pathogen development within the root tissue and to link it to electron microscopy studies. In conclusion, the live cell staining and confocal

imaging established here will enable distinguishing zoosporangium from primary plasmodium in future disease diagnosis.

Previously it had been suggested that once within host cells the contents of a primary zoospore grow by cruciform endomitotic divisions to form a multinucleate primary plasmodium (Bulman and Braselton 2014). Whether the division is an endomitotic division in a uninucleate primary plasmodium to develop into a multinucleate primary plasmodium and then cleaved into multiple zoosporangia, or open mitotic divisions to increase the pathogen number and two rounds of endomitotic division in each unicleate primary plasmodium to produce tetranucleate zoosporangium, remains unknown. Unfortunately, confocal imaging technique established in this study could not provide the resolution for the determination of the mitotic division or meiotic division in primary plasmodia (Fig. 4.4). However, it does establish in a population of pathogen an approximate time-frame for change in a number of important features including change in nuclei number, change in membrane permeability, cytoplasmic cleavage in multinucleate zoosporangia and secondary plasmodia and resting spore formation and maturation. These can be related broadly to the corresponding TEM data gathered from a necessarily smaller number of pathogen. Important events are still missed if confocal live cell imaging is solely used. Even in the era of live cell imaging, electron microscopy analysis remains a useful tool in the examination of pathogen development in great details. For example, TEM in this study provided the ultrastructure of secondary zoospores with flagellar assembly in a zoosporangium, phagocytosis in the secondary plasmodia using a "phagocytosis cup" and different cytoplasmic cleavage models in the multinucleate pathogen stages, that have not previously been recorded. However, sample size and preparation are a constraint and such static imaging does not allow a full understanding of how the parasite develops. Therefore, a comparison with *P. brassicae* development in time-series samples by TEM and confocal microscopy enabled live cell imaging is helpful and promising to define reference points of *P. brassicae* development. Crucially, the use of corresponding serial time-points allowed me to determinate the developmental stage of the pathogen.

4.4.2 Haploid-diploid sexual life cycle

P. brassicae, like many protists, has a complicated life cycle in which nuclear ploidy and development phases may be coupled. A unique type of cruciform nuclear division has been observed in secondary plasmodia (Garber and Aist 1979a; Bulman and Braselton 2014) and a

meiotic process has been observed in late stage secondary plasmodia with the ultimate production of resting spores in roots of Chinese cabbage (Garber and Aist 1979b), suggesting *P. brassicae* has a sexual life cycle (Agrios 2005; Dobson et al. 1983), where haploid secondary zoospores fuse to form binucleate secondary zoospores (prior to secondary infection of the root) that then develop into diploid secondary plasmodia capable of infecting root cortical cells. Only diploid secondary zoospores can infect root cortical cells, whereas primary infection of a root hair or epidermal cell is restricted to haploid primary zoospores (Agrios 2005; Dobson et al. 1983). Other researchers have proposed an asexual life cycle for *P. brassicae* because it is genetically stable through three generations of progeny (Heo et al. 2009).

In this study, an unisexual life cycle of *P. brassicae* is suggested, that involves the alternation between a haploid primary infection cycle and a diploid secondary infection cycle. The alternation between primary infection and secondary infection constitutes the sexual cycle. In previous studies, and confirmed in this study, resting spores are haploid and produced by meiosis of secondary plasmodia (Garber and Aist 1979b; Fig. 4.15, Fig. 4.16, Fig. 4.17, Fig. 4.19). A haploid resting spore germinates into a haploid primary zoospore (Tanaka et al. 2001), that initiates primary infection. Secondary zoospores are produced in zoosporangia developed from primary plasmodia, which was the first intracellular pathogen structure recorded in this study. While unable to observe any changing pathogen structures from primary zoospore to primary plasmodium, my study presents multiple lines of evidence to support a haploid asexual primary infection stage followed by a diploid sexual secondary infection stage: (1) Haploid resting spores produced by meiosis germinate and give rise to haploid primary zoospores (Garber and Aist 1979b; Tanaka et al. 2001). The morphology of zoospores during primary zoosporogenesis and secondary zoosporogenesis is very similar, suggesting that both primary zoospores and secondary zoospores produced by zoosporogenesis, are haploid. (2) Zoosporangia were regularly observed (TEM) containing four daughter cells (secondary zoospores), while smaller uninuclate or binucleate zoosporangium structures were infrequently observed in primary infection, indicating the tetranucleate zoosporangia were produced by two rounds of endomitotic division rather than one round of meiotic division of primary plasmodia, confirmed by meiosis-specific genes not being expressed in primary infection stages. (3) Similar to the haploid immature resting sporangia after meiosis II, secondary zoospores and zoosporangia also lack nucleoli. The absence of nucleoli may reflect the inability of the haploid stage to support the production and organization of a nucleolus. (4)

Expression of PBRA_000175, a gene that putatively encodes a sperm flagellar protein 2, occurs in the zoosporangia and resting spore formation stages, suggesting that both zoosporangia and resting spores are in gamete stages. (5) The meiotic division observed (TEM) in sporulating plasmodia and the expression of meiosis-specific genes at 28 dpi correlated with the production of resting spores from sporulating plasmodia, providing direct evidence of a sexual life cycle. The meiosis-specific genes were not expressed around the time points when zoosporogenesis occurred (between five dpi and 10 dpi) during primary infection, however, non-meiosis-specific genes were expressed around the times points when zoosporogenesis occurred, suggeting an unsexual primary infection process. (6) Haploid secondary zoospores to diploid secondary plasmodia would require diploidization to occur, however, this process has not been observed. In resistant host and non-host plants, the pathogen can complete the primary infection with the production of secondary zoospores, but fusion of secondary zoospores and meiosis, necessary for a complete *P. brassicae* life cycle, have not been observed.

Indicators of true sexual reproduction, consisting of physical observation of cell and/or nuclear fusion, cytological or genetic evidence for meiosis and/or recombination, or change in ploidy levels during the life cycle are found only in eukaryotes. However, completion of a sexual cycle, i.e., plasmogamy (gamete fusion) and karyogamy (nuclear fusion), remains to be demonstrated in *P. brassicae*. Furthermore, direct fusion of both secondary zoospores and nuclei in *P. brassicae* has yet to be reported, probably because fusion of secondary zoospores would occur outside of an obligate parasitic stage and has proven difficult to *in vitro* culture for this parasite. In protists, plasmogamy and karyogamy have received very little attention to date, although the membrane fusion factor, HAPLESS 2 (HAP2) (also called GENERATITIVE CELL SPECIFIC 1 (GCS1)) has been implicated in plasmogamy in eukaryotes distantly related to *P. brassicae* (Wong and Johnson 2010; Liu et al. 2015). The GAMETE EXPRESSED PROTEIN 1 (GEX1) protein family (yeast ortholog: KAR5) represents a potentially conserved karyogamy factor in eukaryotes (Ning et al. 2013). However, neither of these genes have been identified in the *P. brassicae* genome. The observed fusion between zoosporangia walls during primary infection and between sporulating plasmodia membranes during secondary infection indicates that *P. brassicae* is capable of membrane and cytoplasmic fusion, although it is unclear whether karyogamy also occurs when these cells fuse. The cues that trigger cell to cell fusion remain to be indentified.

Dimorphic male and female gametes have not been observed in the *P. brassicae* life cycle, and

mating type loci also have not been identified in the *P. brassicae* genome. However, the meiotic production of resting spores, coincident with the expression of meiosis-specific genes, was observed in this study. It is speculated that *P. brassicae* is a unisexual organism, with the selfing of two identical haploid gametes (two zoospores of *P. brassicae*) to produce a diploid zygote, that subsequently undergoes multiple rounds of mitosis and one final round of meiosis to produce haploid gametes (resting spores) to complete the life cycle. Thus by unisexual reproduction, a single-spore isolate of *P. brassicae* can differentiate and undergo sexual reproduction to complete its life cycle without a sexual partner (Fähling et al. 2004; Xue et al. 2008). Locating a compatible partner and undergoing mating requires time and energy. In addition, sexual reproduction introduces genetic diversity, but in so doing rearranges well-adapted genomic configurations. In contrast, sexual reproduction involving cells of the same type (unisexual reproduction), lowers the barrier to locating a compatible mating partner and ameliorates the cost of losing a well-adapted phenotype while introducing more limited genetic diversity that may enhance the fitness of progeny in response to environmental changes.

4.4.3 Nutrition acquisition

The loss of key biosynthetic pathways is a common feature of parasitic protists, making them heavily dependent on scavenging nutrients from their hosts. There are a limited number of strategies by which intracellular pathogens can divert host nutrients. Such mechanisms depend, in part, on the intracellular locale of the organism within the host. For pathogens living freely in the host cytosol, diffusion and/or transport of host molecules across the plasma membrane or endocytosis of macromolecules from the host cytosol can occur. A few nutrient transporter encoding genes have been indentified in the *P. brassicae* genome (Rofle et al. 2016), however, their functions in nutrient transport remain unknown.

Clubroot symptoms result from the effects of pathogen replication in host cortical cells as well as affects on the functional activity of these cells. Parasitization of host cells results in a nutrient enriched host cytoplasm compared to uninfected neighboring host cells, including accumulation and relocalization of host mitochondria and amyloplasts to the pathogen. In this study, three independent, distinguishable temporally and morphologically, processes for efficient nutrient acquisition by *P. brassicae* have been identified. These processes most likely originated in unicellular protists as means to obtain nutrients from their external environment.

During secondary infection, *P. brassicae* structures increased in volume by more than 100 fold, from one µm diameter secondary zoospore (Fig. 4.7) to 50 µm individual sporulating plasmodium (Fig. 4.15). Over this time period more than 80% of the host cytoplasm is digested to support the asexual growth and sexual replication of the parasite. During the early stage, the myxamoeba at 14 to 17 dpi use pseudopodia extensions to engulf host cytoplasm and organelles and form digestion vacuole, that enables net lipid synthesis within the pathogen. This process is more akin to classical phagocytosis. Vegetative multinucleate plasmodia around 21 dpi create long thin tubular invaginations through the plasma membrane into the cytoplasm to which numerous host organelles attach. Sporulating plasmodia from 24 to 28 dpi fuel meiosis and cytoplasmic cleavage through food vacuoles arising from plasmodial membrane invagination resulting in the ingestion of host cytoplasm and organelles into peripherally or centrally located food vacuoles. Phagotrophic ingestion resulting in peripherally located food vacuoles has been previously observed in sporulating plasmodia of *P. brassicae* (Williams and McNabola 1967). During these three processes the plasmodial membrane, the interface between host and parasite, was very convoluted or invaginated, producing a large surface area for uptake of host cell contents. Host amyloplasts were routinely observed in resulting food vacuoles. Unlike many biotrophic pathogens, the genome of *P. brassicae* does not contain any genes for extracellular invertases that would degrade host apoplastic sucrose (Rolfe et al. 2016). It therefore makes sense that *P. brassicae* takes in host amyloplasts and starch granules as carbohydrate resources. The uptake of host DNA by *P. brassicae* (Bryngelsson et al. 1988) may also result from the observed host content uptaking processes.

Whether the mechanisms of these three morphologically and chronologically distinct nutrient acquisition processes, are the same or not remains largely unknown. Phagocytosis, while required for pathogen survival, also contributes to the pathogenesis of the pathogen by degrading host cell contents. Inhibiting phagocytosis would be a very interesting means of controlling pathogen proliferation and subsequent disease progression.

4.4.4 Distinct cell division cycles within the *P. brassicae* life cycle

Cell cycle is defined as the period between the formation of a cell from the division of its mother cell to the time it divides to form two daughters. During this period, DNA replication is followed by equal segregation of the chromosomes, nuclear division, and lastly cytokinesis of the cell. This

process is somewhat different in *P. brassicae*, since its parasitic form of replication leads to the formation of multinucleate cells, such as the zoosporangia in root hairs and epidermal cells and multinucleate secondary plasmodia in cortical cells. *P. brassicae* nuclear division is thus not immediately followed by cytokinesis. In this study, cell division cycles have been observed occurring at least at four different time points. The dividing forms include: (i) the uninucleate primary plasmodium, resulting from the primary zoospore after release from a haploid resting spore, undergoes a few rounds of mitosis to increase its numbers, (ii) zoosporangium, where two rounds of mitosis produce a tetranucleate zoosporangium from a uninucleate primary plasmodium followed by final cytoplasmic cleavage to produce four secondary zoospores, (iii) diploid uninucleate or binucleate vegetative secondary plasmodium, resulting from the fusion of two secondary zoospores released from zoosporangia, undergo a few rounds of mitosis in the cortical cell to form a multinucleate sporulating secondary plasmodium, and (iv) the diploid multinucleate sporulating plasmodium undergoes one meiotic division to produce haploid resting spores that can survive in the soil for up to 20 years.

4.4.4.1 Nucleus division

P. brassicae divides by mechanisms that are quite different from its host plants. First, plants lack centrioles, while *P. brassicae* similar to mammalian cells, has bipolar centrioles. In animals and fungi, the centrosome is comprised of two centrioles and functions to organize cellular microtubules and cell division. Centrioles ensure the stability, duplication and separation of chromosomes. In this study, I show that in *P. brassicae*, during mitosis and meiosis I, both poles of the spindle contain a pair of centrioles and the centrioles are paired end-to-end, in contrast to the orthogonal arrangement that is found in most mammalian cells (Pearson 2014). Between meiosis I and II, the centrioles, retained in the secondary division, split without duplication resulting in each pole of the meiosis II spindle containing only one centriole that is oriented with its long axis nearly parallel with the spindle axis. The centrioles are also analogous in their triplet microtubule organization reflecting the basal body of a eukaryotic flagellum. All life cycle stages of *P. brassicae*, except for zoospores (both primary and secondary) lack flagella. It is unclear whether the basal bodies of flagella are derived from pre-existing centrioles or are synthesized *de novo*. As a parasitic protist, it is probable that pre-existing centrioles become flagella basal bodies directly to save energy over *de novo* synthesis of basal bodies.

Since both centrioles and flagella are present in the *P. brassicae* life cycle, a correlation is suggested between the presence of the centrioles/basal body and centriole-containing centrosomes during the primary infection stages. During cell division in zoosporangium initiates, the spindle ensures equal separation of the chromosome and the sister chromatids into the daughter cells. The localization of a centriole at each of the poles of the spindle suggests a strategy by *P. brassicae* to ensure equal inheritance of these structures such that all daughter cells are able to produce flagella. Mixed flagellate and non-flagellate progeny were never observed emerging from a single zoosporangium. The production of flagellate secondary zoospores occurred through the production of four daughter cells from a zoosporangium and not by the transformation of a single daughter cell from non-flagellate to flagellate. Basal bodies with associated flagellar axonemes are assembled only during primary and secondary zoospore production. These are both invasive forms of the pathogen, especially secondary zoospores that mark the transition from primary to secondary infection and evoke clubroot disease. As seen in both resistant lines and non-host plants, primary infection is symptomless and it is the transition from primary to secondary infection that is important for subsequent disease development. Mobile secondary zoospores, with flagella, play a vital role in this transition. Given that host plant cells lack centrioles, the presence of centrioles/basal bodies in zoospores provides a potential parasite-specific drug target for inhibiting pathogen invasion and the transition from primary to secondary infection.

P. brassicae cell division occurs in a manner that is quite different from that of its plant hosts. In typical plant cell division, nuclear envelope breakdown/fragmentation occurs during prophase, followed by the rest of the cell division process. Unlike plants, *P. brassicae* has closed cell divisions, without nuclear envelope breakdown, but with polar fenestrae or openings at opposite sides of the nuclear envelope, apparent at metaphase, that provide nuclear access by spindle microtubules. The new nuclear envelope for progeny nuclei is formed from the old nuclear membrane of the mother cell, while in host plant cells that disperse the nuclear envelopes (open mitosis) a new nuclear membrane is formed around each daughter nucleus.

Nuclear divisions in secondary plasmodia, are usually slightly asynchronous and hence the persistence of the nuclear envelope during nuclear division would prevent any intermingling of the meiotic spindles and reduce the possibility of subsequent chromosome imbalance in the daughter cells. It could also be proposed that intranuclear meiosis serves to maintain the internal environment of the nucleus by preventing direct contact between the nucleoplasm and the

cytoplasm. In the multinucleate sporulating secondary plasmodium cell, at the same time as pathogen nuclei are undergoing meiotic division, cytoplasmic cleavage is also occurring and closed nuclear meiotic division prevents any contact between cytoplasmic cleavage elements and nucleoplasm. The unique aspects of the cell divisions in *P. brassicae*, as part of its reproductive strategy, may offer targets to address pathogenesis and control of the pathogen and subsequent control of clubroot disease. While the molecular mechanisms that underlie *P. brassicae* cell divisions remain unknown, an understanding of these mechanisms could provide valuable targets for control of the pathogen life cycle and thereby the development of clubroot disease.

4.4.4.2 Cytoplasmic cleavage

The observations presented here provide the first detailed analysis of membrane development during cytoplasmic cleavage in the two multinucleate stages, zoosporangia in the asexual life cycle and sporulating plasmodia in the sexual life cycle of *P. brassicae*. In many eukaryotes, nuclear division is followed very closely by cytokinesis. In *P. brassicae*, several rounds of close nuclei divisions form multinucleate stages. Once established, a special cytoplasmic cleavage follows where the individual nuclei and associated organelles are partitioned to produce daughter cells. The cytoplasmic cleavage is chronologically easy to distinguish between early zoosporangia from five to 12 dpi and sporulating secondary plasmodia from 24 to 28 dpi. However, by using standard light microscopy techniques such as DIC or phase contrast, it has been difficult to identify the mechanism(s) of membrane development and cleavage in each of these stages due to an inherent lack of sufficient contrast relative to the surrounding cytoplasm.

Using the lipophilic vital fluorescent dye, FM4-64, as a marker for membrane development, the division of zoosporangium cytoplasm into individual zoospores by means of small vesicles coalescing to form cleavage elements was observed. FM4-64 incorporates into the outer leaflet of the plasma membrane. Once incorporated into the membrane, the stain enters the cytoplasm through endocytosis. Before cytoplasmic cleavage, the whole zoosporangia fluoresced red, the result of small endocytotic FM4-64 containing vesicles in the zoosporangium cytoplasm. After coalescing and assembling into an interconnected cytoplasmic element, fused with the plasma membrane, the immature zoospore membrane was formed and visible by FM4-64. No internal membrane labelling was observed in *P. brassicae* zoosporangia with immature or mature secondary zoospores after cytoplasmic cleavage, which indicates secondary zoospores were

incapable of endocytosis.

A difference between the cytoplasmic cleavage to produce secondary zoospores and that to produce resting spores became obvious in this study. At the initiation of resting sporogenesis, numerous vacuoles and vesicles were observed in the multinucleate plasmodium. However, these vacuoles did not pre-align around the nuclei. The cytoplasmic division of the sporulating secondary plasmodia appeared to be the result of an electron-lucent membranous bilayer (Fig. 4.16), morphologically similar to prenuclear ER in vegetative secondary plasmodia (Fig. 4.13), that efficiently partitioned each nucleus undergoing meiosis with its surrounding cytoplasm. The electron-lucent membranous bilayers, which were called cytoplasmic cleavage initials in this study, rapidly elongated and expanded throughout the cytoplasm to the plasma membrane. Finally, resting spores were delimited by the fusion of the cytoplasmic cleavage plane and the plasma membrane. This is a different mechanism for resting spore production to that previously suggested (William and McNabola 1967). William and McNabola (1967) supported the model of a prealignment and subsequent fusion of membrane vesicles along future cleavage planes similar to that observed in zoosporangia in this study. A difference between the cytoplasmic cleavage in zoosporangia resulting in secondary zoospores and that in sporulating secondary plasmodium resulting in resting spores might be expected in *P. brassicae*. Secondary zoospores are formed as individual units following nuclear division, each surrounded by a simple plasma membrane, whereas the nuclei in a sporulating plasmodium are undergoing meiosis simultaneously with cytoplasmic cleavage, a state that requires more accurate and efficient cleavage. The use of FM4-64 as a membrane vital stain has allowed the visualization of membrane development during secondary zoospore formation, which had previously been undetectable in living zoosporangia. These observations, combined with the ultrastructures observed by TEM, provide a more comprehensive understanding than previously reported of the events of zoosporogenesis in *P. brassicae* (William and McNabola 1967).

4.4.5 Terminology

In the literature, there is some confusion around the terminology of the life cycle stages of *P. brassicae*, especially in the primary infection stage and the transmission between secondary zoospores and secondary uninucleate plasmodium. It is accepted that during the primary infection stage, the primary zoospores begin to grow by cruciform division to form multinucleate primary

plasmodia and that, after a few days, then cleave into multiple zoosporangia (Kageyama and Asano 2009). The term "sporangial plasmodia", referring to development stages leading to zoosporangia containing zoospores, has often been used for this stage (Braselton 1995; Bulman and Braselton 2014). Now with the observation of uninucleate primary plasmodia and zoosporogenesis within tetranucleate, uncleaved zoosporangia and mature zoosporangia with four secondary zoospores, a more precise terminology is highly desirable. I propose that the term "primary plasmodia" should be used to describe the uninucleate primary plasmodia in root hair and epidermal cells, that develop into thin-wall tetranucleate young zoosporangia, while "young uncleaved zoosporangia" should be used to describe the thin-walled, tetranucleate zoosporangia up to when the four immature secondary zoospores are formed and "young cleaved zoosporangia' should be used for all forms thereafter, until the four condensed mature secondary zoospores are established (prior to release) in "mature zoosporangia". Mature thin-walled zoosporangia, containing fully formed flagellated zoospores, have been previously observed in infected root hairs of Chinese cabbage (Braselton 1995; Buczacki and Clay 1984), however, this is the first study to describe the ultra-structures of uncleaved zoosporangia and young cleaved zoosporangia preceding mature zoosporangia.

In the secondary infection stage, secondary zoospores invade cortical cells and develop into myxamoeba with pseudodopodia-like structures, that develop into round-shaped secondary plasmodia surrounded with a single thick layer of plasma membrane. These round-shaped secondary plasmodia are easy to distinguish, not only by their spherical shape but also by their lack of DAPI and FM4-64 staining. Such plasmodia, that are undergoing cruciform mitotic division, have been called "sporogenic plasmodium" (Braselton 1995; Bulman and Brasemton 2014). A transitional stage has been used to describe the situation where sporogenic plasmodia reach maturity, growth ceases and noncruciform division, interpreted as meiotic division, occurs instead of cruciform mitotic division (Bulman and Brasemton 2014). This is not entirely accurate, as TEM enabled the visualization of meiosis and cytoplasmic cleavage in plasmodia to form resting spores. I propose the term "vegetative secondary plasmodia" be used to describe secondary plasmodia undergoing cruciform mitotic division prior to meiosis, and "sporulating secondary plasmodium" be used for all forms thereafter until resting spore separation.

In this study I have begun to map the time-course of major events and correct some published reports on pathogen structures in the *P. brassicae* life cycle although there are many cellular details and molecular functions that still remain to be identified. It is hoped that this approach will assist

plant-*P. brassicae* interaction analysis of this highly complex lifecycle, and facilitate experimental studies on primary plasmodium division and secondary zoospore assembly and release. Such information is essential for designing strategies to block differentiation from stage to stage within a host or to prevent transition from primary to secondary infection. The primary infection stage of *P. brassicae* is disease symptom silent and can occur in both resistant host and non-host plants. Therefore, the primary infection stage of the *P. brassicae* life cycle or transition stage between primary and secondary infection constitutes ideal targets for potential disease control treatments.

Chapter 5 Alteration of Polar Auxin Transport Modulates Clubroot Disease Symptom Development during the Arabidopsis-*Plasmodiophora brassicae* Interaction

5.1 Abstract

Plasmodiophora brassicae is the causal agent of clubroot disease, which is characterized by abnormal tumorous swellings of infected roots. Several observations suggest that the tumorous swellings on the roots result from an alteration in auxin and/or cytokinin metabolism in infected cells. In the early stages of a *P. brassicae*-host plant interaction, there is an auxin accumulation in infected root tissues and cortical cell divisions are re-initiated, with subsequent cell enlargement, to form club-shaped roots. This auxin accumulation could be due to auxin directly secreted by *P. brassicae* or could be a result of redirected auxin transport towards the infection site.

Transcript analysis of infected tissue showed that host auxin transport was upregulated in early infection stages and down-regulated at the later stages of gall formation. I have studied the role of the auxin transport system governed by the AUX1 influx protein and the PIN-family efflux proteins during clubroot development in *A. thaliana*. T-DNA insert mutants of individual auxin transporters were screened and used in infection studies to determine possible roles for the different auxin transport proteins during *P. brassicae* infection and clubroot progression. Mutants in auxin eflux proteins PIN1 and PIN3 bear smaller galls suggesting that auxin import into the infected cell is needed for gall formation. Expression of some *PIN* genes appears to be suppressed in late stages of gall formation, probably to prevent auxin drainage.

5.2 Introduction

The most prominent symptoms of clubroot disease are the appearance of distinctive swollen gall-like structures in the root and disease symptoms in the leaves that resemble nutrient or water deficiency as a result of impaired root function (Mithen and Magrath 1992). Four weeks after inoculation, club-shaped tumor-like growths form on the root system and hypocotyls in canola, resulting in wilting and stunting of the aboveground parts of the plant (Fig. 5.1).

Figure 5.1 Disease symptoms on roots of canola grown under controlled conditions at 28 dpi inoculated with *P. brassicae* pathotype 3.

A. Uninfected, B. Infected.

Many plant disease symptoms, where normal tissue is converted to tumorous swellings are dependent on an alteration in auxin and/or cytokinin metabolism. A role for auxin in clubroot gall development has been suggested since the 1970s when an increased auxin pool detected in clubroot galls appeared to correlate with cell expansion and differentiation of root galls, and the up-regulation of several auxin-related genes, after infection with *P. brassicae* (Raa 1971; Butcher et al. 1974; Kavanagh and Williams 1981; Ludwig- Müller et al. 1993, 1996, 1999a and b; Grsic-Rausch et al. 2000; Neuhaus et al. 2000; Devos et al. 2005; Siemens et al. 2006). The level of indole-3-acetic acid or auxin, in plant tissue, is controlled through a variety of mechanisms including biosynthesis, conjugation to amino acids, transcriptional repression, influx and efflux transporters, and other means (Woodward and Bartel 2005) (Fig. 5.2).

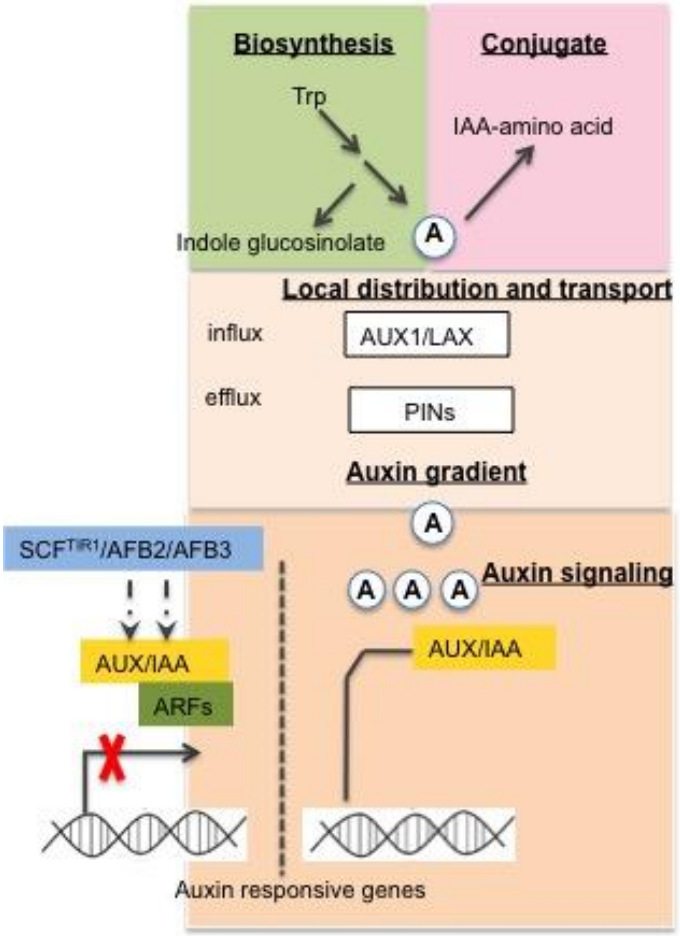

Figure 5.2 Key elements contributing to cellular auxin levels.

Elements of the auxin (A) pathways involved in biosynthesis, degradation, transport, and signaling are shown. AFB: auxin signaling F-box; ARF: auxin response factor; AUX/IAA: auxin/indole acetic acid; PIN: pin-formed; SCF: Skp1p, Cdc53p/cullin, and F-box protein; TIR1: transport inhibitor response1; Trp: Tryptophan.

Auxin is mainly synthesized in the shoot and transported with a single basipetal, or rootward pattern from shoot to the root tips, where it accumulates in the quiescent-center cells and upper tiers of the root-cap columella. From this center, auxin is redistributed radially to more peripheral tissues of the cap, and then transported towards the root elongation zone. In roots, there are two auxin transport polarities, localized to distinct tissue layers, that are linked to distinct developmental and physiological processes. Shootward (or basipetal) transport through the epidermal cell file is tied to gravitropism (Chen et al. 1998; Swarup et al. 2005; Lewis et al. 2007; Rigas et al. 2013) and root elongation, whereas rootward (acropetal) transport through the center cylinder of the root provides the auxin essential for lateral root emergence and the subsequent elongation or growth of these roots (Fig. 5.3; Bhalerao et al. 2002; Overoorde et al. 2010).

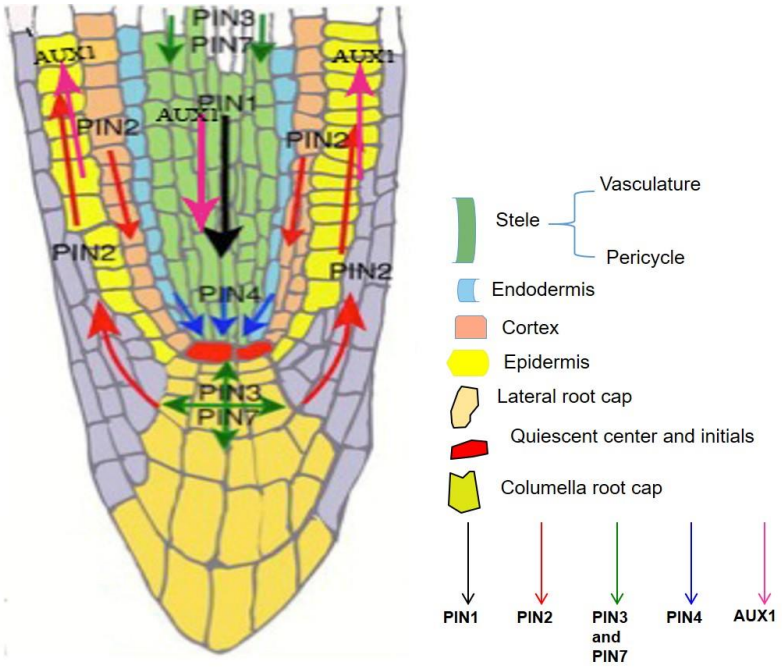

Figure 5.3 Distribution of PIN and AUX1 proteins mediating auxin flow in the *Arabidopsis* root.

Schematic of PIN and AUX1 proteins in the Arabidopsis root tip. Arrows indicate polar auxin transport. Adapted from Michniewicz et al. (2007) and Feraru and Friml (2008).

Polar auxin is transported between cells via AUXIN1/LIKE (AUX1) influx facilitators and PIN-FORMED (PIN) efflux carriers, that together are responsible for the regulation of auxin distribution. All PIN proteins contain a central hydrophilic loop, that separates two hydrophobic regions each with four to five predicted transmembrane domains. According to the length of the hydrophilic loop, PIN proteins have been divided into two sub-classes: type 1 (PIN1, PIN2, PIN3, PIN4 and PIN7) with a long hydrophilic region and atypical type 2 (PIN5, PIN6 and PIN8) with a shorter hydrophilic region (reviewed by Zažímalová et al. 2010a). The cellular localization of PIN proteins seems to be predetermined by their respective hydrophilic regions. Type 1 PIN proteins are associated with the plasma membrane, whereas type 2 proteins, such as PIN5, are found on the endoplasmic reticulum (ER) (reviewed by Zažímalová et al. 2010a).

Each member of the PIN family has different physiological roles and expression patterns. In Arabidopsis roots, PIN1 is expressed in the vascular bundle of the root, with a basal subcellular localization on the plasma membrane (Benková et al. 2003; reviewed by Feraru and Friml 2008). PIN1 also has a polar subcellular localization in leaves and forms convergence points at the margins of leaves, creating localized auxin activity maxima that are required for the outgrowth of serrations, thus *pin1* usually presents fused rosette leaves in seedlings (Bilsborough et al. 2010). Moreover *pin1* presents a nearly naked stem (a pin-like inflorescence stem), from where the *PIN* gene name came (Krecek et al. 2009).

PIN2 regulates the root gravitopic response and meristem enlargement. PIN2 localizes apically in epidermal and lateral root cap cells and predominantly in cortical cells of the root epical meristem (reviewed by Feraru and Friml 2008). Immuno-cytological analysis has localized AtPIN2 at both the anti- and periclinal sides of cortical cells (Müller et al. 1998). *pin2* presents short roots and a loss of gravitropic response in the roots (Müller et al. 1998; Vieten et al. 2005; Kleine-Vehn and Friml 2008). PIN2 has been reported to be the most important of PIN proteins for the regulation of meristem enlargement in the root (Kleine-Vehn and Friml 2008). *pin1pin2* double mutant and all triple and quadruple *pin* mutants containing *pin2* exhibit a growth defect in the root meristem (Blilou et al. 2005). However, the meristem of *pin2* mutants is not much smaller than that of wild type. In the absence of PIN2, PIN1 is expressed in the PIN2 expression domain of the root and it is thought that this PIN1 ectopic expression may compensate for PIN2 function in meristem elongation (Blilou et al. 2005; Vieten et al. 2005).

In roots, PIN3 is expressed without pronounced polarity in tiers two and three of the columella

cells, at the basal side of vascular cells, and to the lateral side of the pericycle of the elongation zone. The expression and function of PIN3 overlap with those of PIN7. Both are expressed in the stele of the central and distal elongation zone as well as the columella cells in the roots (reviewed by Feraru and Friml 2008). PIN3 and PIN7 also have partial functional redundancy with PIN1. Single *pin3* or *pin7* mutants usually show growth phenotypes similar to wild type when they are grown under normal conditions, while the *pin3/pin7* double mutant has a slightly shorter root elongation than wild type and a loss of gravitropic response (Friml et al. 2002a. Blilou et al. 2005, Kleine-Vehn and Friml 2008, Kleine-Vehn et al. 2010). Polar localization of PIN3 in the Arabidopsis shoot contributes to the phototropism response, as shown by *pin3* seedlings being defective in phototropic, hypocotyl bending (Ding et al. 2011; Rakusová et al. 2011). PIN4 is expressed in the quiescent center and close surrounding cells, and localizes basally in provascular cells, suggesting functional redundancy with PIN1, PIN3 and PIN7 (reviewed by Feraru and Friml 2008). The *pin4* mutant has no visible phenotype under normal growth conditions (Friml et al. 2002b; Blilou et al. 2005).

The AUX1/LAX membrane protein, that facilitates anionic auxin influx from the apoplast to the cytoplasm, also participates in auxin distribution in the root (Kramer 2004; Swarup and Péret 2012). An epitope-tagging approach showed that the AUX1 protein is expressed in protophloem, columella, lateral root cap, and epidermal cells in the Arabidopsis root apex (Swarup et al. 2001). In protophloem cells, AUX1, apically localized to the plasma membrane, opposite the basally localized PIN1 in the same cell, is proposed to promote the acropetal, post-phloem movement of auxin to the root apex (Swarup et al. 2001; Benková et al. 2003). In epidermal cells, AUX1 localizes on both apical and basal sides of the cell without pronounced asymmetric distribution. In other cell types, such as columella cells and the lateral root cap, AUX symmetrically localizes on the plasma membrane (Swarup et al. 2001).

In summary, two auxin transport streams have been delineated in roots (Fig. 5.3). In one stream, shoot-derived IAA moves toward the root columella cells through the vasculature and central cylinder, a flow that is polarized by the auxin influx AUX1, and efflux, PIN1, PIN3 and PIN7, carriers. In the second stream, IAA moves away from columella cells through the lateral root cap and epidermis, reaching the root's elongation zone. The second auxin transport stream is polarized by PIN2 and the auxin influx carrier, AUX1.

Auxin transport also plays an important role in plant-microbe interactions. Plant parasitic

nematodes (Grunewald et al. 2009) and rhizobia (Wasson et al. 2006) block auxin transport in roots and thus cause localized increases in auxin concentration. Cyst nematodes (CNs) manipulate the auxin distribution route (Grunewald et al. 2009), by enhanced expression of AUX1 (auxin influx) at nematode feeding sites (NFS) (Mazarei et al. 2003), downregulation of PINI and PIN7 (auxin efflux) and relocalization of PIN3 and PIN4 from the basal side of the vascular cell membrane of uninfected cells to the outer and inner lateral sides of syncytial cells (Grunewald et al. 2009). Arabidopsis *pin1* mutants show a reduced number of cysts and *pin3* and *pin4* mutants only support smaller cysts (Goverse et al. 2000; Grunewald et al. 2009). The cyst nematode, *Heterodera schachtii*, effector HS19C07 directly interacts with the LAX (Like-AUX1)3 auxin importer from Arabidopsis and both *aux1/lax3* and *aux1/lax1/lax2/lax3* mutants showed reduced infectivity when challenged with *H. schachtii* (Lee et al. 2011).

In contrast to cyst nematode infection, the role of auxin transport in clubroot development is poorly understood. An increase in auxin and cytokinin content during clubroot development has been well-documented and the biosynthetic pathway leading to these increases have been identified in Arabidopsis (Ludwig-Müller et al. 2009). Generally, auxin appears to accumulate early and locally within *P. brassicae* infected cells and as such probably has a major role in gall development. Auxin levels in a gall may be increased further by the production of flavonoids, by host plants, that could act as auxin efflux modulators thereby contributing to increased auxin levels locally in *P. brassicae* infected cells (Päsold et al. 2010). Indeed, blocking IAA transport with the chemical inhibitor, *N*-1-naphthylphthalamic acid (NPA), in early stage infections, disturbs clubroot development in both Arabidopsis and oilseed rape (*B. napus*) (Devos and Prisen 2006; Xu et al. 2016). In addition, an Arabidopsis mutant *alh1* (ACC-related long hypocotyl 1), which showed inhibited auxin transport and had a defect in the crosstalk between ethylene and auxin, was found to be more tolerant to clubroot (Vandenbussche et al. 2003; Devos et al. 2006). Transcription studies have shown the auxin transporter genes, *PIN1*, *PIN3*, *AUXI*, *LAX1* and *LAX3* to be up-regulated in the early infection stage, but unchanged or down-regulated at later stages of infection (Irani et al. 2018; Siemens et al. 2006). With *aux1* presenting wild type-sized galls after infection, it has been suggested that LAX1, LAX2 and LAX3 function redundantly with AUX1 (Siement et al. 2002; Lee et al. 2011). The role of auxin transporters during gall development is currently unknown and this lack of understanding prompted me to investigate the role, in Arabidopsis roots, of AUX1/LAX and PIN proteins after *P. brassicae* infection and during clubroot development.

5.3 Results

5.3.1 Mutant screening and characterization

5.3.1.1 Characterization of pin1 mutants

Of the two Arabidopsis SALK lines associated with the *PIN1* gene, PCR confirmed homozygous knockout mutant SALK_097144, with a T-DNA insertion in the fifth exon, displayed a defective developmental phenotype (Fig. 5.4). *pin1* produced one or three cotyledons in the early seedling stage (Fig. 5.4B), fused leaves in the vegetative growing stage (Fig. 5.4C), and pin-like naked inflorescence in the flowering stage (Fig. 5.4D).

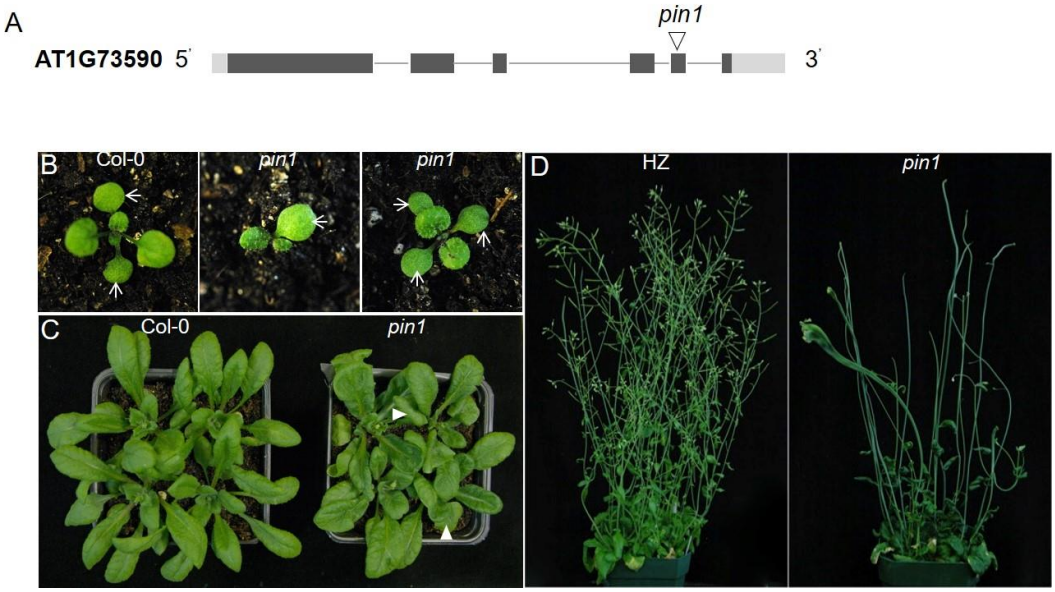

Figure 5.4 Phenotypic analysis of the *pin1* mutants.

A) Schematic diagram of the *PIN1* gene with the location of the T-DNA insertion site indicated. Black boxes represent coding sequences (CDS), grey lines represent introns, grey boxes represent untranslated regions (UTRs), triangle indicates location of T-DNA insertion.
B) *pin1* showing one or three cotyledons in the early seedling stage. Arrows indicate cotyledons.
C) *pin1* showing fused leaves (arrowheads) in the vegetative growing stage.
D) *pin1* showing pin-like naked inflorescence in the flowering stage.

5.3.1.2 Characterization of pin2 mutants

Two SALK lines associated with the *PIN2* gene, SALK_122916 and CS859601, with T-DNA insertions in the first exon and fifth exon respectively, were confirmed as knockout mutants and both displayed agravitropic root growth when grown in vertically placed 100×100×15 mm square Petri dishes (Fig. 5.5).

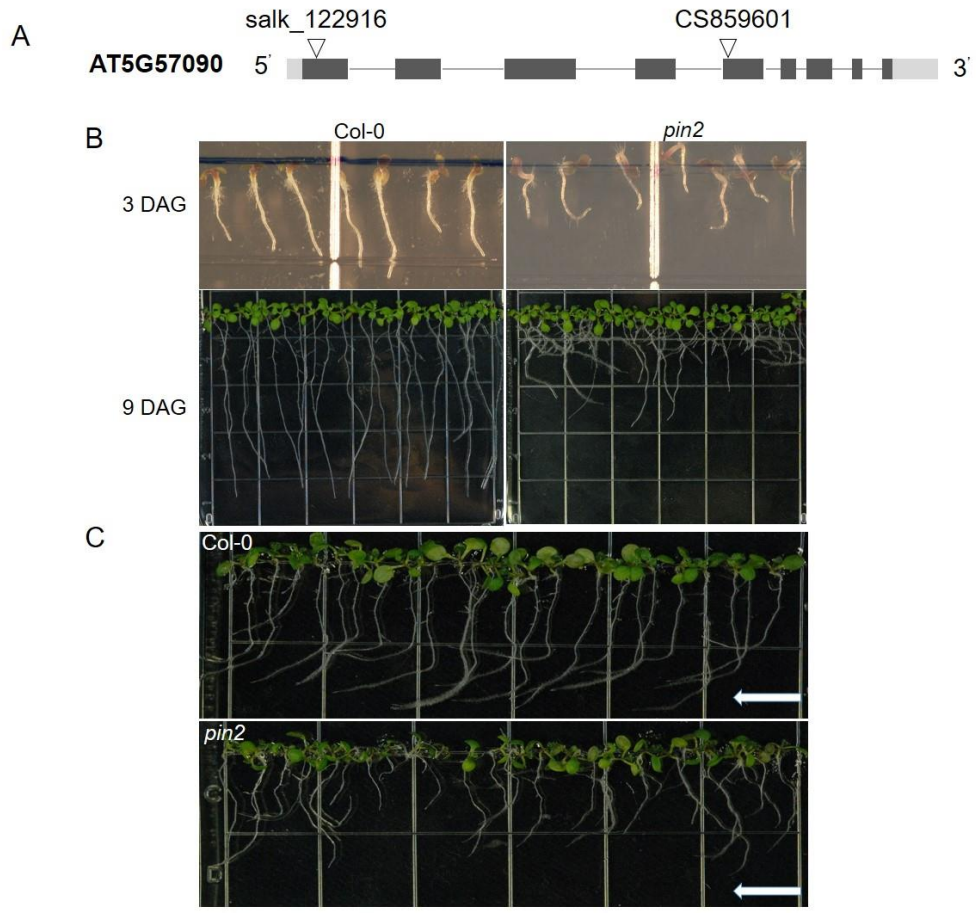

Figure 5.5 *pin2* (SALK_122916) mutants showing defective gravitropic response.

A) Schematic diagram of the *PIN2* gene with T-DNA insertion sites in SALK_122916 and CS859601. Black boxes represent coding sequences (CDS), grey lines represent introns, grey boxes represent untranslated regions (UTRs), triangles indicate locations of T-DNA insertions.
B) *pin2* seedlings grown on vertically oriented agar plates showing agravitropic root growth, DAG: days after germination.
C) Re-orientation of plates by 90° for one day, *pin2* showing defective root bending. Arrows show direction of gravity.

5.3.1.3 Characterization of pin3 mutants

pin3-5 (SALK_005544) carried a T-DNA insertion in the 5-UTR of *PIN3* and *pin3-6* (SALK-113246) carried a T-DNA insertion in the first exon of *PIN3* (Fig. 5.6A). Under photo stimulation, hypocotyl bending in *pin3-5* and *pin3-6* was less pronounced than that of wild type seedlings (Fig. 5.6B). Both *pin 3-5* and *pin3-6* showed an early flowering phenotype when grown in soil (Fig. 5.6C, Fig. 5.10, Fig.5.11). In addition to the decreased phototropic response, *pin3-5* and *pin3-6* seedlings displayed longer hypocotyls and roots (Fig. 5.6B) and shorter lateral roots than wild-type seedlings (data not shown).

5.3.1.4 Characterization of pin4 and pin7 mutants

pin4-3 (cs9368) has a transposon insertion in the second exon and *pin7* (SALK_044687) had a T-DNA insertion in the third exon (Fig. 5.7A). *pin4-3* was previously reported to have no obvious phenotypic difference to wild type plants when grown under optimal conditions (Swarup et al. 2004). However, both *pin4-3* and *pin7* seeds (ABRC) showed a yellow color phenotype (Fig. 5.7B). In order to further characterize the *pin4-3* and *pin7* phenotypes, homozygous lines of *pin4-3* and *pin7* were identified by PCR and lack of expression of *AtPIN4* and *AtPIN7*, in seedling of each mutant, was also confirmed (Fig. 5.7C). In generating multiple mutant combinations, the *pin4-3* and *pin7* mutants were selected by RT-PCR for the absence of a wild-type band by using the gene-specific primers for RT-PCR.

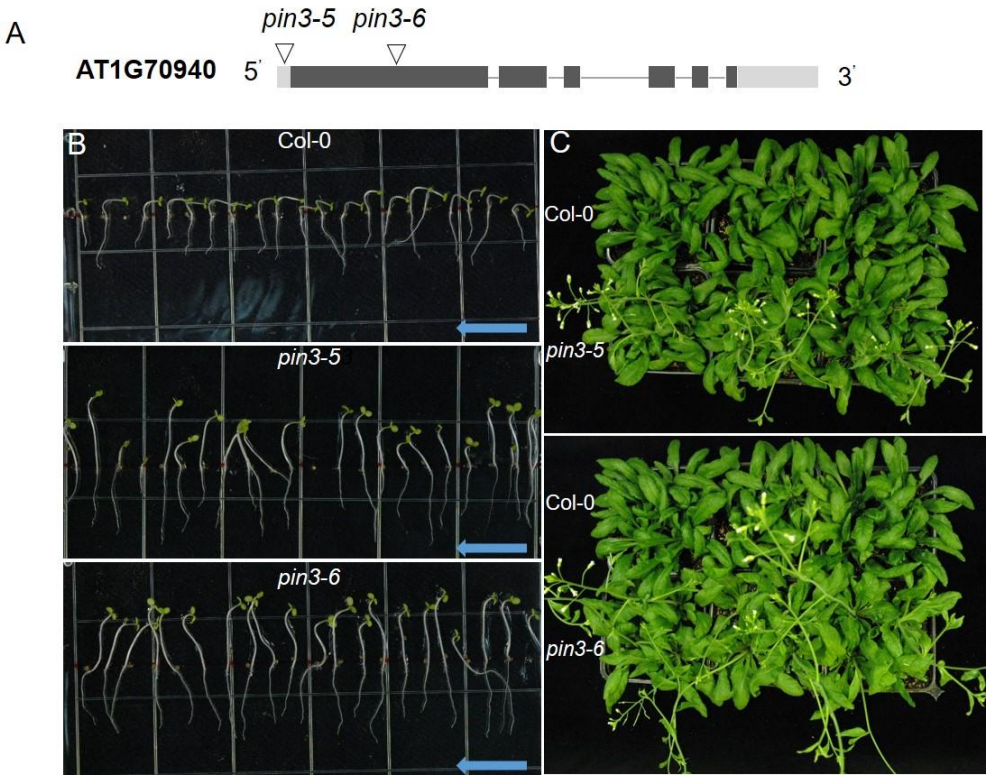

Figure 5.6 *pin3* mutants showing defective phototropic response.

A) Schematic diagram of the *PIN3* gene with T-DNA insertion sites. Black boxes represent coding sequences (CDS), grey lines represent introns, grey boxes represent untranslated regions (UTRs), triangles indicate locations of T-DNA insertions .

B) Images of two day-old etiolated seedlings of wild-type (Col-0) and *pin3-5* and *pin3-6* mutants grown on vertical plates, after exposure to unilateral LED light for 12 h. Both *pin3* mutants show defective hypocotyl phototropic response. Arrows indicate the direction of light.

C) 31 day-old seedlings were grown in soil and observed for the difference in growth phenotype. *pin3* mutants flowered earlier than wild type.

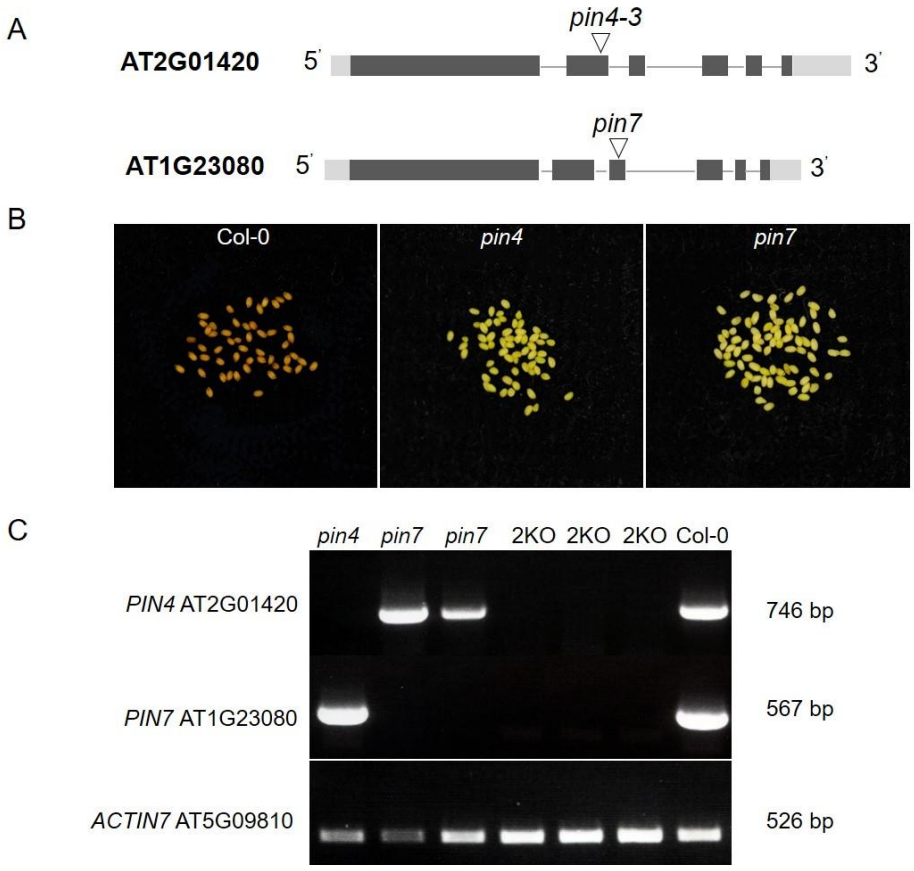

Figure 5.7 Characterization of *pin4-3* and *pin7* knock out mutants.

A) Schematic diagram of the *PIN4 and PIN7* genes with locations of transposon and T-DNA insertion sites, respectively. Black boxes represent coding sequences (CDS), grey lines represent introns, grey boxes represent untranslated regions (UTRs), triangles indicate insertion locations.

B) Yellow-seed phenotype of *pin4-3* and *pin7*.

C) RT-PCR analysis of *PIN4* and *PIN7* transcripts in Col-0 and *pin4*:*pin7* double knock out (2KO). RT-PCR was performed with total RNAs from four-week-old seedlings using gene-specific primers for *PIN4* and *PIN7* and 36 cycles. *AtACTIN7* transcript was used as an internal control to normalize cDNA template. *PIN4* and *PIN7* transcript was absent from *pin4* or *pin7*, respectively and both *PIN4* and *PIN7* transcripts were absent from *pin4:pin7* (2KO) double mutant, confirming that *pin4*, *pin7* and 2KO are null mutants.

5.3.2 Pathogenicity of *P. brassicae* in *pin* mutants

To examine whether auxin efflux PIN transporters are required for clubroot development, the *A. thaliana* mutants *pin1*, *pin2*, *pin3*, *pin4* and *pin7* were grown in soil and inoculated with a resting spore suspension at 5×10^6 (low-inoculum pressure) and 5×10^7 (high-inoculum pressure) spores/mL. Disease index was scored at 21 dpi, when galls are clearly visible and cell division, as well as cell elongation occurred in the infected roots. High inoculum pressure was used to investigate tolerance or resistance phenotypes, because plants that show a level of tolerance against *P. brassicae* would show a low disease index compared to susceptible wild type plants with a high disease index. On the contrary, low inoculum pressure can show higher susceptibility. While the disease index here are expected to be lower for the wild type plants, mutant lines with a higher disease index are regarded as more susceptible than the wild type. When harvested at 21 dpi, low inoculum pressure and high inoculum pressure can also indicate different stages of *P. brassicae* development and clubroot progression. For low inoculum pressure, when harvested at 21 dpi, wild type plants started to show visible swelling on roots where *P. brassicae* was in vegetative secondary plasmodium stage. However, under high inoculum pressure, when harvested at 21 dpi, wild type plants have big clubbed roots where most of *P. brassicae* was in sporulating secondary plasmodium stage as well as the resting spore stage (Fig. 5.9, Fig. 5.10, Fig. 5.11).

5.3.2.1 Pathogenicity of P. brassicae on pin1 mutants

Homozygous *pin1* (SALK_097144) is sterile and was maintained as *PIN1/pin1* heterozygous seeds. At 10 days after germination (DAG), *pin1* homozygous mutants, identified by the one or three cytoledon phenotype described above, were transferred to new pots for inoculation. At 21 dpi and low inoculum pressure, no difference in above ground phenotype or disease index ($p = 0.87$) was observed between *pin1* and wild type plants (Fig. 5.8B). However, at 21 dpi under high inoculum pressure, *pin1* demonstrated increased resistance to *P. brassicae* (Fig. 5.8C, D), with wild type plants presenting a wilted phenotype with smaller and thinner leaves than *pin1* plants. The disease index of *pin1* plants was significantly ($p = 0.017$) lower than that of wild type plants (Fig. 5.8C, D).

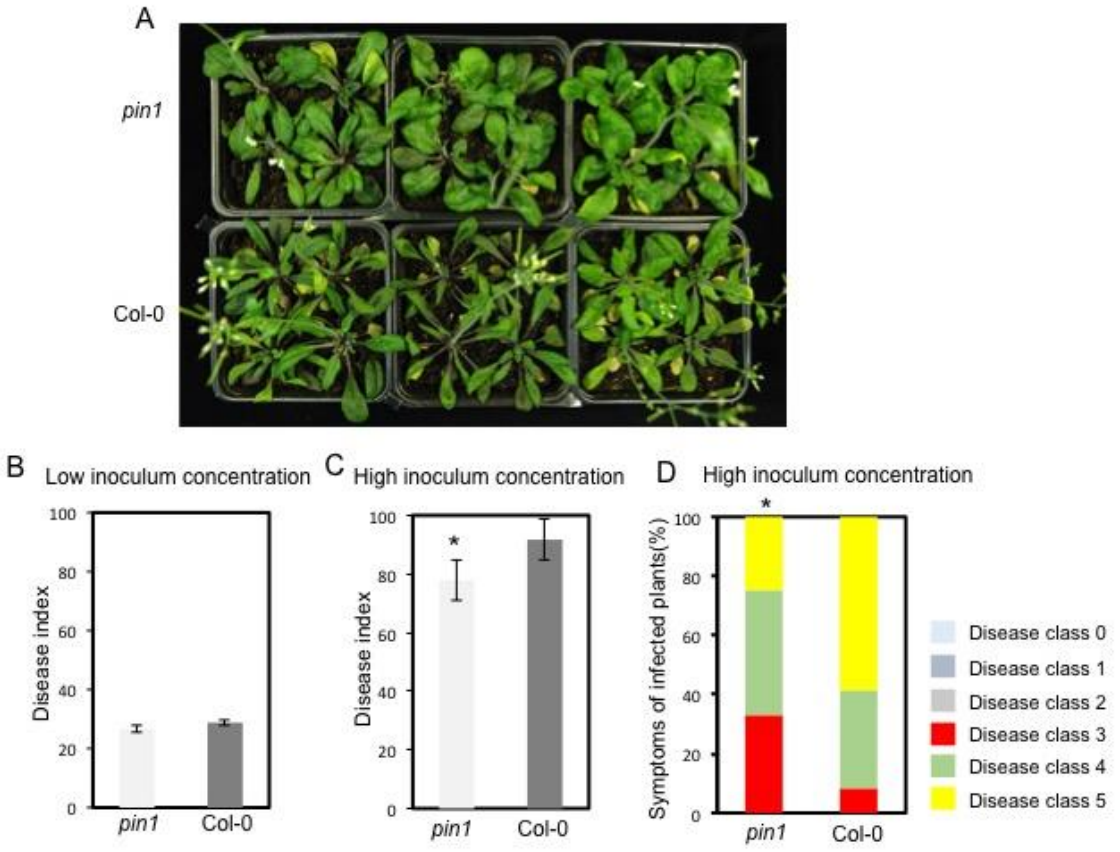

Figure 5.8 *pin1* mutants showing less susceptibility to *P. brassicae* infection than wild type plants at high inoculum pressure.

pin1 and wild type (Col-0) plants were inoculated with *P. brassicae* at low (5×10^6 spores/mL) and high (5×10^7 spores/mL) inoculation pressure and disease index was accessed at 21 dpi. Results are the mean of three replicates.

(A) Above ground clubroot disease phenotype at 21 dpi under high inoculation pressure.

(B) Disease index at low inoculation pressure. Average data from three independent experiments with standard error.

(C) Disease index at high inoculation pressure. Average data from three independent experiments with standard error.

(D) Evaluation of pathogenecity of *P. brassicae* on *pin1* under high inoculation pressure. The scoring scheme follows the disease index described in this study.

Significant differences were determined by two-tailed Student's t-test: * $P<0.05$.

5.3.2.2 Pathogenicity of P. brassicae on pin3 mutants

Under low inoculum pressure, *pin3* mutants (*pin3-5* and *pin3-6*) showed significantly decreased susceptibility ($p = 0.017$ and $p = 0.012$, respectively) to *P. brassicae* infection compared to wild type plants (Fig. 5.9) . At 21 dpi, *pin3* did not show clubroot swellings on roots (disease class 0, see disease class and disease index in Chapter 2; Fig.5.9A) or stunted growth of shoots. These class 0 clubroot symptoms represented about 80% of the total *P. brassicae* inoculated *pin3* plants (Fig. 5.9C, E). Small swellings on lateral roots, diagnostic of disease class 1 occurred on wild-type plants, representing about half of the total clubroot swellings (Fig. 5.9A, C, E).

At high inoculum pressure, leaves of the wild type plants started to turn purple while leaves of *pin3* were still green at 14 dpi. At 21 dpi, *pin3* plants demonstrated increased resistance to *P. brassicae* infection (Fig. 10, Fig. 5.11). The disease index of *pin3-5* and *pin3-6* plants decreased significantly ($p = 0.019$ and $p = 0.001$, respectively) when compared to that of the wild type (Fig. 5.10C, Fig. 5.11C). Large tumorous swellings, that destroyed infected roots and caused wilting of infected plant seedlings of susceptible wild type, were not observed in *pin3* at 21 dpi (Fig. 5.10A, B, Fig. 5.11A, B). Shoot growth was inhibited in both mutants and wild type when compared to mock-inoculated plants, however, *pin3* mutants were more healthy than the wild type.

The single mutants *pin2* (SALK_122916), *pin4-3* (cs9368), *pin7* (SALK_044687) and the *aux1*:*axr4-2* double mutant (cs8040) did not show any difference in phenotype or disease index when compared to the wild type, under both low and high inoculum pressure (Fig. 5.12).

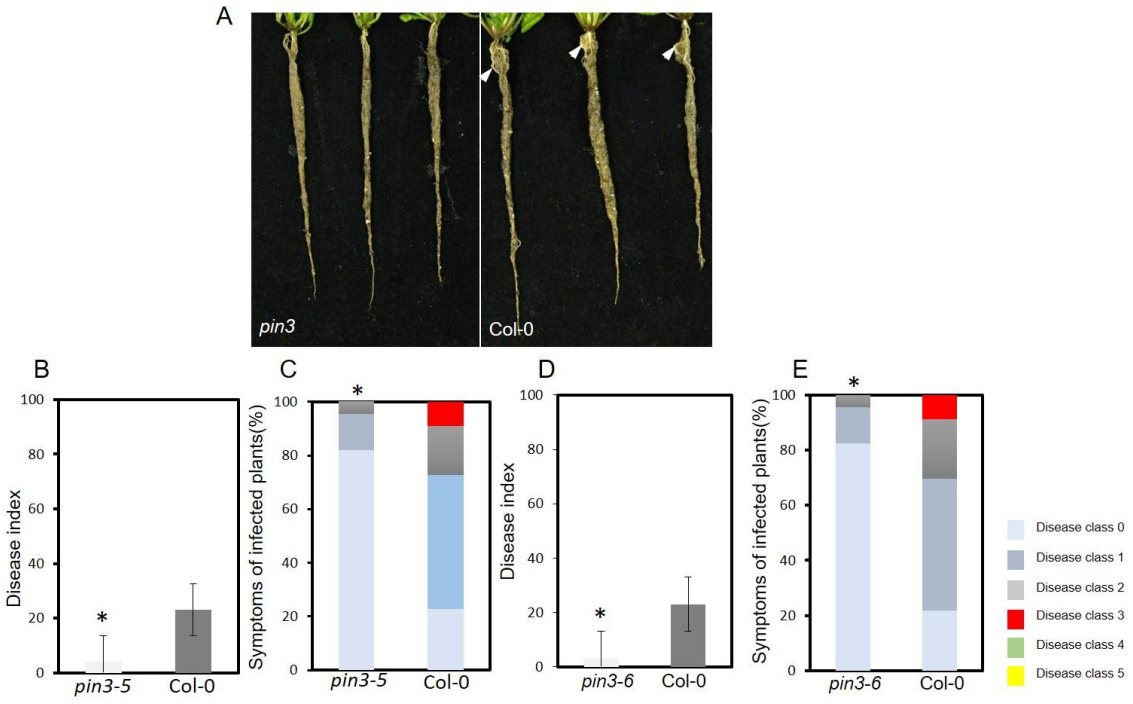

Figure 5.9 Both *pin3* mutant lines showing less susceptibility to *P. brassicae* infetion than wild type at low inoculum pressure.

pin3 (*pin3-5* and *pin3-6)* and wild type (Col-0) plants were inoculated with *P. brassicae* at low inoculation pressure (5×10^6 spores/mL) and disease index was assessed at 21dpi. Results are the mean of three replicates.

(A) Typical below ground clubroot disease class 1(wild type) and class 0 (*pin3*), note slight swellings indicated by white arrowheads.

(B) and (D) Disease index of *pin3-5* (B) and *pin3-6* (D) at low inoculation pressure. Average data from three independent experiments with standard error.

(C) and (E) Quantitative evaluation of pathogenecity of *pin3-5* (C) and *pin3-6* (E) under low inoculum pressure. The scoring scheme follows the disease index described in this study. Significant differences were determined by two-tailed Student's t-test: * $P<0.05$.

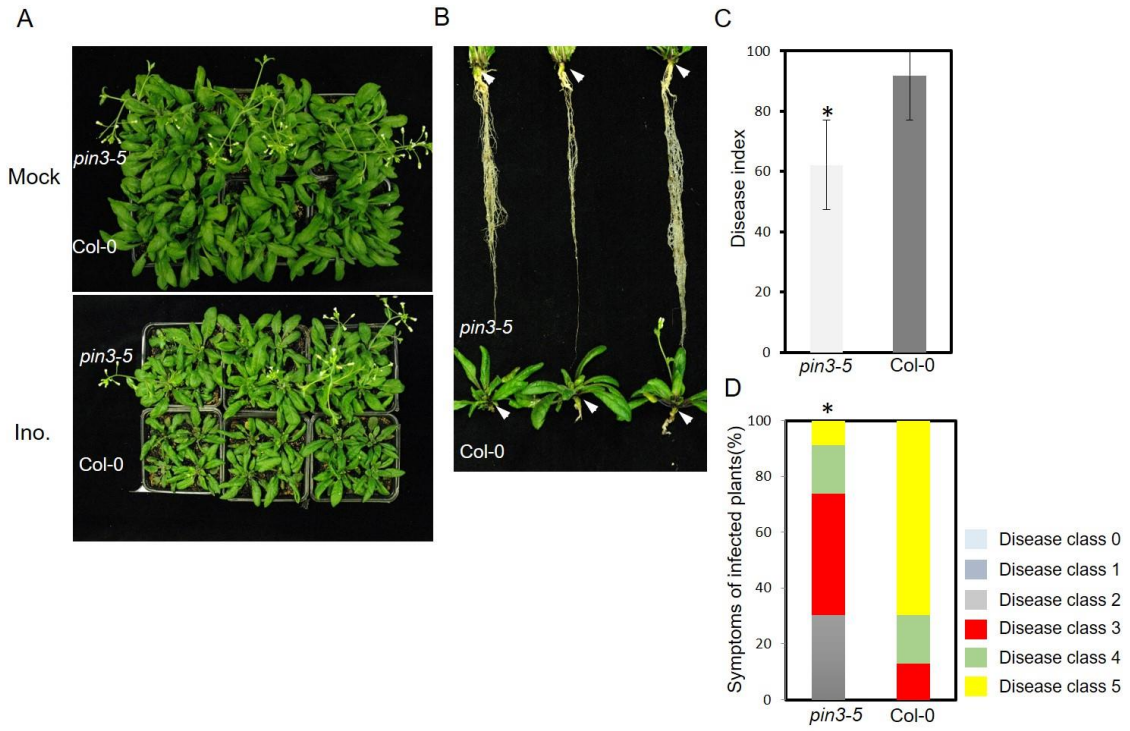

Figure 5.10 *pin3-5* mutants showing less susceptibility to *P. brassicae* infection than wild type at high inoculum pressure.

pin3-5 and wild type (Col-0) plants were inoculated with *P. brassicae* at high inoculation pressure (5×10^7 spores/mL) and disease index was assessed at 21 dpi. Results are the mean of three replicates.

(A) Typical above ground clubroot disease phenotype as demonstrated by Col-0 plants and less susceptible phenotype of *pin3-5*.

(B) Typical below ground clubroot disease class 3 (*pin3-5*) and class 5 (wild type), note the swellings indicated by white arrowheads.

(C) Disease index at high inoculation pressure. Average data from three independent experiments with standard error.

(D) Quantitative evaluation of pathogenecity of *pin3-5* at high inoculation pressure. The scoring scheme follows the disease index described in this study.

Significant differences were determined by two-tailed Student's t-test: * $P<0.05$, ** $P<0.01$.

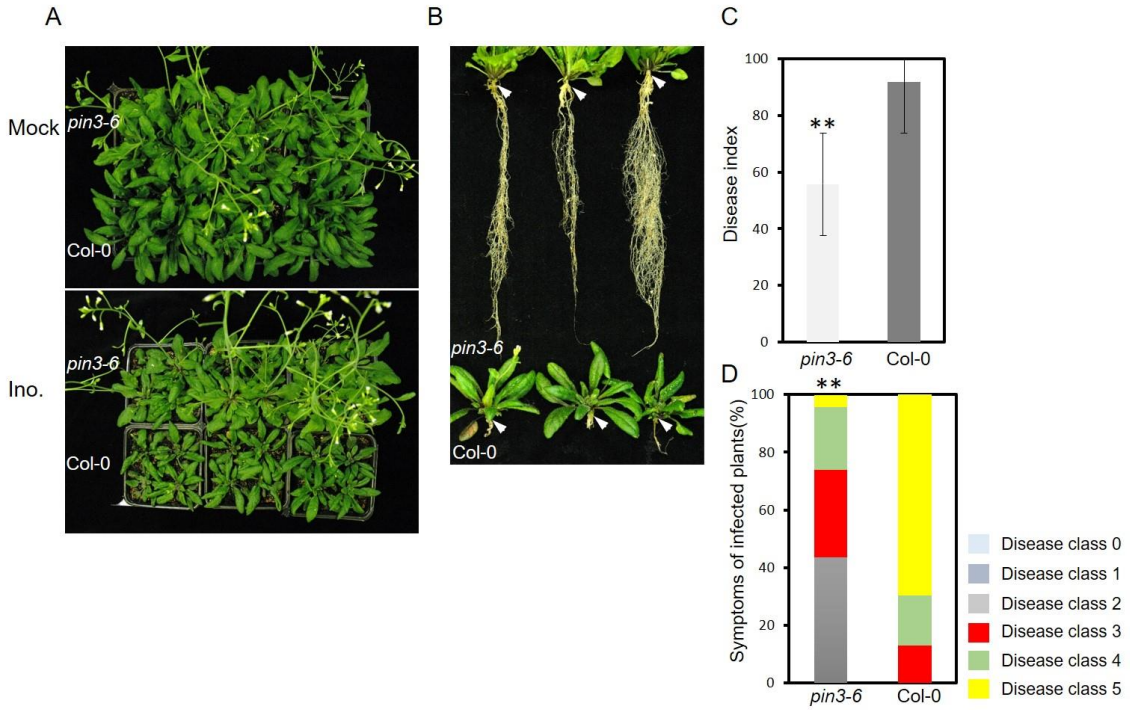

Figure 5.11 *pin3-6* mutants are less susceptible to *P. brassicae* infection than wild type at high inoculum pressure.

pin3-6 and wild type (Col-0) plants were inoculated with *P. brassicae* at high inoculation pressure (5×10^7 spores/mL) and disease index was assessed at 21 dpi. Results are the mean of three replicates.

(A) Typical above ground clubroot disease phenotype as demonstrated by Col-0 plants and the less susceptible phenotype of *pin3-6*.

(B) Typical below ground clubroot disease class 3 (*pin3-6*) and class 5 (wild type), note the swellings indicated by white arrowheads.

(C) Disease index at high inoculation pressure. Average data from three independent experiments with standard error.

(D) Quantitative evaluation of pathogenecity of *pin3-6* at high inoculation pressure. The scoring scheme follows the disease index described in this study.
Significant differences were determined by two-tailed Student's t-test: ** $P<0.01$.

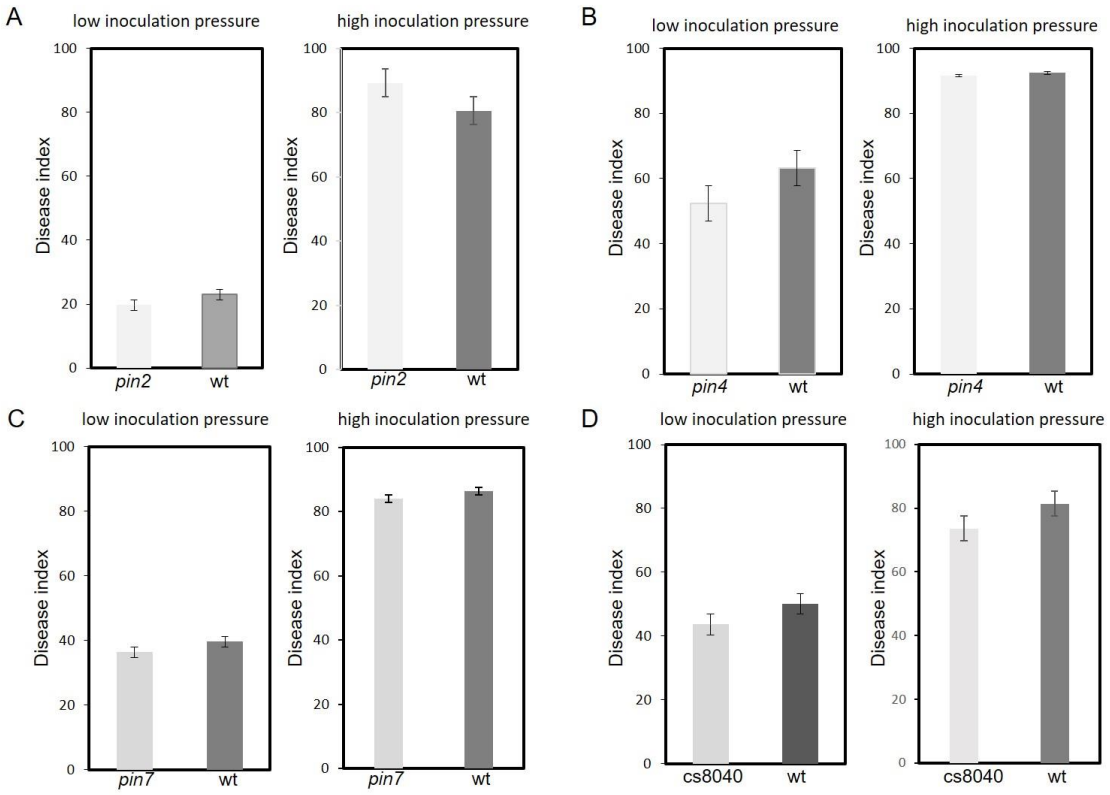

Figure 5.12 *pin2*, *pin4*, *pin7* and *aux1-7:axr4-2* mutants show the same disease index as wild type at both low and high inoculum pressure.

(A) Disease index of *pin2* and wild type at both low and high inoculation pressure. Average data from three independent experiments with standard error.
(B) Disease index of *pin4* and wild type at both low and high inoculation pressure. Average data from three independent experiments with standard error.
(C) Disease index of *pin7* and wild type at both low and high inoculation pressure. Average data from three independent experiments with standard error.
(D) Disease index of *aux1-7:axr4-1* (cs8040) and wild type at both low and high inoculation pressure. Average data from three independent experiments with standard error.
No significant differences were determined using two-tailed Student's t-test.

5.4 Discussion

Auxin is transported throughout the plant by means of a complex interacting network of influx and efflux carriers. In *P. brassicae* infected cells, the increased local auxin response can therefore be the result of increased auxin influx and/or inhibition of auxin efflux. Auxin transporter expression was upregulated early in response to *P. brassicae* infection, suggesting acropetal auxin transport down the root is needed to deliver auxin to the site of infection to stimulate pathogen attraction or to relax the host cell wall for easy pathogen penetration. At later stages of infection, when clubroot symptoms were showing, *P. brassicae* directly or indirectly downregulated auxin transporter expression, in order to inhibit auxin transport out of infected cells/galls, thereby increasing the local auxin concentration.

pin1 and *pin3* polar auxin efflux transporter mutants are less susceptible to both root knot nematode and cyst nematode infection and gall development (Grunewald et al. 2009; Kyndt et al. 2016). IAA levels, within apical root regions of *pin1* and *pin3* plants have been shown to be consistently lower than those found in comparable regions of wild type roots (Marchant et al. 2002; Zhang et al. 2014). Although both *pin1* and *pin3* were less susceptible to *P. brassicae* infection, infection studies suggested that PIN3 plays a role during disease processes after *P. brassicae* infection. Both *pin3* mutants showed lower susceptibility under low and high inoculum pressures, suggesting that local auxin maxima at the root tip direct *P. brassicae* penetration and establishment in host roots, as well as infected cell expansion. Under low inoculum pressure, the high percentage of *pin3* plants without swelling demonstrated that *P. brassicae* is unable to induce expansion of infected cells. As well as a phototropic phenotype, *pin3* mutants also displayed an early flowering phonotype (Fig. 5.10, Fig. 5.11). Previous studies have shown that later flowering plants developed more severe clubroot symptoms than earlier flowering plants (Fuchs and Sacristán 1996). This difference in *P. brassicae* infection response may be attributed to the two competing carbon sinks of flower and gall.

Transcript analyses of *PIN2* have produced contrary results: an upregulation at both early and late stages of infection according to microarray data (Siemens et al. 2006), but strong downregulation at a later stage (24 dpi) of infection according to more recent RNA-seq analysis (Irani et al. 2018). These contrasting data are not surprising, as PIN2 is expressed in a very different manner to the other PIN proteins in uninfected plants. In contrast to the other PIN proteins, PIN2 is not expressed during embryogenesis, or in mature root cells, or during early lateral root growth

(Müller et al. 1998). Further, my infection studies determined that a *pin2* mutant had no effect on *P. brassicae* infection and subsequent clubroot disease progression. *pin2* also had no effect on cyst nematode infection and gall development (Grunewald et al. 2009). In addition, in cortical cells neighbouring infected epidermal cells in the root elongation zone, PIN2 might be involved in a polar localization change resulting in export of auxin from cortical cells towards the infected epidermal cells, in support of pathogen development and resulting in clubroot swelling. In late stages, when clubroot swellings were showing, root structure was destroyed, root elongation was inhibited and radial swelling promoted, *PIN2* expression was decreased. PIN4 is expressed primarily and located without polarity in cells of the root quiescent center, where it is known to regulate auxin homeostasis and patterning through sink mediated auxin distribution at the root tip (Friml et al. 2002b). My results showed that *pin4*, reported to accumulate higher auxin levels in the root tips (Friml et al. 2002b), does not show a difference in disease development when compared to the wild type. This IAA accumulation in the root tips may contribute to *P. brassicae* attraction rather than clubroot development (Kyndt et al. 2016). Similarly, *pin7* showed no significant differences in disease development when compared to the wild type. However, an overlap in localization of PIN3 and PIN7 suggests that PIN3 may compensate for *pin7*, which could partially explain why *pin7* showed no decrease in susceptibility to clubroot disease (reviewed by Feraru and Friml 2008). The difference in disease susceptibility in *pin3* and *pin7* mutants may further suggest that PIN3 and PIN7 have different functions in transporting auxin from shoot to root after *P. brassicae* infection.

The data presented herein support a model in which *P. brassicae* infection of plant roots causes a change in auxin distribution patterns, within the root, leading to clubroot development. Auxin transport from source (above ground) to sink (root) seems to be mediated by the concerted actions of PIN1 and PIN3, ultimately leading to auxin accumulation within the *P. brassicae* infected root cells during early stage infection. Local auxin maxima correlate with the initiation sites of organ primordia in roots and most likely clubroot (De Smet et al. 2010; results in section 3.3.3). Moreover, auxin is also known to facilitate radial expansion of cells in the root elongation zone (Strader et al. 2010), site of *P. brassicae* primary infection initiation and subsequent establishment of clubroot disease, supporting a role for auxin in cell expansion and ultimate root swelling. I suggest that at the early infection stage, a local auxin maxima plays an important role in pathogen infection and disease establishment. Once the disease is established, a down regulation of expression of auxin

transporters probably prevents auxin drainage away from infected cells, leading to enhanced auxin levels within infected cells. While my studies on auxin transport mutants have demonstrated that auxin transport from source to sink plays an important role in disease initiation, whether it is actually *P. brassicae* that influences this modulation of polar, subcellular localization of auxin transport components during pathogen infection and disease development, has still to be determined.

Chapter 6 General Conclusions and Future Work

Clubroot disease significantly contributes to canola yield loss around the world. Clubroot is the result of an infection by the cellular parasitic protist *P. brassciae*. In order to ensure the sustainably of increased canola production, the *P. brassicae* infection cycle and plant host response to *P. brassicae* must be examined to identify novel targets for crop improvement and disease control. The main objectives of this work were to use a axenic culture and soil inoculation system to study the life cycle of *P. brassicae* in the model plant *A. thaliana* and subsequent gall development in *A. thaliana* during *P. brassicae* infection. Overall, the research presented in this thesis has advanced our understanding of *P. brassicae,* especially the pathogen life cycle.

An axenic culture system, removing contaminating soil-borne microbes from *P. brassicae* infected canola galls, was established to produce pure resting spore inoculum. Subsequently, using the pure inoculum and combinations of fluorescent dyes, *P. brassciae* was selectively labelled and differentiated from host cellular organelles. The pure inoculum remained fully virulent and the complete *P. brassicae* life cycle was supported by the axenic culture on Arabidopsis and canola. Further more, the uninucleated primary plasmodia structures, previously identified by TEM in root hair and epidermal cells of Chinese cabbage (*B. rapa*) (Aist and William 1972; https://people.ohio.edu/braselto/
plasmodiophorids/plasmos/zspor.html), were confirmed by live-cell imaging in the axenic culture system. The axenic culture system is a sound cellular biology method for the accurate and rapid monitoring of *P. brassciae* life cycle progression in Arabidopsis root from the very early stage (three days post inoculation) of infection, especially after primary zoospore penetration of root epidermal cell and root hairs.

By observing sequential samples, over the time course of *P. brassicae* infection and using a combination of laser scanning confocal microscopy (LSCM) and transmission electron microscopy (TEM), detailed observations were made of the life cycle of *P. brassciae* from early uninucleate primary plasmodial development through to the development of uninucleate mature resting spores. The double live cell staining techniques, established in Chapter 3 enabled observations of the various stages in the *P. brassicae* life cycle within the root tissues and to couple these observations

with TEM studies. These coupled techniques have increased our understanding of the *P. brassicae* infection process, especially the early stages of infection, where accurate observations are essential to identify the different developmental stages of *P. brassicae* in non-host, resistant host and susceptible host plants. The initial stage in *P. brassicae* pathogenesis, the primary infection of root hairs and epidermal cells, has been previously observed in non-host, resistant and susceptible host plants (Friberg et al. 2006; Hwang et al. 2017). However, the later stages of infection, culminating in the production of mature resting spores and clubroot galls, is limited to susceptible hosts. The coupled microscopy techniques herein provide methodologies to help in answering the burning question of what happens in resistant cultivars and non-host cultivars, in relation to their susceptible relatives, to prevent secondary cortical infections from being established.

During primary infection, susceptible hosts show no symptoms. However, during secondary infection, clubroot disease symptoms develop rapidly. As *P. brassicae* progresses through its life cycle during secondary infection, the pathogen degrades ~80% of the infected host cell contents. This process provides a source of lipids and carbohydrates and creates space within the cell for pathogen growth and proliferation. The pathogen uses three distinct pathways for host content uptake: i) pseudopodia of the myxamoeba-stage surrounded and "engulf" host cell cytoplasm, forming digestive vacuoles, ii) host content-containing vesicles or tubules from invagination of the pathogen plasma membrane continue the uptake of host contents as the pathogen matures into vegetative secondary plasmodia, and iii) mature sporulating secondary plasmodia, through invagination of the pathogen plasma membrane again produce digestive vacuoles. Understanding these pathways may help to identify new strategies for the control of clubroot disease.

During the life cycle, the pathogen adopts at least eight different forms, making life cycle and disease diagnosis quite complicated to assess. However, during each stage, *P. brassicae* shows unique structural features or staining patterns. Molecular markers, as stage specific indicators, were identified in the *P. brassicae* genome and confirmed by RT-PCR in the time course of the *P. brassicae* life cycle. Good correlation between selected marker expression *in planta* and specific life cycle stage structures, determined by microscopy, was evident. Using RT-PCR for stage specific molecular marker genes will eliminate the factors that could influence the results of inoculation and visual assessment, as different inoculum concentration, different inoculation timing and plant stages and different disease index assement timing will cause different disease progress and different disease index. Inoculation and root gall counting or disease index assessment

requires an expertise to quantify the inoculum concentration, detect early stages of gall formation and to maintain the consistency of experiments. In my preliminary experiments and published papers, difference in inoculation concentration, host disease severity observed by different researchers and time to assess disease severity by different research group were noted (Intrenaitonal Clubroot Workshop, 2018). RT-PCR with stage specific marker genes is likely to be more precise for determining pathogen infection, intensity and pathogen developmental stages. In future studies, more life-cycle stage specific marker genes need to be explored as indicator of pathogen developmental stages in host cells. It will be very important to establish where in the pathogen life cycle, during the transition from primary to secondary infection, the onset of resistance occurs and to identify these stage specific effectors.

The auxin transport pathway has been closely examined in Arabidopsis after infection, to identify specific steps crucial for clubroot gall formation. Although, auxin has been implicated in clubroot disease, at present there is limited literature addressing auxin transport mutants and their response to clubroot disease development. Both *pin1* and *pin3* single mutants showed reduced clubroot symptoms after *P. brassicae* infection in comparison to wildtype plants. The reduction in clubroot symptoms suggests a requirement of shoot derived auxin for clubroot formation. This is the first genetic evidence that auxin transport plays a role in clubroot formation. It will be important to include PIN-GFP transgenic plants in future work alongside WT and *pin* mutants, to study the auxin transporter dynamic after *P. brassciae* infection.

References

Agarwal, A., Kaul, V., Faggian, R. and Cahill, D. M. (2009). Development and use of a model system to monitor clubroot disease progression with an Australian field population of *Plasmodiophora brassicae*. Aust. Plant Pathol. 38: 120-127.

Agarwal, A., Kaul, V., Faggian, R., Rookes, J. E., Ludwig-Müller, J. and Cahill, D. M. (2011). Analysis of global host gene expression during the primary phase of the *Arabidopsis thaliana-Plasmodiophora brassicae* interaction. Functional Plant Biol. 38: 462-478.

Agrios, G. N. (2005). Plant Pathology. Elsevier Academic Press, Amsterdam.

Aist, J. R. and Williams, P. H. (1971). The cytology and kinetics of cabbage root hair penetration by *Plasmodiophora brassicae* Wor. Can. J. Bot. 49: 2023-2034.

Alix, K., Lariagon, C., Delourme, R. and Manzanares-Dauleux, M. J. (2007). Exploiting natural genetic diversity and mutant resources of *Arabidopsis thaliana* to study the *A. thaliana-Plasmodiophora brassicae* interaction. Plant Breed. 126: 218-221.

Ando, S., Asano, T., Tsushima, S., Kamachi, S., Hagio, T. and Tabei, Y. (2005). Changes in gene expression of putative isopentenyl transferase during clubroot development of Chinese cabbage (*Brassica rapa* L.). Physiol. Mol. Plant Pathol. 67: 59-67.

Asano, T., Kageyama, K. and Hyakumachi, M. (2000). Germination of surface disinfected resting spores of *Plasmodiophora brassicae* and their root hair infection in turnip hairy roots. Mycoscience. 41: 49-54.

Asano, T. and Kageyama, K. (2006). Growth and movement of secondary plasmodia of *Plasmodiophora brassicae* in turnip suspension-culture cells. Plant Pathol. 55: 145-151.

Asano, T., Kodama, A. and Kageyama, K. (2006). Susceptibility of hairy root lines of Brassica species to *Plasmodiophora brassecae* and in an in vitro subculture system. J. Gen. Plant Pathol. 72: 85-91.

Archibald, J. M. and Keeling, P. J. (2004). Ubiquitin and actin protein sequences support a cercozoan/foraminiferan ancestry for the plasmodiophorid plant pathogens. J. Eukar. Microbiol. 51: 1-6.

Auer, S. and Ludwig-Müller, J. (2014). Effects of the endophyte *Acremonium alternatum* on oilseed rape (*Brassica napus*) development and clubroot progression. Albanian J. Agric. Sci. 13: 15-20.

Azevedo, J. L., Maccheroni, W., Pereira, J. O. and Luiz de Araújo, W. (2000). Endophytic microorganisms: a review on insect control and recent advances on tropical plants. Electron J. Biotechnol. 3: 40-65.

Benková, E., Michniewicz, M., Sauer, M., Teichmann, T., Seifertová, D., Jürgens, G. and Friml, J. (2003). Local, efflux-dependent auxin gradients as a common module for plant organ formation. Cell. 111: 591-602.

Bennett, R. N., Wenke, T., Freudenberg, B., Mellon, F. A. and Ludwig-Müller, J. (2005). The *tu8* mutation of *Arabidopsis thaliana* encoding a heterochromatin protein 1 defects in the induction of secondary metabolite biosynthesis. Plant Biol. 7: 348-357.

Bhalerao, R. P., Eklof, J., Ljung, K., Marchant, A., Bennett, M. and Sandberg, G. (2002). Shoot-derived auxin is essential for early lateral root emergence in Arabidopsis seedlings. Plant J. 29: 325-332.

Blilou, I., Xu, J., Wildwater, M., Willemsen, V., Paponov, I., Friml, J., Heidstra, R., Aida, M., Palme, K. and Scheres, B. (2005). The PIN auxin efflux facilitator network controls growth and patterning in Arabidopsis roots. Nature. 433: 39-44.

Bilsborougha, G. D., Runionsb, A., Barkoulasa, M., Jenkinsa, H. W., Hassonc, A., Galinhaa, C., Laufsc, P., Haya, A., Prusinkiewiczb, P. and Tsiantisa, M. (2010). Model for the regulation of *Arabidopsis thaliana* leaf margin development. Proc. Natl. Acad. Sci. USA. 108: 3424-3429.

Braselton, J. P. (1982). Karyotypic analysis of *Plasmodiophora brassicae* based on serial thin sections of pachytene nuclei. Can. J. Bot. 60: 403-408.

Braselton, J. P. (1995). Current status of the plasmodiophorids. Crit. Rev. Microbiol. 21: 263-275.

Brodmann, D., Wiemken, A., Boller, T., Wingler, A., Schuller, A., LudwigMüller, J. and Aeschbacher, R. A. (2002). Induction of trehalase in Arabidopsis plants infected with the trehalose-producing pathogen *Plasmodiophora brassicae*. Mol. Plant-Microbe Interact. 15: 693-700.

Bryan, R. J., Trese, A. T. and Braselton, J. P. (1996). Molecular karyotypes for the obligate, intracellular, plant pathogens, *Plasmodiophora brassicae* and *Spongospora subterranea*. Mycologia. 88: 358-360.

Bryngelsson, T., Gustafsson, M., Gréen, B. and Lind, C. (1988). Uptake of host DNA by the parasitic fungus *Plasmodiophora brassicae*. Physiol. Mol. Plant Pathol. 33: 163-171.

Buczacki, S. T. and Clay, C. M. (1984). Some observations on secondary zoospore development in *Plasmodiophora brassicae*. Trans. Br. Mycol. Soc. 82: 339-344.

Bulman, S. R., Kuhn, S. F., Marshall, J. W. and Schnepf, E. (2001). A phylogenetic analysis of the SSU rRNA from members of the Plasmodiophorida and Phagomyxida. Protist. 152: 43-51.

Bulman, S., Candy, J. M., Fiers, M., Lister, M., Conner, M. J. and Eady, C. C. (2011). Genomics of biotrophic, plant-infecting plasmodiophorids using in vitro dual cultures. Protist. 162: 449-461.

Bulman, S. R. and Braselton, J. P. (2014). Rhizaria: Phytomyxea. Pp. 99-112. In: McLaughlin, D. J. and J. W. Spatafora (eds.), The Mycota VII, 2nd Edition, Systematics and Evolution, Part A, Springer-Verlag, Berlin-Heidelberg.

Burki, F. and Keeling, P. J. (2014). Rhizaria. Current Biol. 24: 103-107.

Burki, F., Kudryavtsev, A., Matz, M. V., Aglyamova, G. V., Bulman, S., Fiers, M., Keeling, P. J. and Pawlowski, J. (2010). Evolution of rhizaria: new insights from phylogenomic analysis of uncultivated protists. BMC Evol. Biol. 10: 377.

Butcher, D. N., El-Tigani, S. and Ingram, D. S. (1974). The role of indole glucosinolates in the clubroot disease of the cruciferae. Physiol. Plant Pathol. 4: 127-140.

Cavalier-Smith, T. and Chao, E. E.Y. (2003). Phylogeny and classification of phylum cercozoa (protozoa). Protist. 154: 341-358.

Chen, F., ĎAuria, J. C., Tholl, D., Ross, J. R., Gershenzon, J., Noel, J. P. and Pichersky, E. (2003). An *Arabidopsis thaliana* gene for methylsalicylate biosynthesis, identified by a biochemical genomics approach, has a role in defense. Plant J. 36: 577-588.

Chen, J., Jing, J., Zhan, Z., Zhang, T., Zhang, C. and Piao, Z. (2013). Identification of novel QTLs for isolate-specific partial resistance to *Plasmodiophora brassicae* in *Brassica rapa*. PLoS ONE 8: e85307.

Chen, J., Pang, W., Chen, B., Zhang, C. and Piao, Z. (2016). Transcriptome analysis of *Brassica rapa* near-isogenic lines carrying clubroot-resistant and -susceptible alleles in response to *Plasmodiophora brassicae* during early Infection. Front. Plant Sci. 6:1183.

Chen, R., Rosen, E. and Masson, P. H. (1999). Gravitropism in higher plants. Plant Physiol. 120: 343-350.

Chu, M., Song, T., Falk, K. C., Zhang, X., Liu, X., Chang, A., Lahlali, R., McGregor, L., Gossen, B. D., Yu, F. and Peng, G. (2014). Fine mapping of *Rcr1* and analyses of its effect on transcriptome patterns during infection by *Plasmodiophora brassicae*. BMC Genomics 15: 1166.

Conrath, U., Thulke, O., Katz, V., Schwindling, S. and Kohler, A. (2001). Priming as a mechanism in induced systemic resistance of plants. Eur. J. Plant Pathol. 107: 113-119.

De la Jara, A., Mendoza. H., Martel. A., Molina. C., Nordstron. L., de la Rosa. V. and Diaz, R. (2003). Flow cytometric determination of lipid content in a marine dinoflagellate, *Crypthecodinium cohnii*. J. Appl. Phycol. 15: 433-438.

De Smet, I., Lau, S., Voss, U., Vanneste, S., Benjamins, R., Rademacher, E. H., Schlereth, A., De Rybel, B., Vassileva, V., Grunewald, W., Naudts, M., Levesque, M. P., Ehrismann, J. S., Inzé, D., Ehrismann, J. S., Inzé, D., Luschnig, C., Benfey, P. N., Weijers, D., Van Montagu, M. C., Bennett, M. J., Jürgens, G. and Beeckman, T. (2010). Bimodular auxin response controls organogenesis in Arabidopsis. Proc. Natl. Acad. Sci. USA. 107: 2705-2710.

Dekhuijzen, H. M. (1975). The enzyme isolation of secondary vegetative plasmodia of *Plasmodiophora brassicae* form callus tissue of *Brassicae campestris*. Physiol. Plant Pathol. 6: 187-192.

Deora, A., Gossen, B. D., Walley, F. and McDonald, M. R. (2011). Boron reduces development of clubroot in canola. Can. J. Plant Pathol. 33: 475-484.

Deora, A., Gossen. B. D. and McDonald M. R. (2013). Cytology of infection, development and expression of resistance to *Plasmodiophora brassicae* in canola. Ann. Appl. Biol.163: 56-71.

Desoignies, N., Carbonell, J., Moreau, J. S., Conesa, A., Dopazo, J. and Legreve, A. (2014). Molecular interactions between sugar beet and *Polymyxa betae* during its life cycle. Ann. Appl. Biol. 164: 244-256.

Devos, S., Vissenberg, K., Verbelen, J. P. and Prinsen, E. (2005). Infection of Chinese cabbage by *Plasmodiophora brassicae* leads to a stimulation of plant growth: impacts on cell wall metabolism and hormone balance. New Phytol. 166: 241-250.

Devos, S., Laukens, K., Deckers, P., Van Der Straeten, D., Beeckman, T., Inze, D., van Onckelen, H., Witters, E. and Prinsen, E. (2006). A hormone and proteome approach to picturing the initial metabolic events during *Plasmodiophora brassicae* infection on Arabidopsis. Mol. Plant-Microbe Interact. 19: 1431-1433.

Devos, S. and Prinsen, E. (2006). Plant hormone: a key in clubroot development. Comun. Agric. Alli. Biol. Sci. 71 (3 Pt B): 869-872.

Diederichsen, E., Frauen, M. and Ludwig-Müller, J. (2014). Clubroot disease management challenges from a German perspective. Can. J. Plant Pathol. 36: 85-98.

Ding, Z., Galva´n-Ampudia, C. S., Demarsy, E., Langowski, L., Kleine-Vehn, J., Fan, Y., Morita, M. T., Tasaka, M., Fankhauser, C., Offringa, R. and Friml, J. (2011). Light mediated polarization of the PIN3 auxin transporter for the phototropic response in Arabidopsis. Nat. Cell Biol. 13: 447-452.

Dixon, G. R. (2009). The occurrence and economic impact of *Plasmodiophora brassicae* and clubroot disease. J. Plant Growth Reg. 28: 194-202.

Dixon, G. R. (2014). Special issue: clubroot (*Plasmodiophora brassicae* Woronin) – an agricultural and biological challenge worldwide. Can. J. Plant Pathol. 36: 5-18.

Doan, T. T., Jäschke, D. and Ludwig-Müller, J. (2010). An endophytic fungus induces tolerance against the clubroot pathogen *Plasmodiophora brassicae* in *Arabidopsis thaliana* and *Brassica rapa* roots. Acta. Hortic. 867: 173-180.

Dobson, R. L. and Gabrielson, R. L. (1983). Role of primary and secondary zoospores of *Plasmodiophora brassicae* in the development of clubroot in Chinese cabbage. Phytopathol. 73: 559-561.

Donald, E. C. and Porter, I. J. (2004). A sand-solution culture technique used to observe the effect of calcium and pH on root hair and cortical stages of infection by *Plasmodiophora brassicae*. Aust. Plant Pathol. 33: 585-589.

Donald, E.C., Lawrence, J. M. and Porter, I. J. (2004). Influence of particle size and application method on the efficacy of calcium cyanamide for control of clubroot of vegetable brassicas. Crop Prot. 23: 297-303.

Fähling, M., Graf, H. and Siemens, J. (2004). Characterization of a single spore isolate population of *Plasmodiophora brassicae* resulting from a single club. J. Phytopathol.152: 438-444.

Fei, W., Feng, J., Rong, S., Strelkov, S. E., Gao, Z. and Hwang, S. F. (2016). Infection and gene expression of the clubroot pathogen *Plamodiophora brassicae* in resistant and susceptible canola cultivars. Plant Dis. 100: 824-828.

Feraru, E. and Friml, J. (2008). Polar auxin targeting. Plant Physiol. 147:1553-1559.

Fishe, K. E., Lowry, D. S. and Roberson, R.W. (2000). Cytoplasmic cleavage of living zoosporangia of *Allomyces macrogynu*. J. Microsc. 199: 260-269.

Friberg, H., Lagerlöf, J. and Rämert, B. (2006). Usefulness of nonhost plants in managing *Plasmodiophora brassicae*. Plant Pathol. 55: 690-695.

Friml, J., Winiewska, J., Benková, E., Mendgen, K. and Palme, K. (2002a). Lateral relocation of auxin effux regulator PIN3 mediates tropism in Arabidopsis. Nature 415: 806-809.

Friml, J., Benková, E., Blilou, I., Wisniewska, J., Hamann, T., Ljung, K., Woody, S., Sandberg, G., Scheres, B., Jürgens, G. and Palme, K. (2002b). AtPIN4 mediates sink-driven auxin gradients and root patterning in Arabidopsis. Cell 108: 661-673.

Friml, J., Vieten, A., Sauer, M., Weijers, D., Schwarz, H., Hamann, T., Offringa, R. and Jurgens, G. (2003). Efflux-dependent auxin gradients establish the apical-basal axis of Arabidopsis. Nature 426: 147-153,

Fuchs, H. and Sacristan, M. D. (1996). Identification of a gene in *Arabidopsis thaliana* controlling resistance to clubroot (*Plasmodiophora brassicae*) and characterization of the resistance response. Mol. Plant-Microbe Interact. 9: 91-97.

Garber, R. C. and Aist, J. R. (1979a). The ultrastructure of mitosis in *Plasmodiophora brassicae* (Plasmodiophorales). J. Cell Biol. 57: 2509-2518.

Garber, R. C. and Aist, J. R. (1979b). The ultrastructure of meiosis in *Plasmodiophora brassicae* (Plasmodiophorales). Can. J. Bot. 57: 2509-2518.

Glazebrook, J. (2005). Contrasting mechanisms of defense against biotrophic and necrotrophic pathogens. Annu. Rev. Phytopathol. 43: 205-227.

Gossen, B. D., Strelkov, S. E., Manolii, V. P., Rennie, D. C., Cao, T., Hwang, S. F., Peng G. and McDonald M. R. (2015). Spread of *Plasmodiophora brassicae* on canola in Canada, 2003–2014: Old pathogen, new home. Can. J. Plant Pathol. 37: 403-413.

Goverse, A., Overmars, H., Engelbertink, L., Schots, A. and Helder, J. (2000). Both induction and morphogenesis of cyst nematode feeding cells are mediated by auxin. Mol. Plant-Microbe Interact. 13: 1121-1129.

Graf, H., Sokolowski, F., Klewer, A., Diederichsen, E., Luerben, H. and Siemens, J. (2001). Electrophoretic karyotype of the obligate biotrophic parasite *Plasmodiophora brassicae* Wor. J. Phytopathol. 149: 313-318.

Graf, H., Faehling, M. and Siemens, J. (2004). Chromosome polymorphism of the obligate biotrophic parasite *Plasmodiophora brassicae*. J Phytopathol. 152: 86-91.

Gravot, A., Deleu, C., Wagner, G., Lariagon, C., Lugan, R., Todd, C., Wendehenne, D., Delourme, R., Bouchereau, A. and Manzanares-Dauleux, M. J. (2012). Arginase induction represses gall development during clubroot infection in Arabidopsis. Plant Cell Physiol. 53: 901-911.

Grsic, S., Kirchheim, B., Pieper, K., Fritsch, M., Hilgenberg, W. and Ludwig-Muller, J. (1999). Induction of auxin biosynthetic enzymes by jasmonic acid and in clubroot diseased Chinese cabbage plants. Physiol. Plant 105: 521-531.

Grsic, S., Kobelt, P., Siemens, J., Bischoff, M. and Ludwig-Müller, J. (2000). Expression and localization of nitrilase during symptom development of the clubroot disease in *Arabidopsis thaliana*. Plant Physiol. 122: 369-378.

Grunewald, W., Cannoot, B., Friml, J. and Gheysen, G. (2009). Parasitic nematodes modulate PIN-mediated auxin transport to facilitate infection. PLoS Pathol. 5: e1000266.

Guenot, B., Bayer, E., Kierzkowski, D., Smith, R. S., Mandel, T., Zádníková, P., Benková, E. and Kuhlemeier, C. (2012). PIN1-independent leaf initiation in Arabidopsis. Plant Cell. 159: 1501-1510.

Guo, S., Mao, Z., Wu, Y., Hao, K., He, P. and He, Y. (2013). Genome sequencing of *Bacillus subtilis* strain XF-1 with high efficiency in the suppression of *Plasmodiophora brassicae*. Genome Announc 1: e00066-13.

Guzmán, H. M., De la Jara A., Duarte, L. C. and Presmanes, K. F. (2010). Estimate by means of flow cytometry of variation in composition of fatty acids from *Tetraselmis suecica* in response to culture conditions. Aquacult. Int. 18: 189-99.

Guzmán, H. M., Valido A, De La J, Duarte, L. C. and Presmanes, K. F. (2011). Analysis of interspecific variation in relative fatty acid composition: use of flow cytometry to estimate unsaturation index and relative polyunsaturated fatty acid content in microalgae. J. Appl. Phycol. 23: 7-15.

Haga, K. and Sakai, T. (2012). PIN auxin efflux carriers are necessary for pulse-induced but not continuous light-induced phototropism in Arabidopsis. Plant Physiol. 160: 763-776.

Hatakeyama, K., Suwabe, K., Tomita, R.N., Kato, T., Nunome, T., Fukuoka, H. and Matsumoto, S. (2013). Identification and characterization of *Crr1a*, a gene for resistance to clubroot disease (*Plasmodiophora brassicae* Woronin) in *Brassica rapa* L. PLoS One 8: e54745.

Hasan, M. J. and Rahman, M. (2016). Genetics and molecular mapping of resistance to *Plasmodiophora brassicae* pathotypes 2, 3, 5, 6 and 8 in rutabaga (*Brassica napus* var. *napobrassica*). Genome. 59: 1-11.

Hentrich, M., Bötcher, C., Düchting, P., Cheng, Y., Zhao, Y., Berkowitz, O., Masle, J., Medina, J. and Pollmann, S. (2013). The jasmonic acid signaling pathway is linked to auxin homeostasis through the modulation of YUCCA8 and YUCCA9 gene expression. Plant J. 74: 626-637.

Heo, S. H., Jang S. J., Choi, J. S., Jang C. S., Song J. Y. and Kim, H. J. (2009). Chinese cabbage clubroot pathogen, *Plasmodiophora brassicae*, is genetically stable. Mycobiol. 37: 225-229.

Hirai, M., Harada, T., Kubo, N., Tsukada, M., Suwabe, K. and Matsumoto, S. (2004). A novel locus for clubroot resistance in *Brassica rapa* and its linkage markers. Theor. Appl. Genet. 108: 639-643.

Huot, B., Yao, j., Montgomery B. L. and He, S. Y. (2014). Growth–defense tradeoffs in plants: a balancing act to optimize fitness. Mol. Plant. 7: 1267-1287.

Hwang, S. F., Ahmed, H. U., Zhou, Q., Strelkov, S. E., Gossen, B. D., Peng, G. and Turnbull, G. D. (2011). Influence of cultivar resistance and inoculum density on root hair infection of canola (*Brassica napus*) by *Plasmodiophora brassicae*. Plant Pathol. 60: 820-829.

Hwang, S. F., Strelkov, S. E., Ahmed, H. U., Manolii, V. P., Zhou, Q., Fu, H., Turnbull, G., Fredua-Agyeman, R. and Feindel, D. (2017). Virulence and inoculum density dependent interactions between clubroot resistant canola (*Brassica napus*) and *Plasmodiophora brassicae.* Plant Pathol. 66: 1318-1328.

Ingram, D. S. and Tommerup, I. C. (1972). The life history of *Plasmodiophora brassicae* Woron. Proc. Royal Soc. 180: 103-112.

Ira, K. G. (2001). Probing the link between proton transport and water content in lipid membranes. J. Phys. Chem. B. 105: 1484-1488.

Irani, S., Trost, B.,Waldner, M., Nayidu, N., Tu, J., Kusalik A. J., Todd C. D., Wei, Y. and Bonham-Smith, P. C. (2018). Transcriptome analysis of response to *Plasmodiophora brassicae* infection in the Arabidopsis shoot and root. BMC Genomics. 19:23.

Jäschke, D., Dugassa-Gobena, D., Karlovsky, P., Vidal, S. and Ludwig-Müller, J. (2010). Suppression of clubroot (*Plasmodiophora brassicae*) development in *Arabidopsis thaliana* by the endophytic fungus *Acremonium alternatum*. Plant Pathol. 59: 100-111.

Joo, G. J., Kim, Y. M., Kim, J. W., Kim, W. C., Rhee, I. K., Choi, Y. H. and Kim, J. H. (2004).

Biocontrol of cabbage clubroot by the organic fertilizer using *Streptomyces* sp. AC-3. Kor. J. Microbiol. Biotechnol. 32: 173-178.

Jahn, L., Mucha, S., Bergmann, S., Horn, C., Siemens, J., Staswick, P., Steffens, B. and Ludwig-Müller, J. (2013). The clubroot pathogen (*Plasmodiophora brassicae*) influences auxin signaling to regulate auxin homeostasis. Plants 2: 726-749.

Jubault, M., Lariagon, C., Taconnat, L., Renou, J. P., Gravot, A., Delourme R. and Manzanares-Dauleux, M. J. (2013). Partial resistance to clubroot in Arabidopsis is based on changes in the host primary metabolism and targeted cell division and expansion capacity. Funct. Integr. Genomics. 13: 191-205.

Kageyama, K. and Asano, T. (2009). Life cycle of *Plasmodiophora brassicae*. J. Plant Growth Regul. 28: 203-221.

Kavanagh, J. A. and Williams, P. H. (1981). Indole auxins in Plasmodiophora infected cabbage roots and hypocotyls. Trans. Br. Mycol. Soc. 77:125-129.

Kimura, K., Yamaoka. M. and Kamisaka, Y. (2004). Rapid estimation of lipids in oleaginous fungi and yeasts using Nile red fluorescence. J. Microbiol. Methods. 56: 331-338.

Kleine-Vehn, J. and Friml, J. (2008). Polar targeting and endocytic recycling in auxin-dependent plant development. Annu. Rev. Cell Dev. Biol. 24: 447-473.

Kleine-Vehna, J., Ding, Z., Jones, A. R., Tasakac, M., Morita, M. T. and Friml, J. (2010). Gravity-induced PIN transcytosis for polarization of auxin fluxes in gravity-sensing root cells. Proc. Natl. Acad. Sci. USA. 107: 22344-22349.

Knaust, A. and Ludwig-Müller, J. (2013). The ethylene signalling pathway is needed to restrict root gall growth in Arabidopsis after infection with the obligate biotrophic protist *Plasmodiophora brassicae*. J. Plant Growth Regul. 32: 9-21.

Kobelt, P., Siemens, J. and Sacristan, M. D. (2000). Histological characterisation of the incompatible interaction between *Arabidopsis thaliana* and the obligate biotrophic pathogen *Plasmodiophora brassicae*. Mycol. Res. 104: 220-225.

Kopischke, M., Westphal, L., Schneeberger, K., Clark, R., Ossowski, S., Wewer, V., Fuchs, R., Landtag, J., Hause G., Dörmann, P., Lipka, V., Weigel, D., Schulze-Lefert, P., Scheel, D. and Rosahl, S. (2013). Impaired sterol ester synthesis alters the response of *Arabidopsis thaliana* to *Phytophthora infestans.* Plant J. 73: 456-468.

Koo, Y. J., Kim, M. A., Kim, E. H., Song, J. T., Jung, C., Moon, J. K., Kim, J. H., Seo, H. S., Song,

S. I., Kim, J. K., Lee, J. S., Cheong, J. J. and Choi, Y. D. (2007). Overexpression of salicylic acid carboxyl methyltransferase reduces salicylic acid-mediated pathogen resistance in *Arabidopsis thaliana*. Plant Mol. Biol. 64: 1-15.

Kramer, E. M. (2004). PIN and AUX/LAX proteins: Their role in auxin accumulation. Trends Plant Sci. 9: 578-582.

Krecek, P., Skupa, P., Libus, J., Naramoto, S., Tejos, R., Friml, J. and Zažímalová, E. (2009). The PIN-FORMED (PIN) protein family of auxin transporters. Genome Biol. 10: 249.

Kucherak, O. A., Oncul. S., Darwich. Z., Yushchenko. D. A., Arntz. Y., Didier. P., Mély, Y. and Klymchenko, A. S. (2010). Switchable Nile Red-Based Probe for Cholesterol and Lipid Order at the Outer Leaflet of Biomembranes. J. Am. Chem. Soc. 132: 4907-4916.

Kyndt, T., Goverse, A., Haegeman, A., Warmerdam, S., Wanjau, C., Jahani, M., Engler, G., de Almeida Engler, J. and Gheysen, G. (2016). Redirection of auxin flow in *Arabidopsis thaliana* roots after infection by root-knot nematodes. J. Exp. Bot. 67:4559-4570.

Lahlali, R., Peng, G., McGregor, L., Gossen, B. D., Hwang, S. F. and McDonald, M. R. (2011). Mechanisms of the biofungicide Serenade (*Bacillus subtilis* GST713) in suppressing clubroot. Biocontrol Sci. Technol. 21: 1351-1362.

Lahlali, R., Peng, G., Gossen, B. D., McGregor, L., Yu, F. Q., Hynes, R. K., Hwang, S. F., McDonald, M. R. and Boyetchko, S. M. (2013). Evidence that the biofungicide Serenade (*Bacillus subtilis*) suppresses clubroot on canola via antibiosis and induced host resistance. Phytopathol. 103: 245-254.

Lahlali, R., McGregor, L., Song, T., Gossen, B. D., Narisawa, K. and Peng, G. (2014). *Heteroconium chaetospira* induces resistance to clubroot via upregulation of host genes involved in jasmonic acid, ethylene, and auxin biosynthesis. PLoS One 9: e94144.

Lahlali, R. and Peng, G. (2014). Suppression of clubroot by *Clonostachys rosea* via antibiosis and induced host resistance. Plant Pathol. 63: 447-455.

Lavy, M. and Estelle, M. (2016). Mechanisms of auxin signaling. Development. 143: 3226-3229.

Lecourieux, D., Ranjeva, R. and Pugin, A. (2006). Calcium in plant defence-signalling pathways. New Phytol. 171: 249-269.

Lee, S. O., Choi, G. J., Choi, Y. H., Jang, K. S., Park, D. J., Kim, C. J. and Kim, J. K. (2008). Isolation and characterization of endophytic actinomycetes from Chinese cabbage roots as antagonists to *Plasmodiophora brassicae*. J. Microbiol. Biotechnol. 18: 1741-1746.

Lee, J., Izzah. N. K., Choi, B. S., Joh, H. J., Lee, S. C., Perumal, S., Seo, J., Ahn, K., Jo, E. J., Choi, G. J., Nou, I. S., Yu, Y. and Yang, T. J. (2015). Genotyping-by-sequencing map permits identifcation of clubroot resistance QTLs and revision of the reference genome assembly in cabbage (*Brassica oleracea* L.). DNA Res. 23: 29-41.

Lee, C., Chronis, D., Kenning, C., Péret, B., Hewezi, T., Davis, E. L., Baum, T. J., Hussey, R., Bennett, M. and Mitchum, M. G. (2011). The novel cyst nematode effector protein 19C07 interacts with the Arabidopsis auxin influx transporter LAX3 to control feeding site development. Plant Physiol. 155: 866-880.

Lemarié, S., Robert-Seilaniantz, A., Lariagon, C., Lemoine, J., Marnet, N., Jubault, M. and Gravot, A. (2015). Both the jasmonic acid and the salicylic acid pathways contribute to resistance to the biotrophic clubroot agent *Plasmodiophora brassicae* in Arabidopsis. Plant Cell Physiol. 56: 2158-2168.

Lewis, D. R., Miller, N. D., Splitt, B. L., Wu, G. and Spalding, E. P. (2007). Separating the roles of acropetal and basipetal auxin transport on gravitropism with mutations in two Arabidopsis multidrug resistance-like ABC transporter genes. Plant Cell. 19: 1838-1850.

Li, R., Sun, R., Hicks, G. R. and Raikhel, N. V. (2015). Arabidopsis ribosomal proteins control vacuole trafficking and developmental programs through the regulation of lipid metabolism. Proc. Natl. Acad. Sci. *USA* 112: 89-98.

Liu, Y., Pei, J., Grishin, N. and Snell, W. J. (2015). The cytoplasmic domain of the gamete membrane fusion protein HAP2 targets the protein to the fusion site in Chlamydomonas and regulates the fusion reaction. Development. 142: 962-971.

Loarce, Y., Navas, E., Paniagua, C., Fominaya, A., Manjón J. L. and Ferrer, E. (2016). Identification of genes in a partially resistant genotype of *Avena sativa* expressed in response to *Puccinia coronata* infection. Front. Plant Sci.7:731.

Lovelock, D. A., Donald, C. E., Conlan, X. A. and Cahill, D. M. (2013). Salicylic acid suppression of clubroot in broccoli (*Brassicae oleracea* var. *italica*) caused by the obligate biotroph *Plasmodiophora brassicae*. Aust. Plant Pathol. 42: 141-153.

Lovelock, D.A., Šola, I., Marschollek, S., Donald, C. E., Rusak, G., Pèe, K. V., Ludwig-Müller, J. and Cahill, D. M. (2016). Analysis of salicylic acid-dependent pathways in *Arabidopsis thaliana* following infection with *Plasmodiophora brassicae* and the influence of salicylic acid on disease. Mol. Plant Pathol. 17: 1237-1251.

Ludwig-Müller, J., Bendel, U., Thermann, P., Ruppel, M., Epstein, E. and Hilgenberg, W. (1993). Concentrations of indole-3-acetic acid in plants of tolerant and susceptible varieties of Chinese cabbage infected with *Plasmodiophora brassicae* Woron. New Phytol. 125: 763-769.

Ludwig-Müller, J., Epstein, E. and Hilgenberg, W. (1996). Auxin-conjugate hydrolysis in Chinese cabbage: characterization of an amidohydrolase and its role during the clubroot disease. Physiol. Plant. 97: 627-634.

Ludwig-Müller, J., Pieper, K., Ruppel, M., Cohen, J.D., Epstein, E., Kiddle, G. and Bennett, R. (1999a). Indole glucosinolate and auxin biosynthesis in *Arabidopsis thaliana* (L.) Heynh. glucosinolate mutants and the development of clubroot disease. Planta. 208: 409-419.

Ludwig-Müller, J., Bennett, R. N., Kiddle, G., Ihmig, S., Ruppel, M. and Hilgenberg, W. (1999b). The host range of *Plasmodiophora brassicae* and its relationship to endogenous glucosinolate content. New Phytol. 144: 443-458.

Ludwig-Müller, J. and Schuller, A. (2008). What can we learn from clubroot: alternation in host roots and hormone homeostasis caused by *Plasmodiophora brassicae*. Eur. J. Plant Pathol. 121: 291-302.

Ludwig-Müller, J. (2009a). Plant defence—what can we learn from clubroots? Aust. Plant Pathol. 38:318-324.

Ludwig-Müller, J. (2009b). Glucosinolates and the clubroot disease: defense compounds or auxin precursors? Phytochem. Rev., 8: 135-148.

Ludwig-Müller, J., Prinsen, E., Rolfe, S. and Scholes, J. (2009). Metabolism and plant hormone action during the clubroot disease. J. Plant Growth Regul. 28: 229-244.

Ludwig-Müller, J., Jülke, S., Geiß, K., Richter, F., Mithöfer, A., Šola, I., Rusak, G., Keenan, S. and Bulman, S. (2015). A novel methyltransferase from the intracellular pathogen *Plasmodiophora brassicae* methylates salicylic acid. Mol. Plant Pathol. 16: 349-364.

Ludwig-Müller, J. (2016). Belowground defence strategies against clubroot (*Plasmodiophora brassicae*). In: Vos C., Kazan K. (eds) Belowground defence strategies in plants. Signaling and Communication in Plants. Springer, Cham.

Manoharan, R. K., Shanmugam, A., Hwang, I., Park, J. I. and Nou, I. S. (2016). Expression of salicyclc acid-related genes in *Brassica oleracea* var. *capitate* during *Plasmodiophora brassicae* infection. Genome. 59: 379-391.

Manzanares-Dauleux, M., Delourme, R., Baron, F. and Thomas, G. (2000). Mapping of one major gene and of QTLs involved in resistance to clubroot in *Brassica napus*. Theor. Appl. Genet. 101: 885-891.

Marchant, A., Bhalerao, R., Casimiro, I., Eklof, J., Casero, P. J., Bennett, M. and Sandberg, G. (2002). AUX1 promotes lateral root formation by facilitating indole-3-acetic acid distribution between sink and source tissues in the Arabidopsis seedling. Plant Cell. 14: 589-597.

Maheshwari, P. and Kovalchuk, I. (2016). Genetic transformation of crops for oil production. In Industrial Oil Crops (pp. 379-412).

Matsumoto, E., Yasui, C., Ohi, M. and Tsukada, M. (1998). Linkage analysis of RFLP markers for clubroot resistance and pigmentation in Chinese cabbage (*Brassica rapa* ssp. *pekinensis*). Euphytica. 104: 79-86.

Matsumoto, E., Ueno, H., Aruga, D., Sakamoto, K. and Hayashida, N. (2012). Accumulation of three clubroot resistance genes through marker-assisted selection in Chinese cabbage (*Brassica rapa* ssp. *pekinensis*). J. Japan. Soc. Hort. Sci. 81: 184-190.

Mazarei, M., Lennon, K. A., Puthoff, D. P., Rodermel, S. R. and Baum, T. J. (2003). Expression of an Arabidopsis phosphoglycerate mutase homologue is localized to apical meristems, regulated by hormones, and induced by sedentary plant-parasitic nematodes. Plant Mol. Biol. 53, 513-530.

McGrann, G. R., Grimmer, M. K., Mutasa-Göttgens, E. S. and Stevens, M. (2009). Progress towards the understanding and control of sugar beet rhizomania disease. Mol. Plant Pathol. 10: 129-141.

Miquel, M., Trigui, G., d'Andréa, S., Kelemen, Z., Baud, S., Berger, A., Deruyffelaere, C., Trubuil, A., Lepiniec, L. and Dubreucq, B. (2014). Specialization of oleosins in oil body dynamics during seed development in Arabidopsis seeds. Plant Physiol. 164: 1866-1878.

Michniewicz, M., Brewer, P. B. and Friml, J. (2007). Polar auxin transport and asymmetric auxin distribution. Arabidopsis Book: doi:10.1199/tab.0108.

Mithen, R. and Magrath, R. (1992). A contribution to the life history of *Plasmodiophora brassicae*: secondary plasmodia development in root galls of *Arabidopsis thaliana*. Mycol. Res. 96: 877-885.

Moxham, S. and Buczacki, S. T. (1983). Chemical composition of the resting spore well of *Plasmodiophora brassicae*. Trans. Br. Mycol. Soc. 80: 297-304.

Müller, A., Guan, C., Gälweiler, L., Tänzler, P., Huijser, P., Marchant, A., Parry, G., Bennett, M., Wisman, E. and Palme, K. (1998). AtPIN2 defines a locus of Arabidopsis for root gravitropism control. EMBO J. 17: 6903-6911.

Murakami, H., Tsushima, S., Kuroyanagi, Y. and Shishido, Y. (2002). Reduction in resting spore density of *Plasmodiophora brassicae* and clubroot severity by liming. Soil Sci. Plant Nutr. 48: 685-691.

Nagaoka, T., Doullah, M. A., Matsumoto, S., Kawasaki, S., Ishikawa, T., Hori, H. and Okazaki, K, (2010). Identification of QTLs that control clubroot resistance in *Brassica oleracea* and comparative analysis of clubroot resistance genes between *B. rapa* and *B. oleracea.* Theor. Appl. Genet. 120: 1335-1346.

Neuhaus, K., Grsic-Rausch, S., Sauerteig, S. and Ludwig-Müller, J. (2000). Arabidopsis plants transformed with nitrilase 1 or 2 in antisense direction are delayed in clubroot development. J. Plant Physiol. 156: 756-761.

Neuhauser, S., Kirchmair, M., Bulman, S. and Bass, D. (2014). Cross-kingdom host shifts of phytomyxid parasites. BMC Evol. Biol. 14: 33.

Ning, J., Otto, T. D., Pfander, C., Schwach, F., Brochet, M., Bushell, E., Goulding, D., Sanders, M., Lefebvre, P. A., Pei, J., Grishin, N. V., Vanderlaan, G., Billker, O. and Snell1, W. J. (2013). Comparative genomics in Chlamydomonas and Plasmodium identifies an ancient nuclear envelope protein family essential for sexual reproduction in protists, fungi, plants, and vertebrates. Genes Dev. 27:1198-1215.

Niwa, R., Nomura, Y., Osaki, M. and Ezawa, T. (2008). Suppression of clubroot disease under neutral pH caused by inhibition of spore germination of *Plasmodiophora brassicae* in the rhizosphere. Plant Pathol. 57: 445-452.

Osaki, K., Fujiyama, S., Nakayama, A., Shimizu, Y., Ito, S. I. and Tanaka, S. (2008). Relation between pathogenicity and genetic variation within *Plasmodiophora brassicae*. J. Gen. Plant Pathol. 74: 281-288.

Overvoorde, P., Fukaki, H. and Beeckman, T. (2010). Auxin control of root development. Cold Spring Harb Perspect. Biol. 2(6): a001537.

Päsold, S., Siegel, I., Seidel, C. and Ludwig-Müller, J. (2010). Flavonoid accumulation in *Arabidopsis thaliana* root galls caused by the obligate biotrophic pathogen *Plasmodiophora brassicae.* Mol. Plant Pathol. 11: 545-562.

Pearson, C. G. (2014). Choosing sides - asymmetric centriole and basal body assembly. J. Cell Sci. 127: 2803-2810.

Peng, G., McGregor, L., Lahlali, R., Gossen, B. D., Hwang, S. F., Adhikari, K. K., Strelkov, S. E. and McDonald, M. R. (2011). Potential biological control of clubroot on canola and crucifer vegetable crops. Plant Pathol. 60: 566-574.

Piao, Z.Y., Deng, Y. Q., Choi, S. R., Park, Y. J. and Lim, Y. P. (2004). SCAR and CAPS mapping of *CRb*, a gene conferring resistance to *Plasmodiophora brassicae* in Chinese cabbage (*Brassica rapa* ssp. *pekinensis*). Theor. Appl. Genet. 108: 1458-1465.

Portman, N., Foster, C., Walker, G. and Šlapeta, J. (2014). Evidence of intraflagellar transport and apical complex formation in a free-living relative of the Apicomplexa. Eukaryot. Cell. 13:10-20.

Raa, J. (1971). Indole-3-acetic acid levels and the role of indole-3-acetic acid oxidase in the normal root and club-root of cabbage. Physiol. Plant. 25: 130-134.

Rahman, H., Peng, G., Yu, F., Falk, K. C., Kulkarni, M. and Selvaraj, G. (2014). Genetics and breeding for clubroot resistance in Canadian spring canola (*Brassica napus* L.). Can. J. Plant Pathol. 36: 122-134.

Rakusová, H., Gallego-Bartolomé, J., Vanstraelen, M., Robert, H. S., Alabadí, D., Blázquez, M. A., Benková, E. and Friml, J. (2011). Polarization of PIN3-dependent auxin transport for hypocotyl gravitropic response in *Arabidopsis thaliana*. Plant J. 67: 817-826.

Ramesh, M. A., Malik, S. B. and Logsdon, J. M. (2005). A phylogenomic inventory of meiotic genes: Evidence for sex in Giardia and an early eukaryotic origin of meiosis. Curr. Biol. 15: 185-191.

Rigas, S., Ditengou, F. A., Ljung, K., Daras, G., Tietz, O., Palme, K. and Hatzopoulos, P. (2013). Root gravitropism and root hair development constitute coupled developmental responses regulated by auxin homeostasis in the Arabidopsis root apex. New Phytol. 197: 1130-1147.

Rocherieux, J., Glory, P., Giboulot, A., Boury, S., Barbeyron, G., Thomas, G. and Manzanares-Dauleux, M. J. (2004). Isolate-specifc and broad-spectrum QTLs are involved in the control of clubroot in *Brassica oleracea*. Theor. Appl. Genet. 108: 1555-1563.

Rolfe, S. A., Strelkov, S. E., Links, M. G., Clarke W. E., Robinson, S. J., Djavaheri, M., Malinowski, R., Haddadi, P., Kagale, S., Parkin, I. A. P., Taheri, A. and Borhan M. H. (2016). The compact genome of the plant pathogen *Plasmodiophora brassicae* is adapted to intracellular

interactions with host *Brassica spp*. BMC Genomics 17: 272.

Rumin, J., Bonnefond, H., Saint-Jean, B., Rouxel, C., Sciandra, A., Bernard, O., Cadoret, J. and Bougaran, G. (2015). The use of fluorescent Nile red and BODIPY for lipid measurement in microalgae. Biotechnol. Biofuels. 8: 42.

Sakamoto, K., Saito, A., Hayashida,N., Taguchi G. and Matsumoto, E. (2008). Mapping of isolate-specific QTL for clubroot resistance in Chinese cabbage (*Brassica rapa* L.ssp. pekinensis). Theor. Appl. Genet. 117: 759-767.

Schuller, A., Kehr, J. and Ludwig-Müller, J. (2014). Laser microdissection coupled to transcriptional profiling of Arabidopsis roots inoculated by *Plasmodiophora brassicae* indicates a role for brassinosteroids in clubroot formation. Plant Cell Physiol. 55: 392-411.

Schuller, A. and Ludwig-Müller, J. (2016). Histological methods to detect the clubroot pathogen *Plasmodiophora brassicae* during its complex life cycle. Plant Pathol. 65: 1223-1237.

Schurko, A. M. and Logsdon, J. M. (2008). Using a meiosis detection toolkit to investigate ancient asexual "scandals" and the evolution of sex. BioEssays. 30(6): 579-589.

Schwelm, A., Fogelqvist, J., Knaust, A., Jülke, S., Lilja, T., Bonilla-Rosso, G., Karlsson, M., Shevchenko, A., Dhandapani, V., Choi, S. R., Kim, H. G., Park, J. Y., Lim, Y. P., Ludwig-Müller, J. and Dixelius, C. (2015). The *Plasmodiophora brassicae* genome reveals insights in its life cycle and ancestry of chitin synthases. Sci. Rep. 5: 11153.

Schwelm, A., Badstöber, J., Bulman, S., Desoignies, N., Etemadi, M., Falloon, R.E., Gachon, C. M. M., Legreve, A., Lukeš, J., Merz, U., Nenarokova, A., Strittmatter, M. Sullivan, B. K. and Neuhauser, S. (2018). Not in your usual Top 10: protists that infect plants and algae. Mol. Plant Pathol. 19: 1029-1044.

Sharma, K., Gossen, B. D. and Mcdonald, M. R. (2011a). Effect of temperature on cortical infection by *Plasmodiophora brassicae* and clubroot severity. Phytopathol. 101: 1424-1432.

Sharma, K., Gossen, B. D. and Mcdonald, M. R. (2011b). Effect of temperature on primary infection by *Plasmodiophora brassicae* and initiation of clubroot symptoms. Plant Pathol. 60: 830-838.

Siemens, J., Nagel, M., Ludwig-Müller, J. and Sacristán, M. D. (2002). The interaction of *Plasmodiophora brassicae* and *Arabidopsis thaliana*: parameters for disease quantification and screening of mutant lines. J. Phytopathol. 150: 592-605.

Siemens, J., Keller, I., Sarx, J., Kunz, S., Schuller, A., Nagel, W., Schmülling, T., Parniske, M. and Ludwig-Müller, J. (2006). Transcriptome analysis of Arabidopsis clubroots indicate a key role for cytokinins in disease development. Mol. Plant-Microbe Interact. 19: 480-494.

Siemens, J., Glawischnig, E. and Ludwig-Müller, J. (2008). Indole glucosinolates and camalexin do not influence the development of the clubroot disease in *Arabidopsis thaliana*. J. Phytopathol. 156: 332-337.

Siemens, J., Graf, H., Bulmen, S., In, O. and Ludwig-Müller, J. (2009). Monitoring expression of selected *Plasmodiophora brassicae* genes during clubroot development in *Arabidopsis thaliana*. Plant Pathol. 58: 130-136.

Siemens, J., Gonzalez, M. C., Wolf, S., Hofmann, C., Greiner, S., Du, Y. J., Rausch, T., Roitsch, T. and Ludwig-Müller, J. (2011). Extracellular invertase is involved in the regulation of clubroot disease in *Arabidopsis thaliana*. Mol. Plant Pathol. 12: 247-262.

Sierra, R., Cañas-Duarte, S. J., Burki, F., Schwelm, A., Fogelqvist, J., Dixelius, C., González-García, L. N., Gile G. H., Claudio, H., Slamovits, C. H., Klopp, C., Restrepo, S., Arzul, I. and Pawlowski J. (2015). Evolutionary origins of rhizarian parasites. Mol. Biol. Evol. 33: 980-983.

Simionato, D., Sforza, E., Carpinelli, E. C., Bertucco, A., Giacometti, G. M. and Morosinotto, T. (2011). Acclimation of *Nannochloropsis gaditana* to different illumination regimes: effects on lipids accumulation. Bioresour. Technol. 102: 6026-6032.

Sinden, R. E., Talman, A., Marques, S. R., Wass, M. N. and Sternberg, M. J. E. (2010). The flagellum in malarial parasites. Curr. Opin. Microbiol. 13: 491-500.

Staswick, P. E. and Tiryaki, I. (2004). The oxylipin signal jasmonic acid is activated by an enzyme that conjugates it to isoleucine in Arabidopsis. Plant Cell. 16: 2117-2127.

Staswick, P. E., Serban, B., Rowe, M., Tiryaki, I., Maldonado, M. T., Maldonado, M. C. and Suza, W. (2005). Characterization of an Arabidopsis enzyme family that conjugates amino acids to indole-3-acetic acid. Plant Cell. 17: 616-627.

Strader, L. C., Chen G. L. and Bartel, B. (2010). Ethylene direct auxin to control root cell expansion. Plant J. 64: 874-884.

Strelkov, S. E., Tewari, J. P. and Smith-Degenhardt, E. (2006). Characterization of *Plasmodiophora brassicae* populations from Alberta, Canada. Can. J. Plant Pathol. 28: 467-474.

Strelkov, S. E., Manolii, V. P., Cao, T., Xue, S. and Hwang, S. F. (2007). Pathotype classification of *Plasmodiophora brassicae* and its occurrence in *Brassica napus* in Alberta. Can. J.

Phytopathol. 155: 06-12.

Strelkov, S. E., Hwang, S.-F., Manolii, V. P., Cao, T. and Feindel, D. (2016). Emergence of new virulence phenotypes of *Plasmodiophora brassicae* on canola (*Brassica napus*) in Alberta, Canada. Eur. J. Plant Pathol. 145: 517-529.

Strelkov, S. E., Hwang S-F., Manolii, V. P., Cao, T., Fredua-Agyeman, R., Harding, M. W., Peng, G., Gossen, B. D., Mcdonald, M. R. and David Feindel, D. (2018) Virulence and pathotype classification of Plasmodiophora brassicae populations collected from clubroot resistant canola (*Brassica napus*) in Canada. Can. J. Plant Pathol, 40: 284-298.

Suwabe, K., Tsukazaki, H., Iketani, H., Hatakeyama, K., Fujimura, M., Nunome, T., Fukuoka, H., Matsumoto, S. and Hirai, M. (2003). Identification of two loci for resistance to clubroot (*Plasmodiophora brassicae* Woronin) in *Brassica rapa* L. Theor. Appl. Genet. 107: 997-1002.

Suwabe, K., Tsukazaki, H., Iketani, H., Hatakeyama, K., Fujimura, M., Kondo, M., Nunome, T., Fukuoka, H., Hirai, M. and Matsumoto, S. (2006). Simple sequence repeat-based comparative genomics between *Brassica rapa* and *Arabidopsis thaliana*: the genetic origin of clubroot resistance. Genetics. 173: 309-319.

Suwabe, K., Suzuki, G., Nunome, T., Hatakeyama, K., Mukai, Y., Fukuoka H. and Matsumoto, S. (2012). Microstructure of a *Brassica rapa* genome segment homoeologous to the resistance gene cluster on Arabidopsis chromosome 4. Breed. Sci. 62: 170-177.

Swarup, R., Friml, J., Marchant, A., Ljung, K., Sandberg, G., Palme, K. and Bennett, M. (2001). Localization of the auxin permease AUX1 suggests two functionally distinct hormone transport pathways operate in the Arabidopsis root apex. Genes Dev. 15: 2648-2653.

Swarup, R., Kramer, E. M., Perry, P., Knox, K., Leyser, H. M., Haseloff, J., Beemster, G. T., Bhalerao, R. and Bennett, M. J. (2005). Root gravitropism requires lateral root cap and epidermal cells for transport and response to a mobile auxin signal. Nat. Cell Biol. 7: 1057-1065.

Swarup, R. and Péret, B. (2012). AUX/LAX family of auxin influx carriers-an overview. Front. Plant Sci. 3: 225.

Takahashi, H., Muraoka, S., Ito, K., Mitsui, T., Hori, H. and Kiso, A. (2001). Resting spores of *Plasmodiophora brassicae* proliferation only in the callus of clubroot disease susceptible turnip but increases PAL activity in the callus of clubroot disease-resistant turnip. Plant Biotechnol. 18: 267-274.

Takahashi, H., Takita, K., Kishimoto, T., Mitsui, T. and Hori, H. (2002). Ca^{2+} is required by clubroot resistant turnip cells for transient increases in PAL activity that follow inoculation with *Plasmodiophora brassicae*. J. Phytopathol. 150: 529-535.

Takahashi, H., Ishikawa, T., Kaido, M., Takita, K., Tayakawa, T., Okazaki, K., Okazaki, K., Itoh, K., Mitsui, T. and Hori, H. (2006). *Plasmodiophora brassicae*-induced cell death and medium alkalization in clubroot-resistant cultured roots of *Brassica rapa*. J. Phytopathol. 154: 156-162.

Tanaka, S. Ito, S. and Kameya-Iwaki, M. (2001). Electron microscopy of primary zoosporogenesis in *Plasmodiophora brassicae*. Mycoscience 42: 389-394.

Taschner, M., and Lorentzen, E. (2017). The intraflagellar transport machinery. Cold Spring Harb Perspect Biol doi: 10.1101/cshperspect.a028092.

Tomita, H., Shimizu, M., Doullah, M.A., Fujimoto, R. and Okazaki, K. (2013). Accumulation of quantitative trait loci conferring broad-spectrum clubroot resistance in *Brassica oleracea*. Mol. Breed. 32: 885-900.

Ueno, H., Matsumoto, E., Aruga, D., Kitagawa, S., Matsumura, H. and Hayashida, N. (2012). Molecular characterization of the *CRa* gene conferring clubroot resistance in *Brassica rapa*. Plant Mol. Biol. 80: 621-629.

Vandenbussche, F., Smalle, J., Le, J., Madeira, J., Saibo, N., De Paepe, A., Chaerle, L., Tietz, O., Smets, P. R., Laarhoven, L., Harren, F. J. M., Onckelen, H. V., Palme, K., Verbelen, J. P. and Straeten, D. (2003). The Arabidopsis mutant *alh1* illustrates a cross talk between ethylene and auxin. Plant Physiol., 131: 1228-1238.

Vieten, A., Vanneste, S., Wisniewska, J., Benková, E., Benjamins, R. and Beeckman, T. (2005). Functional redundancy of PIN proteins is accompanied by auxin-dependent cross-regulation of PIN expression. Development. 132: 4521-4531.

Wasson, A. P., Pellerone, F. I. and Mathesius, U. (2006). Silencing the flavonoid pathway in *Medicago truncatula* inhibits root nodule formation and prevents auxin transport regulation by rhizobia. Plant Cell 18: 1617-1629.

Weedall, G. D. and Hall, N. (2015). Sexual reproduction and genetic exchange in parasitic protists. Parasitology. 142: 120-127.

Werner, S., Diederichsen, E., Frauen, M., Schondelmaier, J. and Jung, C. (2008). Genetic mapping of clubroot resistance genes in oilseed rape. Theor. Appl. Genet. 116: 363-372.

Williams, P. H. and McNabola, S. (1967). Fine structure of *Plasmodiophora brassicae* in sporogenesis. Can. J. Bot. 45: 1165-1169.

Willige, B. C., Ahlers, S., Zourelidou, M., Barbosa, I. C., Demarsy, E., Trevisan, M., Davis, P. A., Roelfsema, M. R., Hangarter, R., Fankhauser, C. and Schwechheimer, C. (2013). D6PK AGCVIII kinases are required for auxin transport and phototropic hypocotyl bending in Arabidopsis. Plant Cell. 25:1674-1688.

Wong, J. L. and Johnson, M. A. (2010). Is HAP2-GCS1 an ancestral gamete fusogen? Trends Cell Biol. 20: 134-141.

Woodward, A. W. and Bartel, B. (2005). Auxin: regulation, action, and interaction. Ann Bot. 95:707-735.

Xu, L., Ren., L., Chen, K., Liu., F. and Fang, X. (2016). Putative role of IAA during the early response of *Brassica napus* L. to *Plasmodiophora brassicae*. Eur. J. Plant Pathol. 145: 601-613.

Xue, S., Cao, T., Howard, R. J., Hwang, S. F. and Strelkov, S. E. (2008). Isolation and variation in virulence of single-spore isolates of *Plasmodiophora brassicae* from Canada. Plant Dis. 92: 456-462.

Yuan, H. M., Xu, H. H., Liu, W. C. and Lu, Y. T. (2013). Copper regulates primary root elongation through PIN1-mediated auxin redistribution. Plant Cell Physiol. 54: 766-778.

Zažímalová, E., Murphy, A. S., Yang, H., Hoyerová, K. and Hošek, P. (2010). Auxin transporters—why so many? Cold Spring Harb Perspect. Biol. 2:1-14.

Zhang, H., Feng, J., Hwang, S. F., Strelkov, S., Falak, I., Huang, X. and Sun, R. (2016). Mapping of clubroot (*Plasmodiophora brassicae*) resistance in canola (*Brassica napus*). Plant Pathol. 65: 435-440.

Zhang, K. X., Xu, H. H., Gong, W., Jin, Y., Shi, Y. Y., Yuan, T. T., Li, J. and Lu, Y. T. (2014). Proper PIN1 distribution is needed for root negative phototropism in Arabidopsis. PloS One 9: e85720.

Zhang, T., Zhao, Z., Zhang, C. Y., Pang, W. X., Choi, S. R., Lim, Y. P. and Piao, Z. (2014). Fine genetic and physical mapping of the *CRb* gene conferring resistance to clubroot disease in *Brassica rapa*. Mol. Breed. 34: 1173-1183.

Zhao, Y. (2014). Auxin biosynthesis. Arabidopsis Book. 12: e0173.

Zhao, Y., Bi, K., Gao, Z., Chen, T., Liu, H., Xie, J., Cheng, J., Fu, Y. and Jiang, D. (2017). Transcriptome analysis of *Arabidopsis thaliana* in response to *Plasmodiophora brassicae* during early infection. Front. Microbiol. 8: 673.

Zhou, L., Zhang, L., He, Y., Liu, F., Li, M. Wang, Z. and Ji, G. (2014). Isolation and characterization of bacterial isolates for biological control of clubroot on Chinese cabbage. Eur. J. Plant Pathol. 140: 159-168.